Analyses of Atmospheric Pollutants in Atlanta and Hong Kong

Using Observation-Based Methods

A Thesis
Presented to
The Academic Faculty

by

Jing Zhang

In Partial Fulfillment
of the Requirements for the Degree
Doctor of Philosophy in the
School of Earth and Atmospheric Sciences

Georgia Institute of Technology
December 2004

Analyses of Atmospheric Pollutants in Atlanta and Hong Kong

Using Observation-Based Methods

Approved by:

Dr. William L. Chameides, Advisor

Dr. Michael H. Bergin

Dr. Carlos Cardelino

Dr. C. S. Kiang

Dr. Tao Wang

July 16, 2004

ACKNOWLEDGEMENTS

I would like to thank my thesis advisor, Prof. William L. Chameides, for his persistent guidance, thoughtful comments, assistance, and encouragement throughout my thesis work. But most of all, I thank him for kindly offering me opportunities to explore my own interests. His scientific knowledge and insight proved to be invaluable to my work.

Sincere thanks to Dr. Carlos Cardelino for his suggestions and support with my work. He provided me the OBM model and helped me understand it. I also thank Dr. Tao Wang for providing me the back trajectories. I thank my other two committee members, Dr. Michael Bergin and Dr. C. S. Kiang, for their suggestions and comments, as well as their time invested in my work.

I am grateful to Dr. David Streets who kindly helped me match up the source type profiles for VOC speciation. Many thanks to Dr. James Schauer, Dr. Karsten Baumann, Dr. Gao Chen, and Dr. Rodney Weber for their help and support through my research. I also enjoyed and appreciated the friendship, help and encouragement from many of my friends and EAS fellows, Qian Tan, Yan Huang, Ping Jing, Yilin Ma, Lei Zhu, Qing Yang, Wei Xu, Yongjiu Dai, Nicholas Meskhidze, Jingzhi Zhao, which carried me through the hardship and difficulties and made my years here at GA Tech most enjoyable.

Finally, I would like to thank my parents for their constant support and understanding through the many years of my Ph.D. education. And I would like to thank my husband for his patience and love for these years.

TABLE OF CONTENTS

LIST OF TABLES

LIST OF FIGURES

SUMMARY

There are two parts in this study. The first part is to test the validity of the assumption of thermodynamic equilibrium between fine particulate ($PM_{2.5}$) nitrate (NO_3^-) and ammonium (NH_4^+) and gas-phase nitric acid ($HNO_3(g)$) and ammonia ($NH_3(g)$). A rough estimation of the characteristic time to achieve thermodynamic equilibrium is first carried out, which suggests that $PM_{2.5}$ and gas-phase species are in thermodynamic equilibrium. Then equilibrium is tested by calculating the equilibrium concentrations of $HNO_3(g)$ and $NH_3(g)$ implied by the $PM_{2.5}$ inorganic composition (i.e. Na^+, NH_4^+, Cl^-, NO_3^- and SO_4^{2-}), temperature and relative humidity observed at the Atlanta Supersite 1999 using ISORROPIA model. The results indicate that the data of the inorganic $PM_{2.5}$ composition are consistent with the assumption of thermodynamic equilibrium provided that the $PM_{2.5}$ SO_4^{2-} concentration measured by the PILS has a systematic overestimate of ~15%, or the $PM_{2.5}$ PILS systematically underestimated the concentration of the alkaline components by ~15%, and/or the ISORROPIA model systematically overestimated the acidity of the $PM_{2.5}$ encountered during the experiment.

The second part of this study is to analyze the ground-level ozone pollution precursor relationships in Hong Kong and the Pearl River Delta (PRD) Pilot Air Monitoring Project. Characteristics of O_3 precursors are explored. Trace gases NO and CO, VOCs, absorption coefficient, temperature and solar radiation are associated with the O_3 formation. Specific VOC and VOC-sources that contribute most to the formation of photochemical smog are identified. The reactivity of VOCs is dominated by anthropogenic VOC and of the anthropogenic VOCs, reactive aromatics dominate in

which m-xylene and toluene are the most important. The accuracy of pollutant emission inventories for Hong Kong and PRD region is also assessed. Standard methods used to speciate VOC inventory provide ratios of species that are inconsistent with observed ratios in Hong Kong and PRD region. Combined with back trajectory information, dCO/dNO_y is used to define whether O_3 is locally or regionally occurred. Five out of nine Hong Kong O_3-episodes studied show a "pollution signature" that is indicative of impact from Guangdong Province, China. Approximately 50-100% of the O_3 increase observed in Hong Kong during O_3 episodes can be explained by photochemical generation within the Hong Kong area provided that HONO is present at the concentrations derived from this study and plays a critical role in getting photochemical reactions start and O_3 formation. An OBM is used to investigate the relative benefits of various emission-control strategies. Generally the formation of O_3 throughout much of Hong Kong area is limited by VOC, in which reactive aromatics are dominant.

CHAPTER 1

INTRODUCTION

1.1 Introduction to Air Pollution

A condition of "air pollution" is defined as a situation in which substances that result from either natural, or more typically, anthropogenic activities are present at concentrations that are sufficiently high to produce a measurable adverse effect on humans, animals, vegetation, or materials (Seinfeld and Pandis, 1997). These substances are generally viewed as "air pollutants". Today, air pollution is widespread over the entire earth. It can, in the case of photochemical smog, affect rural and even remote areas as well as urban/industrial centers, and in the case of chlorofluorocarbons, affect the stratosphere and have global impact.

The first serious type of air pollution to be associated with widespread human mortality or morbidity was that characterized by high concentrations of acidic particles, resulting from combustion of coal and other high-sulfur-containing fuels. The term "London smog" was coined to describe this phenomenon by Dr. Des Voeux in a report proposed at the Smoke Coal Abatement Society Meeting in Manchester, England in 1911. The word smog was formed as a combination of smoke and fog to describe the noxious components of the air pollution and London was used because the phenomenon was first documented in that city. The more serious smog events were generally associated with cold, stagnant meteorological conditions that promoted the presence of liquid fog droplets where dissolved sulfuric acid could form and accumulate and at the same time prevented the venting of the pollution from the boundary layer. One of the most infamous of these types of smog episodes occurred in London on December, 1952.

The concentration of particulate matter with aerodynamic diameter smaller than 10 μm (PM_{10}) reached 14 mg/m^3, which was 56 times the level normally experienced at the time in London; and the levels of sulfur dioxide in the air increased by 7 fold, peaking at around 700ppb (Wilkins, 1954). During the month following the event, thousands of people in London died, about three to four times normal (Bell and Davis, 2001). Cities with this type of air pollution are often in cold climates, and have a heavy reliance on coal burning for electric power generation and domestic heating, a major source of sulfur oxide emissions (Brimblecombe, 1982).

A second common type of air pollution appeared with the widespread use of gasoline as a motor fuel (Haagen-Smit, 1950, 1952; Haagen-Smit et al., 1951, 1954; Tiao et al., 1975; Seinfeld and Pandis, 1997). This type of air pollution, once thought to be exclusive to Los Angeles, now occurs in virtually all metropolitan areas with a heavy reliance on automobiles; they include Tokyo (Wakamatsu et al., 1996, 1999), Athens (Lalas et al., 1983; Gusten et al., 1988; Wakamatsu et al., 1990; Mantis et al., 1992; Moussiopoulos et al., 1995), Mexico City (Raga and Raga, 2000; Raga et al., 2001; Castro et al., 2001), Greater Vancouver (Joe et al., 1996; Gertler et al., 1997; Pryor, 1998; Vingarzan and Taylor, 2003), Perth, Australia (Cope and Ischtwan, 1995; Rye et al., 1996), and Sao Paulo, Brazil (Fishman and Kalish, 1990; Massambani and Andrade, 1994; Seinfeld and Pandis, 1997), etc. This type of air pollution is usually referred to as "photochemical smog" (or sometimes simply smog). However it is far different from the aforementioned London smog. It is a complex mixture of reactants and products of complicated chemistry taking place in the presence of sunlight and an atmosphere laden with organic gases and oxides of nitrogen at high temperature and low wind speed. The

primary pollutants (nitrogen oxides and hydrocarbons) are converted to more harmful secondary pollutants: ozone, organic nitrates, oxidized hydrocarbons, and photochemical aerosols, which constitute photochemical smog. The production of aerosols in photochemical smog is responsible for the hazy conditions and reduced visibility that accompany this phenomenon. The production of ozone and other oxidants, as well as aerosols, is responsible for the phenomenon's deleterious effects on human health and ecosystems.

1.2 Methods to Study Air Pollution

The processes that determine the abundance of air pollutants in the atmosphere are complex and often non-linear. They involve emissions, transport and turbulent dispersion, photochemical reactions that can occur in the gas, aqueous, or particulate phase or heterogeneously, dry/wet deposition, sedimentation, aerosol nucleation/ coagulation, condensation/dissolution/evaporation, freezing/melting/sublimation, and aerosol absorption/scattering of solar radiation. Because of these complexities, mathematical and/or numerical methods are often needed to understand how these processes interact, to analyze data, and to inform policy-makers on how to best mitigate the deleterious effect of air pollution. Generally, two mathematical/numerical approaches have been taken: Emission-Based Methods and Observation-Based Methods.

An Emission-Based Method (EBM) is also called a prognostic method because it aims to predict the concentrations of pollutants from a simulation of the atmospheric processes listed above. Traditionally, the design of pollution-control strategies has largely depended upon the use of EBMs (generally air quality models (AQMs) (Russell and

Dennis, 2000). However, there are significant uncertainties in many aspects of EBMs; e.g., the emission inventories used to define the sources of O_3 precursors (Solomon, 1995; Pierson et al., 1990; Geron et al, 1994; Simpson, 1995; Guenther et al., 2000) and the meteorological fields (Hanna et al., 1996; Kumar and Russell, 1996) and parameterizations used to simulate boundary layer dynamics (Hanna et al., 1996; Kuklin and Seinfeld, 1995).

A complementary approach to the use of EBMs is the application of Observation-Based Analyses and/or Models (Hidy, 2000). Observation-Based Approaches are those methods that use ambient chemical data as the fundamental input for the analysis. These observation-based approaches use measurements of ambient concentrations of chemical compositions to check the applicability of physical/chemical mechanisms for the atmospheric processes, to evaluate the accuracy of existing emission inventories, and for assessing the relative benefits of various proposed emission control strategies for regulatory purposes. Since the observation-based approaches do not use emission inventories and often do not require the simulation of boundary layer dynamics, they avoid some of the uncertainties inherent in EBMs and thus provide a useful independent verification on the results obtained using EBMs. But it has its own limitations, for example, it is restricted by observation uncertainties. In Section 1.3 I will introduce some observation-based approaches used in various studies of air pollution.

1.3 Observation-Based Approaches

For the purposes of this thesis, I define "observation-based approaches" as those approaches that use ambient chemical data as the fundamental input for analysis. These

approaches can be used in various applications; they include emission testing, source-receptor modeling, mechanistic analyses, diagnostic analyses, and assessment of emission control strategies. Below I will briefly discuss each of these types of observation-based applications.

1.3.1 Emission Testing

In emission testing, ambient data is used to test emission inventories. It is different from EBMs which use emissions as input to calculate the atmospheric concentrations of pollutants, but uses atmospheric concentrations of pollutants as input to test the emission inventory. It is also distinct from methods that attempt to derive emission factors from measurements of chemicals emitted from a specific source (e.g., within smoke stack effluent or tunnel/roadside air) in that the later does not involve measurements in ambient air.

Inverse modeling is one method that uses ambient data to test emission inventories (Kalman, 1960). There have been a number of such applications (Cunnold et al., 1983, 1986; Enting and Mansbridge, 1989; Prinn et al., 1990; Hartley and Prinn, 1993; Brown, 1995; Mulhollan and Seinfeld, 1995; Chang et al., 1996, 1997). For example, Hartley and Prinn (1993) used an inverse method to estimate the continental-scale emissions of CFCs by comparing observations and simulations based on a three-dimensional chemical transport model. They utilized a sparse observation network in studying net surface fluxes of trace gases and found that the inverse method was successful with the observations reproduced by the chemical transport model, and that the locations of the existing ALE/GAGE observations sites were sufficient for resolving the primary source regions for $CFCl_3$ which served as a tracer in the model because of its

well known sources and chemistry. Chang et al. (1996, 1997) used an inverse method similar to that of Hartley and Prinn (1993) to estimate CO and isoprene emissions in Atlanta. In their studies, they calculated the concentrations of these pollutants from air quality model Urban Airshed Model (UAM) driven by emissions, meteorology, and boundary and initial conditions and compared them with observations. They found that for ubiquitous biogenic emission of isoprene, the simulations of isoprene and O_3 were improved and the simulation was not significantly constrained by the UAM resolution. While for inhomogeneous spatial distribution of emission of CO, the simulation was limited by the model resolution constraints and could be improved by introducing relatively small errors in the spatial distribution of the emission inventory. Although it is a potentially powerful tool to resolve the magnitude and spatial allocation of emissions and of values in both scientific understanding and policy making, inverse modeling method is limited by the uncertainties of observations as well as the models used in the application.

Apart from the inverse modeling mentioned above, various statistical methods, for example chemical mass balance (CMB), have been also used to test inventories for gas-phase pollutants and particulate matter (PM). CMB was first used by Miller et al. (1972) and Friedlander (1973). It utilizes chemical element signatures of specific emission sources to estimate source contributions to atmospheric samples taken at receptor air monitoring sites. Glen Cass and coworkers (Cass and McRae, 1983; Schauer et al., 1996; Schauer and Cass, 2000; Zheng et al., 2002) have done a lot of work in this area. For example, Cass and McRae (1983) estimated the source contributions to airborne particulate matter using CMB and tracer models (multivariate statistical models) with

different elements as tracers of various sources. With use of data from local and Federal monitoring network in Los Angeles area during the period of 1965 to 1977, it was found that most monitoring sites were exposed to aerosol containing about 20% highway vehicle exhaust, 1-2% fuel oil fly ash, 20-50% soil dust or road dust, with sulfates and nitrates each present at about 15% of total mass. Organic compounds can also serve as tracers (Schauer et al., 1996; Schauer and Cass, 2000; Zheng et al., 2002) in this method. This method can be used for policy makers to determine the contributions of different sources. But it also has limitations: the composition of source emissions needs to be constant with time; all sources that contribute to ambient concentrations at the receptor are identified; and the sources are sufficiently different in terms of their chemical signatures so that source contributions may be easily distinguished in the receptor measurement.

Another method to test the accuracy of emission inventory is based on the comparison of the species ratios from atmospheric measurements and emission inventory. Parrish et al. (1991) did some work using ambient measurements of primary pollutants (CO, NO_y, SO_2) at rural sites to test emission inventories for the US. They used two ratios CO/NO_y and SO_2/ NO_y to distinguish mobile source from point source with mobile source having high CO/NO_y and low SO_2/ NO_y, while point source the opposite. They found that by considering the photochemical transformation on time scales consistent with transport from source to receptor, the ratio CO/NO_y was consistent with that from emission inventories. This method will be applied and discussed in Chapter 3 in which observations of VOC concentrations are used to test speciated VOC inventories.

1.3.2 Source-Receptor Modeling

Source-receptor modeling attempts to ascribe the dosage of a pollutant at a given location to a set of upwind sources. This method considers transport, chemical reactions, and removal processes, and requires a good deal of meteorological input as well as chemical data. It was used quite extensively during the US National Acid Precipitation Assessment Program (NAPAP) to determine the sources of sulfate being deposited in the Northeastern US or Canada (NAPAP, 1989; NAPAP, 1991; Chang et al., 1987; Dennis et al., 1993; McHenry and Dennis, 1994). For example, one approach taken by NAPAP to analyze source-receptor relationships was the Tagged RADM/EM (Regional Acid Deposition Model/Engineering Model) model system to quantify the attribution of each source to each receptor region. Using the Tagged RADM/EM allows the determination and interpretation of three features regarding source attribution: the influence of US emissions on Canadian deposition and vice versa; the relative contribution of nearby versus distant sources to receptor regions; and the distribution of deposition and ambient concentrations as a result of a specific source region. Taking the first feature as an example, NAPAP (1991) estimated that US sources contributed 50%-75% of the total annual sulfur deposition over substantial portion of southeastern Canada, while the contribution of Canadian sources to the northeastern states of US was about 15%. The farther the distance between the source region and the receptor region, the less influence would be of the source to the receptor. In Europe, especially Scandinavia, similar analyses have been carried out (Hass et al., 1991, 1993; Iversen, 1993; Berge and Jakobsen, 1998). The source-receptor modeling has been used for scientific research of acid deposition and policy making for abatement of SO_2 and NO_x emissions and mitigation of acid precipitation.

Source-receptor modeling considers many atmospheric processes; however, it is still limited by the incompleteness of model design. For example, Dennis et al. (1993) found that the RADM and the related ADOM (Acid Deposition and Oxidant Model) model both underestimated the sulfate deposition compared with observations, and that by modifying the scavenging module of the nonprecipitating cumulus clouds, some of the seasonal variations of the sulfate deposition could be captured, but the regional variations still need improvement.

1.3.3 Mechanistic Analysis

In mechanistic analysis, algorithms or portions of algorithms used in air quality models (and chemical transport models) are driven by observational-datasets and tested against independent measurements from these datasets to assess/evaluate the algorithms. These types of studies include tests of fast photochemical theory in which model-calculated values of OH, HO_2, NO_2:NO ratio, etc are compared to appropriate high-resolution data (Calvert, 1976; Fehsenfeld et al., 1983; Parrish et al., 1986; Chameides et al., 1990; Davis et al., 1993; Ridley et al., 1992; Crawford et al., 1996; Eisele et al., 1996; Poppe et al., 1994; McKeen et al., 1997; Stevens et al., 1997; Brune et al., 1999; Carslaw et al., 2001, 2002; Cantrell et al., 1996, 2003). For example, the relative levels of tropospheric NO_2 and NO are determined by a rapid photochemical cycling of NO_x in sunlight on a time scale much shorter than the production or the destruction of NO_x (Cadle and Johnston, 1952; Leighton, 1961), which establishes a “photostationary state”. Lots of work has been done on examining the photostationary state by comparing the ratio NO_2 to NO calculated from observation-based models based on the photostationary state theory with that inferred from direct observations (Calvert, 1976; Fehsenfeld et al.,

1983; Parrish et al., 1986; Chameides et al., 1990; Davis et al., 1993; Ridley et al., 1992; Crawford et al., 1996). For example, Chameides et al. (1990) compared observationally-driven model-calculated ratios of NO_2:NO to observations in NASA GTE/CITE 2 study. They found reasonably good agreement only when the role of peroxy radicals in the fast photochemical cycling of NO_x was included in their calculations. However, there was still an average 25% bias between the observed and model–calculated ratios, most likely caused by an error either in the measurements or in the model-calculated peroxy radical concentrations or photolysis rate constant of NO_2. This called for more accurate measurements of NO_x and photolysis rate constant of NO_2. As a result of this and similar studies at that time, significant work was undertaken to improve instrumentation for these measurements.

Another example of mechanistic analyses are so-called "aerosol closure experiments" in which PM concentrations and chemical composition data are used to calculate the extinction of sunlight in the atmosphere and then compared to atmospheric radiative measurements. For example, Xu et al. (2003) conducted measurements of aerosol radiative properties at a rural location in the Yangtze delta region of China over one-month period. Comparisons between the observation and the model-calculation of direct aerosol radiative forcing for Photosynthetically Active Radiation (PAR) at the surface showed good agreement. The amount of PAR impinging on the surface over the Yangtze delta region was reduced by ~16% as a result of the direct radiative effect of aerosols. The mean direct aerosol radiative forcing at the top of atmosphere for total solar radiation was about one order of magnitude greater than the estimated global mean aerosol radiative forcing suggested by Intergovernmental Panel on Climate Change

(IPCC) (1996). This study suggested a substantial impact of aerosols on the amount of radiation reaching the region (Bergin et al., 2001; Xu et al., 2002).

Another application of mechanistic analyses that have been undertaken is tests of the applicability of thermodynamic equilibrium between the gas- and particulate-phases in the lower atmosphere. This type of test is in fact the subject of Chapter 2 of the thesis and is therefore not discussed here.

1.3.4 Diagnostic Analysis

In diagnostic analyses, data and algorithms from air quality models are used to derive unobserved parameters and thereby gain insight into the processes controlling the abundances of the relevant species. One example of this approach is gas-phase studies in which CO, VOC, and NO_x data are used to calculate the ozone photochemical tendency (i.e, the net rate of ozone photochemical production/destruction) and thereby determine whether photochemistry is providing a net source or sink of ozone. Since the issues of photochemical production of ozone were raised in 1970s (Chameides and Walker, 1973; Cruzen, 1973), the topic of tropospheric sources and sinks of ozone has been one of intense scientific investigation and debate (Fabian, 1974; Chameides and Walker, 1974; Chatfield and Harrison, 1976; Fabian and Pruchniewicz, 1977; Fishman and Crutzen, 1977; Liu et al., 1980; Chameides and Tan, 1981; Chameides et al., 1987; Davis et al., 1996), and the aforementioned diagnostic analyses were undertaken to address this issue. For example, Chameides et al. (1987) analyzed the relations between O_3, NO, CO, and water vapor measured simultaneously over eastern and central North Pacific Ocean during GTE/CITE 1 fall flight in 1983, and estimated the net rate of ozone photochemical production in these remote regions using a photochemical model. They found that

photochemistry provided a net source of ozone to the free troposphere over the region and a net sink of ozone to the boundary layer over the same region. Their results were similar to those of Davis et al. (1996) who studied the ozone photochemistry in the western North Pacific during the fall 1991. Davis et al. (1996) found that the ozone tendency was typically negative for altitude less than 6 km, while positive for altitude from 6 to 8 km. Both studies suggested that the ozone production in the free troposphere was associated with high NO concentrations which might come from lower stratosphere or upper troposphere from lighting/aircraft emissions and/or deep convection from the continental boundary layer. This type of studies might be limited by not only measurement uncertainties, like other observation-based methods, but also the incompleteness of the models.

Another example of this approach is studies in which the concentrations of the precursors thought to lead to new particle formation along with the concentrations of nano-particles were monitored to get a better understanding of the mechanisms that lead to new particle formation. Weber et al. [1995, 1996, 1997, 1998] carried out such studies at various sites in remote troposphere, in which they measured the concentrations of $H_2SO_{4(g)}$, $H_2O_{(g)}$ and ultrafine condensation nuclei (UCN) simultaneously. Their results suggested that the nucleation mechanism varied with elevation: In colder regions with altitude higher than 4 km, the measurements agreed well with the classical binary nucleation model ($H_2SO_{4(g)} + H_2O_{(g)}$); while in warmer regions closer to the surface, a ternary mechanism ($H_2SO_{4(g)} + H_2O_{(g)} + NH_{3(g)}$) might better explain the observation data (Weber et al., 1999).

1.3.5 Analysis on Ozone Photochemistry Sensitivity

In addition to the applications mentioned above, a special class of observation-based methods has been developed to help inform policy-makers on whether (or when) a locality's ozone photochemistry is VOC- or NO_x-limited. These methods range from those relying solely on air-quality data to more complex methods relying on photochemical models as well as observations to diagnose VOC- or NO_x- limitation.

The most straightforward method analyzes chemical measurements, for example, the reactivity of hydrocarbons (Chameides et al., 1992) and the determination of O_3 production efficiency from observations of O_3 and the oxidized products of NO_x (Trainer et al., 1993, 1995; Olszyna et al., 1994; Chin et al, 1994; Ryerson et al., 1998; Kasibhatla et al., 1998; St. John et al, 1998).

Two other methods rely on photochemical indicators (Sillman, 1999) or smog production (SP) algorithms (Blanchard, 2000). Both methods seek to establish a measurement-based "indicator" for O_3 sensitivity. The "Photochemical Indicator Method" uses measured secondary species – primarily reactive nitrogen and peroxides – to derive information about O_3-NO_x-VOC sensitivity. These secondary species are generally produced simultaneously with ozone and thus provide information about the conditions under which ozone was formed. NO_x or VOC sensitivity indicators are based on results from AQMs. Initially, the indicator approach was presented as a series of rules-of-thumb that would identify whether O_3 was NO_x-sensitive or VOC-sensitive based on ambient measurements. For example, observed ratios of specific chemical species, such as O_3/NO_y, O_3/NO_z, O_3/HNO_3, and H_2O_2/HNO_3 etc, were identified to characterize the regime of precursor sensitivity (Sillman, 1995; Sillman et al., 1997; Sillman and He, 2002). If they exceeded a certain threshold or a transition value, it would be NO_x-

sensitive; otherwise, VOC-sensitive. However, the behavior of indicator ratios may differ in different locations and environmental conditions (Lu and Chang, 1998; Chock et al., 1999). As a result, threshold criteria need be examined and derived for the local conditions rather than adopting simply rules of thumb (Lu and Chang, 1998). In addition, the models from which the indicators were derived are subject to many uncertainties that affect their ability to identify NO_x-sensitive vs. VOC-sensitive conditions. Different assumptions in models may lead to very different results for predicted sensitivity to NO_x and VOC.

The SP algorithm uses ambient measurements in tandem with O_3-NO_x relationships expected from smog-chamber experiments to derive the so-called "extent of reaction" (Blanchard et al., 1999; Chang et al., 1997). The extent of reaction is related to photochemical age and serves as an indicator of the sensitivity of instantaneous ozone production to changes in VOC or NO_x concentrations. This concept suggests that NO_x-sensitive conditions are found when photochemistry has run to completion and most of the emitted NO_x has been removed, while VOC-sensitive conditions are found when the ozone production process has not yet reached completion. But extent of reaction alone is insufficient as an indicator of the sensitivity of ozone concentration to a complex upwind history of emission changes. Daily, hourly, and spatial patterns of extent of reaction are needed to be considered to interpret applications of the SP algorithm.

The "Observation-Based Model" (OBM) (Cardelino and Chameides, 1995, 2000) utilizes air-quality observations of VOC and NO_x to drive a photochemical box model that infers O_3 production sensitivity to precursors on the basis of Carter's Relative Incremental Reactivity factors (Carter and Atkinson, 1987, 1989). It is a mechanistically

relatively complete and time-dependent model that uses observed precursor and ozone concentrations as input. The OBM model calculates the total amount of O_3 photochemically produced during the daylight hours at the measurement sites, as well as the sensitivity of the O_3 photochemical production to changes in the concentrations of the precursors at these sites. Since the concentrations of a given precursor are related to its emission rate, the sensitivity calculated by the model to precursor concentrations can be used to determine the sensitivity of O_3 photochemical production to precursor emissions in the area of the measurements without a detailed or accurate knowledge of these emissions. This method will be discussed in more detail in Chapter 3.

This special class of observation-based methods, like other methods based on observations, is subject to the limitations of measurement uncertainties and/or the constraints of incomplete chemistry used. For example, OBM did not consider the HONO heterogeneous formation during nighttime, thus might underestimate the OH source and the O_3 production during the daytime.

1.4 Outline of This Thesis

In this thesis, a variety of observation-based approaches and models are used to study the air pollution (particulate matter pollution) in Atlanta and (O_3 pollution) in Hong Kong.

This thesis is organized into 4 chapters:

Chapter 2: An evaluation of the thermodynamic equilibrium assumption for fine particulate composition: Nitrate and ammonium during the 1999 Atlanta Supersite Experiment.

Chapter 3: Examination of relationship of ground-level ozone precursors in Hong Kong and Pearl River Delta.

Chapter 4: Conclusion of this study.

In Chapter 2, I will use redundant and consistent $PM_{2.5}$ measurements of high time-resolution (5 to 15 minutes) to test the validity of the thermodynamic equilibrium assumption. In this chapter, I will address the following scientific questions: (1). Is the thermodynamic equilibrium assumption valid for particulate composition based on observations at a particular location? (2). Is the model adequately accurate to describe the thermodynamic equilibrium between particulate composition and gas-phase concentrations at the interested location?

In Chapter 3, I will use averages of high time-resolution measurements at multiple locations during a 3-month measurement campaign to examine the ozone pollution in Hong Kong area. In examining the O_3 photochemistry, I will consider the HONO heterogeneous formation during the nighttime, and compare the O_3 productions with and without considering this factor to see the impact of this reaction. In this chapter, I will address the following scientific/policy-related questions: (1). Which is a more effective way (e.g. NO_x controls or VOC controls) for reducing the ozone pollution in the region interested? (2). If the ozone production is sensitive to VOC, which specific species is dominant in contribution to the ozone production? Where does the dominant species come from? (3). What is the ratio of ozone coming from regional transport, and what from local production? (4). Are present-day source emission inventories are sufficiently accurate for the gas-phase pollutants observed in the region interested?

CHAPTER 2

AN EVALUATION OF THE THERMODYNAMIC EQUILIBRIUM ASSUMPTION FOR FINE PARTICULATE COMPOSITION

2.1 Introduction

Atmospheric aerosols are solid or liquid particles suspended in the gas phase. The particles are composed of water, inorganic salts, carbonaceous materials (e.g., elemental carbon, semi-volatile organic compounds), crustal materials (e.g., silicon), and trace metals. Aerosols have adverse impacts on human health (review by Vedal, 1997) and affect air quality, visibility, and climate (Malm et al., 1994a, b; Groblicki, 1981; Wigley, 1989; Mitchell, 1995; Intergovernmental Panel on Climate Change (IPCC), 1996). The aerosols that are most effective in giving rise to these impacts generally range in diameter 0.1-1.0 microns (μm). In part because of this fact, $PM_{2.5}$ (particulate matter with aerodynamic diameters less than 2.5 μm, also called fine particles) was designated as a criteria pollutant by the US EPA in 1997.

In the continental boundary layer, inorganic salts are usually found to comprise about 25%-75% of the total $PM_{2.5}$ dry mass, and mainly consist of ammonium (NH_4^+), sulfate (SO_4^{2-}), nitrate (NO_3^-), and small amounts of sodium (Na^+) and chloride (Cl^-) (Heintzenberg, 1989; Malm et al., 1994b; Potukuchi et al., 1995). To calculate the inorganic composition of aerosols in air quality models, thermodynamic equilibrium of semi-volatile species between the particulate and the gas phases is generally assumed. Since H_2SO_4 has an extremely low vapor pressure, the amount of sulfuric acid in the gas phase under thermodynamic equilibrium is generally predicted to be negligible. Since acidic particles will absorb gas-phase ammonia ($NH_3(g)$) and nitric acid ($HNO_3(g)$) is

more volatile than sulfuric acid, thermodynamic equilibrium models generally predict negligible amounts of NH_3(g) and particulate NO_3^- as long as the $[NH_4^+]$:$[SO_4^{2-}]$ ratio in the particulate phase is less than 2. If excess NH_3(g) remains after the SO_4^{2-} has been neutralized, larger levels of particulate NO_3^- are predicted to form via formation of solid NH_4NO_3(s)

$$NH_3(g) + HNO_3(g) \Leftrightarrow NH_4NO_3(s) \qquad (2.1)$$

or, if the particles have deliquesced, dissolution of gas-phase nitric acid (HNO_3(g))

$$HNO_3(g) \Leftrightarrow H^+(aq) + NO_3^-(aq) \qquad (2.2)$$

where the subscript "aq" is used here to denote a dissolved species in the particulate phase. In addition to the concentrations of NH_3(g) and HNO_3(g), the direction of Reactions (1) and (2) depend on the ambient temperature and relative humidity, which affect the equilibrium constant and liquid water content of the particles. Thus under thermodynamic equilibrium, the amount of NH_4^+ and NO_3^- in the particulate phase is a complex function of SO_4^{2-} and other strong acids present in the particles, the relative amounts of NH_3(g) and HNO_3(g) present in the atmosphere, as well as temperature which affects the relevant equilibrium constants and relative humidity which affect the deliquescence of the particles.

The use of thermodynamic equilibrium models to predict inorganic $PM_{2.5}$ composition rests on two basic assumptions: 1) whether thermodynamic equilibrium applies, and 2) whether the models used to describe the equilibrium partitioning between the gas and the particulate phases are sufficiently accurate. The first issue has been addressed theoretically by a number of previous investigations (cf., Wexler and Seinfeld, 1991, 1992; Meng and Seinfeld, 1996; Dassios and Pandis, 1999; Capaldo et al., 2000).

For the most part these investigators estimated the time scale needed to achieve gas-particulate equilibrium and compared this time with the characteristic time scale for variations in the concentrations of volatile and particulate species (i.e., typically a few minutes). If the equilibration time was found to be short compared to the time scale for atmospheric variability, it was concluded that thermodynamic equilibrium would hold. These studies indicated that the time scale for equilibration depends upon the size of the particle. Submicron particles were generally predicted to have relatively short equilibration times and able to reach equilibrium with the gas-phase. Super-micron particles, on the other hand, were found to have relatively long equilibration times and thus more likely to exist in non-equilibrium transition states. Since $PM_{2.5}$ contains both sub- and super-micron particles, these studies suggest that thermodynamic equilibrium may or may not be a reasonable approximation for these particles depending upon the degree of accuracy needed and details of the $PM_{2.5}$ size distribution.

The validity of assumptions 1 and 2 have been evaluated empirically by comparing the observed partitioning between the two phases with that predicted by thermodynamic equilibrium models; investigators that focused on the ammonia/nitrate/sulfate system include Stelson et al. (1979), Doyle et al. (1979), Stelson and Seinfeld (1982a, b, c), Fridlind et al. (2000), Fridlind and Jacobson (2000), and Moya et al. (2001). The results of these studies are somewhat ambiguous; in some cases thermodynamic equilibrium appeared to hold, in other cases it did not, and in still others thermodynamic equilibrium was found to only hold for the smaller particles in the distribution. However, all of the aforementioned studies were based on measurements of PM composition using filter-based techniques with relatively long sampling times (i.e., 6

hours to > 1 day). During such long sampling periods, there can be significant variations in the ambient gas-phase and particulate phase composition, as well as the ambient temperature and relative humidity. Since the equilibrium partitioning between the gas- and particulate-phases of individual parcels of air can generally be quite different from the equilibrium partitioning obtained by mixing these parcels together (Perdue and Beck, 1988), the equilibrium predicted on the basis of the average conditions over a sampling periods will not necessarily reproduce the actual partitioning even though equilibrium may apply to each of the individual parcels. This fact along with the susceptibility of filter-based techniques to artifacts (Chow, 1995; Weber et al, 2001; Slanina et al, 1992, 2001) raises some question as to the accuracy of these studies.

The previous studies suggest that thermodynamic equilibrium may or may not apply to $PM_{2.5}$, depending on the degree of accuracy needed and details of the $PM_{2.5}$ size distribution. Therefore a rough estimation of characteristic time scales to achieve thermodynamic equilibrium between $PM_{2.5}$ and gas phase species is carried out following the approach of Wexler and Seinfeld (1990) and using the data collected during the Atlanta Supersite Experiment (Carrico et al., 2003). (A discussion on how equilibration times are calculated and the results of an illustrative calculation of these times is presented in Appendix A.) The estimation shows that the rough characteristic time to reach thermodynamic equilibrium between $PM_{2.5}$ and gas phase species is less than 1 min. Therefore it is expected that the $PM_{2.5}$ and gas phase species are in thermodynamic equilibrium. However it needs to be confirmed by the measurements of $PM_{2.5}$ and gas phase species.

In this work, measurements of $PM_{2.5}$ composition and $HNO_3(g)$ and $NH_3(g)$ concentrations are used to test the validity of the thermodynamic equilibrium assumption. However unlike the aforementioned previous studies, the data used in this study were gathered during 1999 Atlanta Supersite Experiment (Solomon et al, 2003). During this experiment, a suite of techniques was used to measure $PM_{2.5}$ composition on relatively short time scales; the shortest of these being 5 minutes. ($NH_3(g)$ and $HNO_3(g)$ concentrations were also measured on time scales of up to 15 minutes.) There are two unique advantages of this dataset: 1. The high time-resolution of the $PM_{2.5}$ measurements makes it possible to more rigorously test the validity of the thermodynamic equilibrium assumption; and 2. The existence of redundant (and generally consistent) measurements of $PM_{2.5}$ composition by independent techniques lends credence to the validity of the data used (see for example, Weber et al. 2003).

2.2 Experimental Data

The 1999 Atlanta Supersite Experiment was conducted from August 3 to September 1, 1999 at a site in midtown Atlanta (i.e., 4 km NW of downtown). An overview of the experimental objectives, design, and implementation, as well as a description of the instrumentation used during the experiment is provided by Solomon et al. (2003) and the papers cited therein. The data applied in this study were collected from Aug. 18 to Sept. 1, 1999. In total I made use of 384 distinct data points based on 5-minute averages of the $PM_{2.5}$ concentrations of Na^+, SO_4^{2-}, NH_4^+, NO_3^-, and Cl^-, the gas-phase concentrations of NH_3 and HNO_3, and ambient temperature (T), pressure (p) and relative humidity (RH). (To explore the sensitivity of my results to the data averaging time, I also

carried out calculations using 15 and 20 minute averaging times; my results were virtually unchanged.)

Of the total 384 data points, 272 had data for all relevant particulate and gaseous species. There were 111 data points that lacked data for NH_3(g) (because of missing data) or particulate NH_4^+ (because the ion concentration was below the detection limit); and 1 data point that lacked data for NO_3^- (because the ion concentration was below the detection limit). The sources of these data are discussed below.

2.2.1 Inorganic Ion Data

The inorganic $PM_{2.5}$ composition is based on inorganic ion concentrations of Na^+, SO_4^{2-}, NH_4^+, NO_3^-, and Cl^- measured by the Particle Into Liquid Sampler (PILS) with a 5-minute sampling period and a 7-minute duty cycle. Note, the PILS, which uses ion chromatography to detect and quantify dissolved species, is able, in principle, to detect virtually any dissolved ion in the sampled particles. I only considered concentrations of these 5 ions because these were the only ones consistently identified to be present at significant concentrations. Other data from the Atlanta Supersite Experiment confirm other ionic species (eg. formate, acetate, Ca^{2+}, Mg^{2+}, K^+) generally only contributed a few percent to the total $PM_{2.5}$ mass (e.g. Baumann et al., 2003).

The experimental methodology and a general discussion of the data gathered by PILS are provided by Weber et al. (2001, 2003). The detection limits for these ions were 0.1ug/m^3. The random error in the measurement of each ion was estimated to be ±8% (Diamond, 2002). It is relevant to note that the PILS instrument was one of four non-filter-based, semi-continuous techniques used during the Atlanta Supersite for quantifying the inorganic $PM_{2.5}$ composition (Solomon et al. 2003). For the most part the

data from these various techniques were consistent with each other (see Table 2.2.1 and Weber et al. 2003), however there are some significant inconsistencies (e.g., $[SO_4^{2-}]$ measurements from the Dasgupta method). I elected to use the data from PILS because it was the only instrument that had simultaneous measurements of $PM_{2.5}$ anions and cations and for which the time intervals of its measurements overlapped with the time intervals of measurements of $NH_3(g)$ and $HNO_3(g)$ at the Supersite – a prerequisite for being able to rigorously evaluate the thermodynamic equilibrium assumption. A brief discussion of how my results and conclusions would have been affected had I been able to use any of these alternate datasets for inorganic $PM_{2.5}$ composition is presented later in this work.

Table 2.2.1 Comparison of $[SO_4^{2-}]$ and $[NH_4^+]$ measured by PILS[(1)] with measurements made by other semi-continuous techniques used during the Atlanta Supersite Experiment. (Adopted from Weber et al. 2003)

	Ratio of Means	Ratio of Medians
A. $[SO_4^{2-}]$ Measurements		
PILS:ECN[(2)]	1.03	1.04
PILS:Dasgupta[(3)]	1.42	1.32
PILS:Hering[(4)]	1.04	1.02
B. $[NH_4^+]$ Measurements		
PILS:ECN[(2)]	1.16	1.07

(1) For PILS see Weber et al (2001, 2003) and text
(2) For ECN see Slanina et al. (2001)
(3) For Dasgupta see Simon and Dasgupta (1995)
(4) For Hering see Stolzenburg and Hering (2000)

2.2.2 Gas Phase Data

$NH_3(g)$ concentrations used here are based on the measurements of the ECN SJAC-Aerosol Sampler (Slanina et al. 2001), while the $HNO_3(g)$ concentrations are based on ARA instrument described by Edgerton et al (2000a). The ECN instrument was operated with a time resolution of 15 minutes and the ARA instrument was operated with

a time resolution of 10 minutes. The reported detection limits for $NH_3(g)$ and $HNO_3(g)$ are 0.015ppbv, and 0.05ppbv, respectively. The measurement uncertainty was estimated to be approximately ±20% for both instruments (Edgerton, private communication, 2002, Slanina, private communication, 2001).

These measured $NH_3(g)$ and $HNO_3(g)$ concentrations were parsed into 5-minute averages so as to overlap with the 5-minute-averaged $PM_{2.5}$ composition data obtained from the PILS. When the time-period of an individual $NH_3(g)$ or $HNO_3(g)$ measurement was not coincident with the 5-minute periods of the $PM_{2.5}$ measurements, appropriate weighted averages of the gas-phase measurements were used.

2.2.3 Meteorological Data

Temperature (T), air pressure (p) and relative humidity (RH) were monitored with 1-minute time resolution during the experiment by two independently operated sets of meteorological equipment. Information on the measurement techniques used and the meteorological conditions encountered during the experiment are provided by Edgerton et al (2000b) and St John et al (unpublished manuscript, 2001). In this study, 5-minute averages of T, p, and RH were adopted from a simple average of the data obtained from the two sets of instruments; the five-minute intervals were chosen to overlap with those obtained from the $PM_{2.5}$ data. In the rare cases when data was missing from either set of meteorological equipment, simple linear interpolation was used to fill in the data gaps.

2.3 Model Calculations

The model ISORROPIA of Nenes et al. (1998) is used here to calculate the equilibrium concentrations of $HNO_3(g)$ and $NH_3(g)$ on the basis of the aforementioned

observations of the $PM_{2.5}$ composition and meteorological conditions. The model has a number of distinct advantages; these include the facts that: (i) the model is relatively fast and stable; and (ii) it considers interactions between two or more salts that can lead to mutual deliquescence. Moreover the model is able to simulate two types of deliquescence case: (i) a so-called "deliquescent branch," where particles are assumed to exist as aqueous solutions at relative humidities above the nominal deliquescence points and as solids below; and (ii) an "efflorescent branch," where metastable aqueous solutions are allowed at relative humidities below the nominal deliquescence points. A potential disadvantage of ISORROPIA is its implicit assumption that inorganic ions are internally mixed within $PM_{2.5}$; this may or may not lead to inaccuracies depending upon the actual properties of the $PM_{2.5}$ samples during the Supersite experiment.

2.3.1 Standard Method

For my Standard Model calculations, the observed $PM_{2.5}$ composition was used to calculate the equilibrium concentrations of $HNO_3(g)$ and $NH_3(g)$ in a straightforward manner:

1. Each set of 5-minute averaged observations of $[Na^+]$, $[SO_4^{2-}]$, $[NH_4^+]$, $[NO_3^-]$, and $[Cl^-]$, as well as T and RH was used as input to ISORROPIA;
2. The equilibrium concentrations of $HNO_3(g)$ and $NH_3(g)$ were then calculated for each 5-minute data point using ISORROPIA. Calculations were carried out specifying both the deliquescent and efflorescent (i.e., metastable) branches. However the deliquescent-branch solutions generally yielded unrealistically large $HNO_3(g)$ concentrations and thus only the efflorescent-branch solutions are reported here. (My results in this regard are similar to those of Ansari and Pandis

(2000) who found that, under conditions similar to those encountered during the Atlanta Supersite Experiment with relatively low concentrations of [NO_3^-], the deliquescent and efflorescent branches can differ significantly and that only the efflorescent branch was capable of approximating the observations.)

3. The calculated equilibrium concentrations were then compared to the overlapping measured concentrations for HNO_3(g) and NH_3(g).

In addition to the method described above, I carried out sensitivity calculations using an alternate method: (i) instead of specifying the observed [NH_4^+] and [NO_3^-] concentrations in step 1 and calculating equilibrium concentrations of HNO_3(g) and NH_3(g) to compare to the observed gas-phase concentrations, I specified the total amount of ammonia and nitrate in the system based on the sum of the gas-phase plus particulate phase observations and then calculated the equilibrium partitioning between the phases and compared these results to the observed partitioning. As discussed later, this other approach yielded essentially the same conclusions.

2.3.2 Iterative Method

As demonstrated below, the calculated equilibrium HNO_3(g) and NH_3(g) concentrations are quite sensitive to pH. A small change, for example, in the ratio of [SO_4^{2-}] to [NH_4^+] used in the model calculations causes a large change in the resulting concentrations calculated for HNO_3(g) and NH_3(g). To explore this effect in more detail I also adopted an alternate Iterative Method that independently inferred the "Acidity" of the $PM_{2.5}$ needed to produce an equilibrium HNO_3(g) concentration and an equilibrium NH_3(g) concentration equal to their respective observed concentrations. The steps in this case were:

1. Each set of 5-minute averaged observations of $[Na^+]$, $[NH_4^+]$, $[NO_3^-]$, and $[Cl^-]$, as well as T and RH was used as input to ISORROPIA.
2. The secant method was then used to adjust the value for $[SO_4^{2-}]$ input into ISORROPIA for each 5-minute data point so that the calculated equilibrium $HNO_3(g)$ matched the observed $HNO_3(g)$ concentration for that data point to within 10%.
3. The required change in "Acidity" for thermodynamic equilibrium (i.e., the difference between the inferred $[SO_4^{2-}]$ and the observed $[SO_4^{2-}]$) was calculated.
4. Steps 1 – 3 were then repeated for $NH_3(g)$.
5. The results for $HNO_3(g)$ and $NH_3(g)$ were then compared.

It should be noted that the observed concentration of $NH_3(g)$ was not used to calculate $[SO_4^{2-}]$ in Step 2 and the observed concentration of $HNO_3(g)$ was not used in Step 4. Thus the two sets of results are numerically independent of each other. This suggests that if the two sets of results are consistent with each other, some mechanism must exist that couples $PM_{2.5}$ acidity to both $HNO_3(g)$ and $NH_3(g)$. One such mechanism is that related to the establishment of thermodynamic equilibrium.

2.4 Results and Analysis

2.4.1 General Trends in $PM_{2.5}$ Inorganic Composition

The $PM_{2.5}$ concentrations of Na^+, NH_4^+, SO_4^{2-}, and NO_3^- measured by the PILS as a function of time are shown in Figure 2.4.1; the measured Cl^- were generally too small to appear in the Figure with the scale chosen and are not illustrated. Also illustrated in Figure 2.4.1 is the apparent acidity, denoted here by "Acidity" and given by

$$\text{“Acidity”} = [SO_4^{2-}] + [NO_3^-] - [NH_4^+] - [Na^+] \qquad (2.3)$$

where [I] is the concentration of species I in the particulate phase in units of μeq/m^3 of air.

Inspection of Figure 2.4.1 reveals that the concentrations of SO_4^{2-} and NH_4^+ generally dominate over those of NO_3^- and Na^+. Moreover, $[NH_4^+]$:$[SO_4^{2-}]$ tends to hover around a value of about 1.2, and, thus for most of the dataset “Acidity” > 0. There are three notable intervals, however, when the apparent acidity fell below zero: 1. During the beginning of the sampling period (Julian Dates 230 – 232); 2. About midway through the sampling period (Julian Dates 237 – 239); and 3. Near the end of the sampling period (Julian Dates 243 – 244). The later two intervals corresponded to periods of rainfall and were characterized by unusually low $PM_{2.5}$ ratios of SO_4^{2-} mass-to-organic carbon mass; i.e., on a typical day the ratio was generally ~ 1, but during portions of these rainy periods the ratio was 0.1 – 0.2 (Weber et al., 2003).

As illustrated in Figure 2.4.2, there are significant correlations between $[SO_4^{2-}]$, $[NH_4^+]$, and “Acidity,” but no correlations between these three parameters and temperature and humidity. By comparison, $[NO_3^-]$ is uncorrelated with $[SO_4^{2-}]$, $[NH_4^+]$, and “Acidity,” but weakly correlated with RH and, to a lesser extent anticorrelated with T (see Figure 2.4.3). These results are not surprising. Given the low volatility of sulfate, we would not expect $[SO_4^{2-}]$ to be strongly affected by meteorological factors, and, in as much as sulfate is the major anion, it follows that “Acidity” would be correlated with $[SO_4^{2-}]$. Since acidic particles should tend to react with NH_3(g), it follows that $[NH_4^+]$ would also correlate with $[SO_4^{2-}]$. The correlation of $[NO_3^-]$ with RH probably reflects the greater dissolution of HNO_3(g) onto deliquescent particles as the amount of liquid water

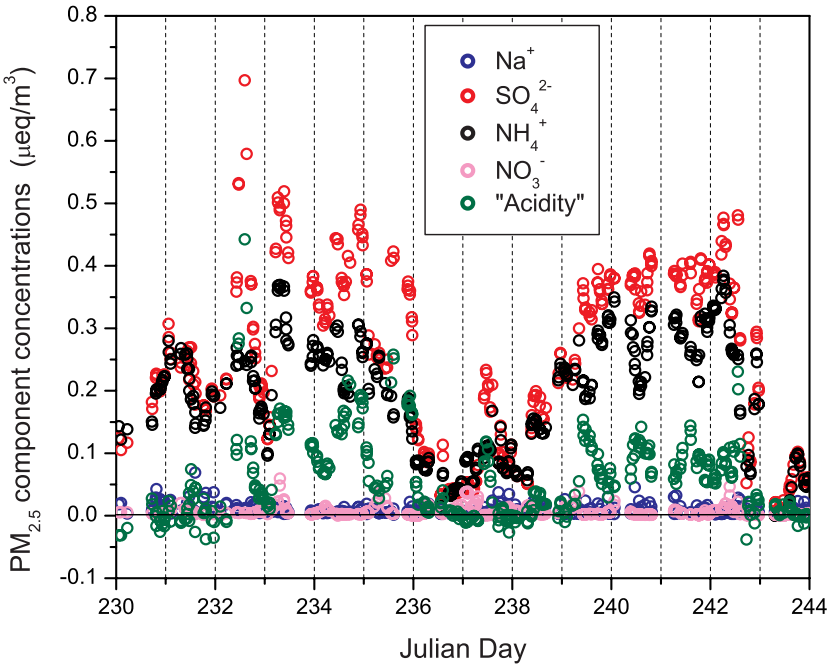

Figure 2.4.1 Concentrations of fine particle composition vs. Julian Day of the measurements from August 18, 1999 to August 31, 1999 during the Atlanta Supersite Experiment.

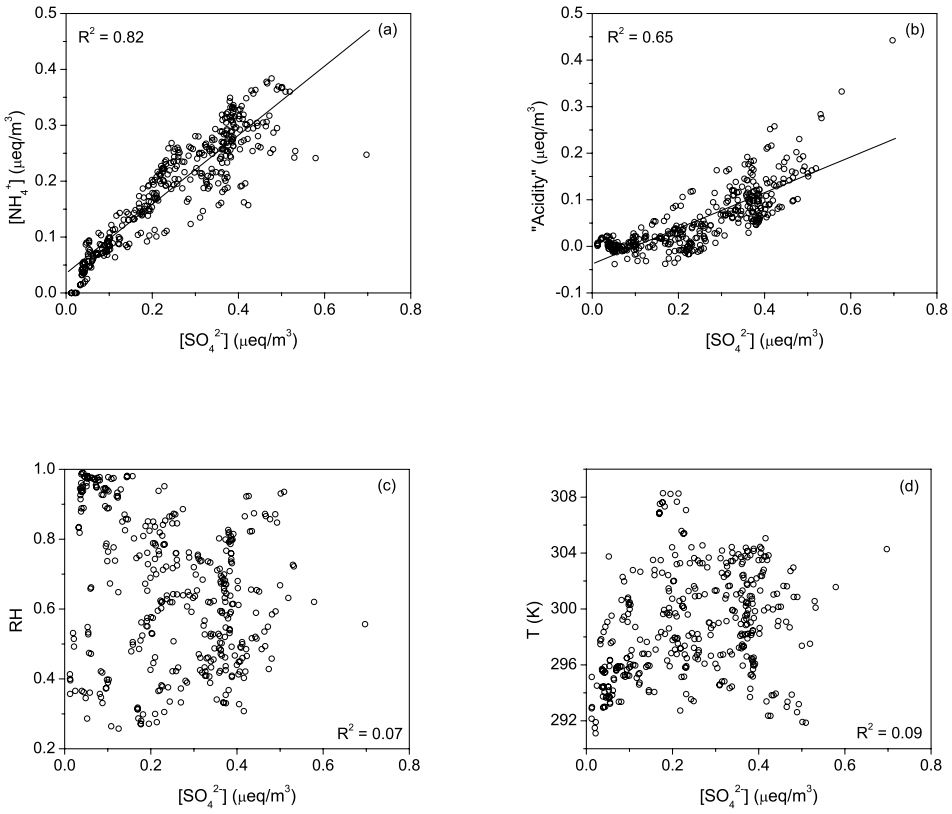

Figure 2.4.2 Scatterplots of $[SO_4^{2-}]$ vs. (a) $[NH_4^+]$, (b) "Acidity", (c) RH, and (d) T.

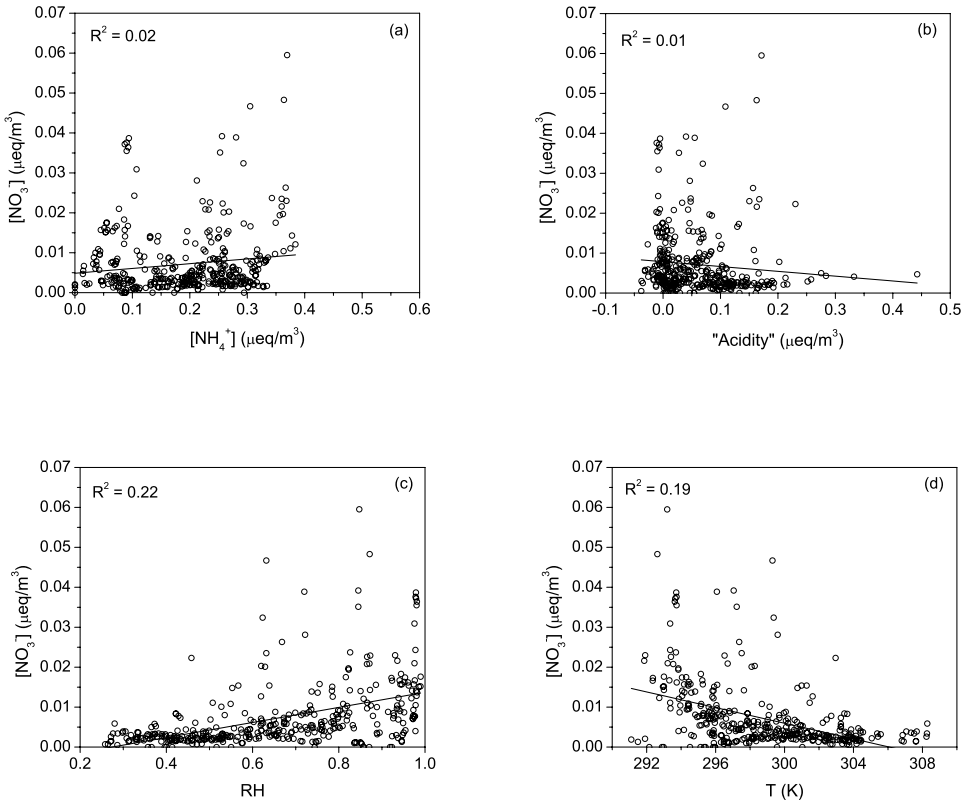

Figure 2.4.3 Scatterplots of $[NO_3^-]$ vs. (a) $[NH_4^+]$, (b) "Acidity", (c) RH, and (d) T.

on these particles increases with increasing RH. Since RH generally tends to increase with decreasing T, this would also explain the weak anticorrelation of [NO_3^-] with T.

2.4.2 Results Using Standard Method

A scatterplot comparing observed concentrations of NH_3(g) with model calculated concentrations using the Standard Method is presented in Figure 2.4.4. A similar scatterplot for HNO_3(g) is presented in Figure 2.4.5. Inspection of the figures reveals an absence of correlation between the calculated equilibrium concentrations and the observed concentrations for both species. Further note that the measured and calculated concentrations differ by orders of magnitude, and thus the discrepancy far exceeds the estimated uncertainty in the measurements. This result would appear to suggest that thermodynamic equilibrium does not apply to the data collected during the Atlanta Supersite Experiment and/or ISORROPIA is not able to accurately simulate such a state for the conditions encountered during the experiment. This is surprising since the estimation of the equilibration times shown in Appendix A suggests that the $PM_{2.5}$ and the gas phase species can reach equilibrium in less than 1 min which is much shorter than 5 min, the time period over which the $PM_{2.5}$ and the gas phase species are averaged. Therefore, a more detailed examination of the results is done below, which suggests the viability of another interpretation.

Figures 2.4.6 and 2.4.7 show the dependences of the measured and calculated concentrations of NH_3(g) and HNO_3(g), respectively, on "Acidity." Inspection of the figures reveals the presence of some interesting trends. I find that the calculated NH_3(g) is generally lower than the measured NH_3, suggesting that the observed NH_3(g) is shifted towards the gas phase relative to the calculated equilibrium concentration. On the other hand, the calculated HNO_3(g) is generally larger than the measured concentration, i.e.,

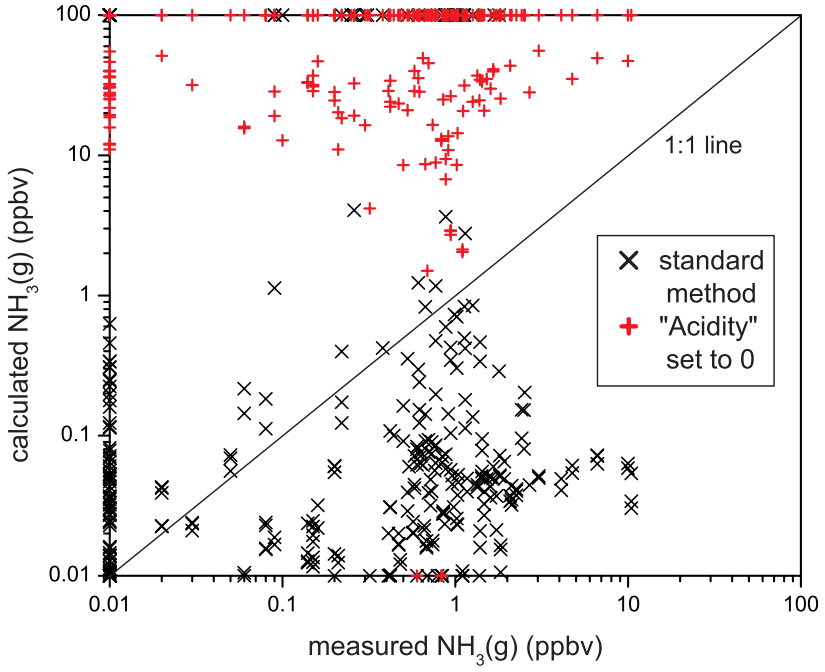

Figure 2.4.4 Scatterplot of measured and calculated equilibrium $NH_3(g)$ concentrations.

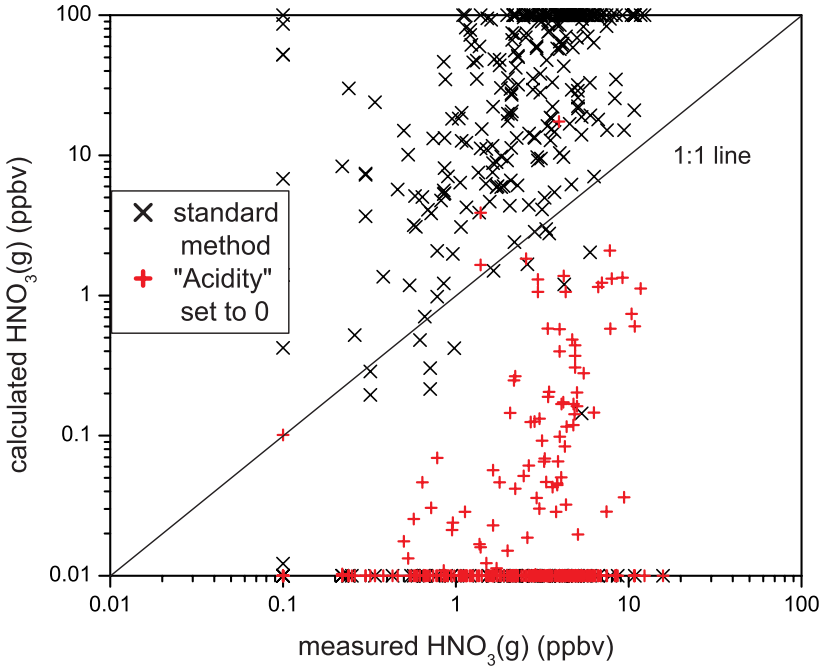

Figure 2.4.5 Scatterplot of measured and calculated equilibrium $HNO_3(g)$ concentrations.

while the observed $NH_3(g)$ appears to be shifted in favor of the gas-phase, the observed $HNO_3(g)$ appears to be shifted towards the particulate phase.

The finding of these disequilibria in both the nitrate and ammonium systems seems to be reasonably independent of the method used to do the calculations. For example, inputting the data as 15- and 20-minute averages instead of 5-minute averages, yields the same underestimate in $NH_3(g)$ and overestimate in $HNO_3(g)$. When using the alternate approach for the Standard Method described in Section 2.3.1, I overestimate $[NH_4^+]$, underestimate $NH_3(g)$, and both overestimate and underestimate the relatively small values for $[NO_3^-]$. It is also unlikely that the implicit assumption in my calculations of an internal mixture of particles is the source of the discrepancy. For example, Perdue and Beck (1988) found that when an external mixture of cloud drops in equilibrium with a collection of trace gases are collected in a bulk sample the resulting sample will be supersaturated with respect to the existing trace composition. However, in my calculations I found an apparent undersaturation with respect to NH_3.

Despite the quantitative disagreements described above, Figures 2.4.6 and 2.4.7 indicate a rough qualitative consistency between the observed and model-calculated dependence of the gas-phase concentrations on "Acidity." The measured and the calculated equilibrium $NH_3(g)$ both exhibit a trend toward an anti-correlated with the "Acidity," while a trend toward positive correlation is found in the case of $HNO_3(g)$. It is also interesting to note that the exceptions to the trend of underestimates by the model in $NH_3(g)$ and overestimates in $HNO_3(g)$ generally occur when the "Acidity" is less than zero (i.e. when the PILS measurements suggest that the $PM_{2.5}$ is basic or alkaline). One implication of this result is that the disagreement between the calculated and the

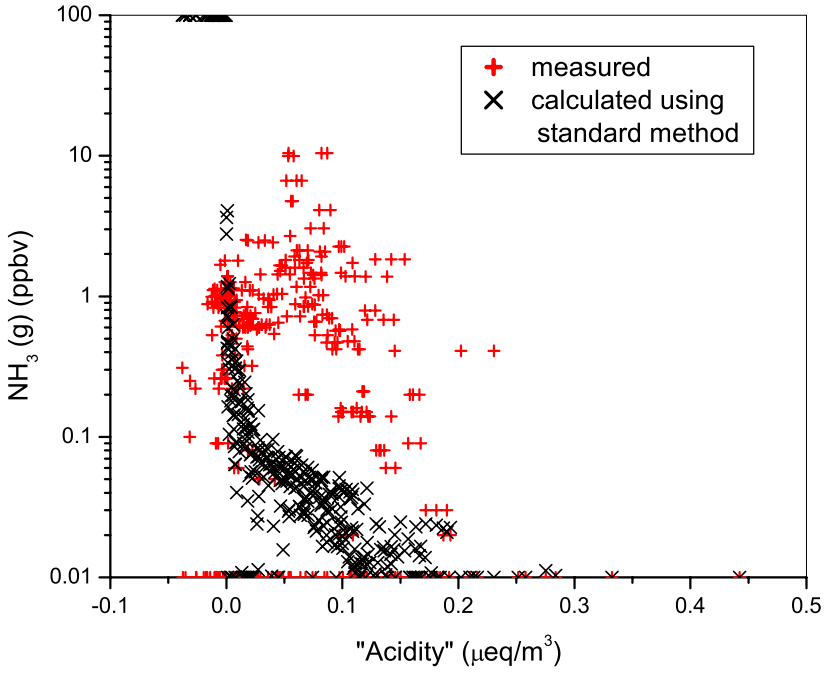

Figure 2.4.6 Dependence measured and calculated $NH_3(g)$ concentrations on "Acidity". Note: points with $NH_3(g) > 100$ppbv are made equal to 100ppbv; points with $NH_3(g) < 0.01$ppbv are made equal to 0.01ppbv.

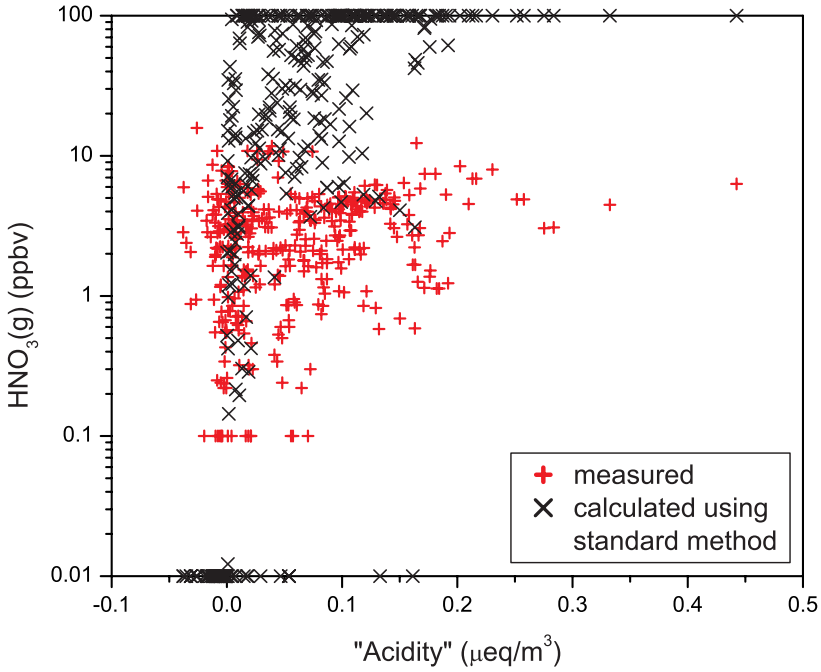

Figure 2.4.7 Dependence of measured and calculated $HNO_3(g)$ concentrations on "Acidity". Note: points with $HNO_3(g) > 100$ppbv are made equal to 100ppbv; points with $HNO_3(g) < 0.01$ppbv are made equal to 0.01ppbv.

measured concentrations is not due to an absence of thermodynamic equilibrium but to an error in the apparent acidity of $PM_{2.5}$ inferred from the inorganic ion concentration measurements of Weber et al (2001) and/or ISORROPIA. This possibility is examined below.

I first examine what happens if "Acidity" is set to zero. In principle this change could be accomplished via the addition of some cation and/or the reduction in the concentration of one or more of the observed anions. For simplicity I have carried out these calculations by appropriately adjusting the value for $[SO_4^{2-}]$ input into ISORROPIA for each 5-minute data point and keeping all other ion concentrations constant. Scatterplots between these newly calculated equilibrium $NH_3(g)$ and $HNO_3(g)$ concentrations (along with the original calculated concentrations) and the measured concentrations are illustrated in Figures 2.4.4 and 2.4.5, respectively. Note that these newly-calculated $NH_3(g)$ concentrations are generally greater than the observed concentrations (i.e., the points are shifted to the upper side of 1:1 line in Figure 2.4.4), and similarly, the newly-calculated equilibrium $HNO_3(g)$ concentrations are generally lower than the observed concentrations (i.e., the points are shifted to the lower side of 1:1 line in Figure 2.4.5).

The results described above suggest that for most data points there is some value for "Acidity" between that inferred from the measurements and zero that will yield calculated equilibrium $NH_3(g)$ and $HNO_3(g)$ concentrations that are equal to their observed concentrations. To explore this possibility and its implications in more detail I carried out model calculations using the Iterative Method as described below.

2.4.3. Results Using the Iterative Method

For the purposes of this discussion I will use the following nomenclature:

1. "Acidity"$_{obs}$ = the observed apparent acidity;
2. "Acidity"$_{HNO3}$ = the apparent acidity required to obtain agreement with the $HNO_3(g)$ observation;
3. "Acidity"$_{NH3}$ = the apparent acidity required to obtain agreement with the $NH_3(g)$ observation;
4. δ(diff) = the relative inferred "Acidity" difference

   = ("Acidity"$_{NH3}$ - "Acidity"$_{HNO3}$)/$[SO_4^{2-}]_{obs}$

where $[SO_4^{2-}]_{obs}$ is the observed sulfate concentration in unit of $\mu eq/m^3$.

Figure 2.4.8 illustrates the variation of the 3 apparent acidities as a function of their time of observation. In Figure 2.4.8a I present the results for all 272 5-minute averaged data points for which I had data for all parameters needed for my calculations. Inspection of this figure reveals that while for most of the data points there appears to be a relatively close correspondence between all apparent acidities, there are 15 data points, all occurring during Julian Date 237 and 238, when "Acidity"$_{HNO3}$ is found to be much greater than both "Acidity"$_{obs}$ and "Acidity"$_{NH3}$. For reasons that are not immediately obvious these datapoints are anomalous; for example, the sulfate corrections required to obtain agreement with the $HNO_3(g)$ observations for these 15 datapoints lie outside the 99.9% confidence intervals of the sulfate corrections required for nitrate equilibrium for the remaining 257 datapoints. It is also interesting to note that these 15 datapoints all correspond to a rainy period during the Supersite Experiment when both $[SO_4^{2-}]$ and the ratio of $PM_{2.5}$ $[SO_4^{2-}]$-to-organic C mass was unusually low (see discussion in Section 2.4.1). In the discussion that follows, the results from these 15 datapoints are excluded.

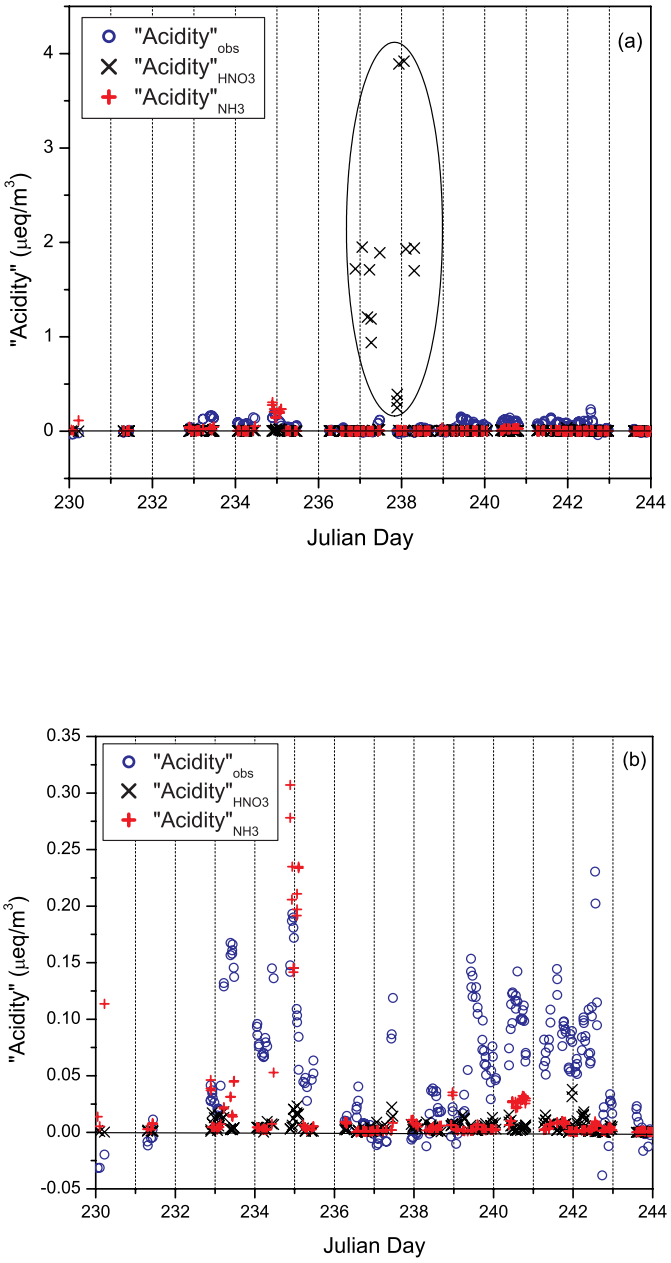

Figure 2.4.8 Measured and calculated "Acidity" as a function of Julian Day. (a) All 272 data points included. (b) Same as (a), but with the 15 data points circled in (a) excluded (see text).

Figure 2.4.8b illustrates the apparent acidities as a function of time for the remaining 257 datapoints. Inspection of this figure, with its expanded scale, reveals two trends: 1. Both "Acidity"$_{HNO3}$ and "Acidity"$_{NH3}$ generally tend to be less than "Acidity"$_{obs}$ confirming that a reduction in [SO_4^{2-}] was in fact needed to bring the calculated thermodynamic equilibrium HNO_3(g) and NH_3(g) concentrations into agreement with the observations; and 2. For most of the datapoints considered here, there is a fairly close correspondence between "Acidity"$_{HNO3}$ and "Acidity"$_{NH3}$. There are 16 datapoints that contradict this later trend. For these datapoints, which occur during Julian Dates 230, 232, and 234, "Acidity"$_{HNO3}$ is significantly less than "Acidity"$_{NH3}$. For many of these 16 datapoints, "Acidity"$_{NH3}$ is greater than "Acidity"$_{obs}$. The anomalous behavior of these 16 datapoints is even more apparent in Figure 2.4.9a where I illustrate, δ(diff), the relative difference between "Acidity"$_{HNO3}$ and "Acidity"$_{NH3}$, as a function of time for the aforementioned 257 datapoints. While the discrepancies between the two inferred apparent acidities obtained for these 16 datapoints are not nearly as large as that obtained for the 15 datapoints excluded earlier, they are nevertheless quite significant (i.e., ranging from ~20% to almost 100%). It turns out that all of these points are characterized by extremely low observed concentrations of NH_3(g) (i.e., ≤ 0.05ppbv, within a factor of 3 of the stated detection limit).

In Figure 2.4.9b δ(diff) is plotted as a function of time after excluding both the 16 datapoints with low observed NH_3(g) concentrations as well as the 15 datapoints discussed earlier (i.e., a total of 241 datapoints). Figure 2.4.10 illustrates the magnitude in the apparent acidity corrections needed for HNO_3 and NH_3 as a function of time. Note that the corrections in the apparent acidity needed to reproduce the HNO_3(g) and NH_3(g)

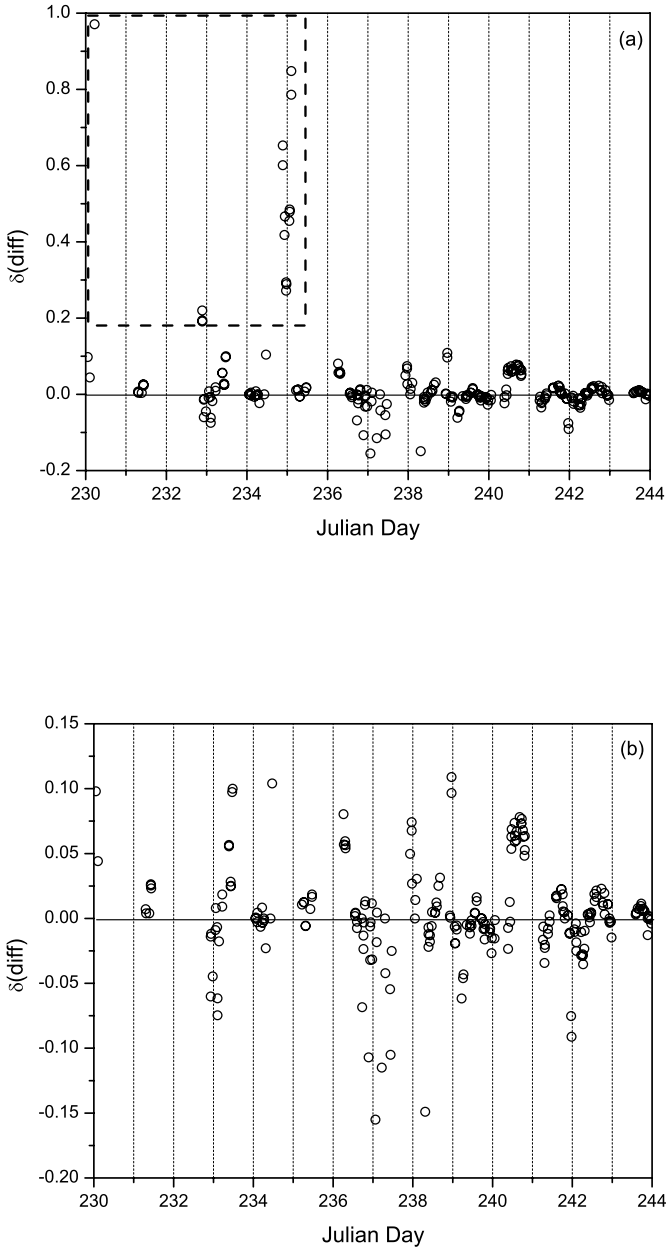

Figure 2.4.9 Relative difference in the "Acidity" corrections for NH_3(g) and HNO_3(g) as a function of Julian Day. (a) Results for all 257 data points; (b) Results excluding the 16 data points in the dashed rectangle in (a) (see text).

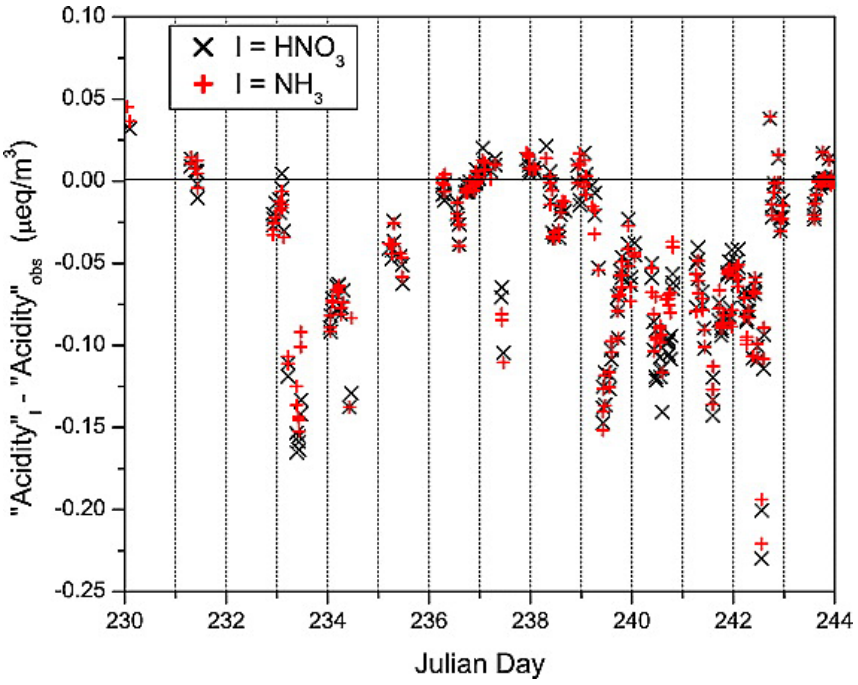

Figure 2.4.10 Absolute corrections of "Acidity" for $NH_3(g)$ and $HNO_3(g)$ for the 241 data points (i.e. excluding the 15 low $[SO_4^{2-}]$ data points and the 16 low $NH_3(g)$ data points).

observations for the 241 datapoints are relatively small and quite consistent with each other. The average apparent acidity correction needed to reproduce the $NH_3(g)$ and $HNO_3(g)$ observations are –0.046 μeq/m^3 and –0.048 μeq/m^3, or –13.7% and –14.1% of $[SO_4^{2-}]_{obs}$, respectively. The average relative difference in the two corrections is only 0.39% and the standard error of the difference ($\sigma/\sqrt{N-1}$) is 0.24%.

2.4.4. Implications of Results Using the Iterative Method

The quantitative consistency between the "Acidity"$_{NH3}$ and "Acidity"$_{HNO3}$ suggests that thermodynamic equilibrium did in fact apply during the Atlanta Supersite Experiment, which confirms the suggestion from the calculation of characteristic times to achieve equilibrium following the method of Wexler and Seinfeld (1990) and using the data collected during the Atlanta Supersite Experiment (Carrico et al., 2003) as shown in Appendix A. As noted above, the average of the two apparent acidities for the 241 datapoints agree to within 0.4%. Linear regression between the two relative "Acidity" corrections yields a correlation coefficient of 0.96, a slope of 1.04, and an intercept of –0.0002 (see Figure 2.4.11). Given the large number of data points involved in the analysis (241), the probability that this correlation is fortuitous is much less than 0.1%. Since the calculation of "Acidity"$_{NH3}$ was carried out independently of the calculation of "Acidity"$_{HNO3}$, the strong correlation between the two parameters suggests the existence of some mechanism that mutually couples the $PM_{2.5}$ acidity to both the concentration of $NH_3(g)$ and that of $HNO_3(g)$; one such mechanism is that of thermodynamic equilibrium. Thus the data collected during the Atlanta Supersite Experiment are consistent with thermodynamic equilibrium between $PM_{2.5}$ and $NH_3(g)$ and $HNO_3(g)$ on the time scale of 5 minutes.

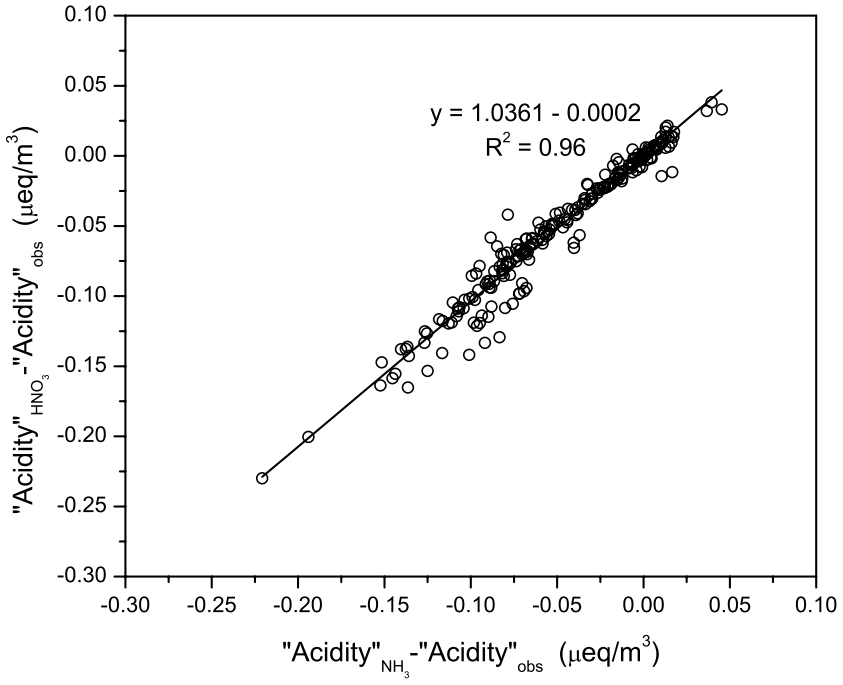

Figure 2.4.11 Scatterplot of absolute "Acidity" corrections for $HNO_3(g)$ vs. that for $NH_3(g)$ for the 241 data points.

However, if thermodynamic equilibrium did apply during the Supersite Experiment, it follows that some aspect or combination of the input data and model calculations used in my analysis to calculate the $PM_{2.5}$ "Acidity" was in error. One possible source of error is ISORROPIA; the discrepancy between the "Acidity" used in the Standard and Iterative Methods could be due to the model systematically overestimating the acidity of particulate matter encountered during the Supersite Experiment.

Another potential source of error is the PILS measurements. Recall that my calculations suggest that an average relative correction in the apparent acidity of about -14% is needed to make the $NH_3(g)$ and $HNO_3(g)$ observations consistent with thermodynamic equilibrium. On the other hand, the PILS single point measurement random error for each ion is estimated at ±8% (Diamond, 2002). A simple propagation of error analysis suggests the random error in each inferred value of "Acidity" is ~ 50%. This implies that the approximate average error in "Acidity" for the entire population of 241 data points ($\sigma/\sqrt{N-1}$) is about 3%. Thus the required average –14% adjustment in the calculated "Acidity" is significantly larger than the average uncertainty in the measurements and suggests the existence of a systematic error in the data. This systematic error could arise in two ways: 1. A failure to identify a significant alkaline component in $PM_{2.5}$ (e.g. organic base if any); and/or 2. An error in the concentrations of one or more ions identified by PILS. With regard to the second possibility it is interesting to note that on average the PILS-measured $[SO_4^{2-}]$ was in fact about 20% larger than the $[SO_4^{2-}]$ measured from chemical analysis of 24-hour integrated filter samples (Weber et al. 2003).

However, if the error did in fact arise from the PILS measurements, it is likely that similar errors would have been obtained had I been able to use data from the other semi-continuous instrumentation operating during the Supersite Experiment. Inspection of Table 2.2.1 indicates that use of the ECN or Hering [SO_4^{2-}] instead of that of the PILS would decrease the calculated "Acidity" by only a few percent – too small a correction to remove the discrepancy. Use of the ECN [NH_4^+] would further increase the calculated "Acidity" and thus worsen the discrepancy. Use of the Dasgupta [SO_4^{2-}] would overcompensate and produce a calculated "Acidity" that is too small to yield thermodynamic equilibrium.

2.5 Summary

A thermodynamic equilibrium model, ISORROPIA, was applied to 5-minute-averaged measurements of $PM_{2.5}$ inorganic composition and gas-phase concentrations of NH_3 and HNO_3 to determine the viability of the assumption of thermodynamic equilibrium. It is found that the partitioning of ammonium/ammonia and nitrate/nitric acid between the particulate and gas-phases is highly sensitive to the apparent acidity of the particulate phase. Adjustments in the apparent acidity using [SO_4^{2-}] as a free variable, suggest that the $PM_{2.5}$ acidity required to make the equilibrium NH_3(g) concentration equal to its observed concentration is essentially the same as the acidity required to make the equilibrium HNO_3(g) concentration equal to its observed concentration for ~90% of the datapoints analyzed here. Moreover, the average correction required to produce this acidity is larger than the estimated random error in the apparent acidity inferred from the measurements. These results suggest that: 1. The data collected during the Atlanta

Supersite Experiment are consistent with the assumption of thermodynamic equilibrium on the time scale of 5 minutes; and 2. ISORROPIA is, for the most part, capable of reproducing the partitioning of inorganic species between particulate and gas-phases during the experiment. For this to be the case however, one or more of the following must apply: 1. The $PM_{2.5}$ SO_4^{2-} concentration measured by the PILS has a systematic overestimate of ~15%; 2. The $PM_{2.5}$ PILS systematically underestimated the concentration of the alkaline components by ~ 15%; and/or 3. The ISORROPIA model systematically overestimated the acidity of the $PM_{2.5}$ encountered during the experiment. This work confirms the result of the calculation of characteristic time to achieve equilibrium following the method of Wexler and Seinfeld (1990), and using the data collected during the Atlanta Supersite Experiment (Carrico et al., 2003) as shown in Appendix A.

It should be noted that there were 31 data points (out of a total of 272) that either had inconsistent sulfate corrections or unrealistically large sulfate corrections. These 31 data points were characterized by either anomalously low concentrations of $[SO_4^{2-}]$ or $NH_3(g)$. The inconsistencies in these cases may have been caused by inaccuracies in the data. However I cannot preclude the possibility that physico-chemical processes not accounted for in my model calculations were at work in these instances. For example, the low $[SO_4^{2-}]$ cases occurred during rainy periods and were characterized by unusually low ratios of sulfate to organic carbon, and it is possible that the preponderance of organic carbon affected the particle-to-gas partitioning (see for example, Cruz et al., 2000). This is certainly an issue that requires further study.

Another limitation of this work is that it only considered data collected during one summer in Atlanta. For the most part, these data were collected during periods of high temperatures and relative humidities. Investigations during cooler, dryer conditions would no doubt help provide more insight into the general applicability of thermodynamic equilibrium to $PM_{2.5}$.

CHAPTER 3

GROUND-LEVEL OZONE POLLUTION IN HONG KONG

3.1 Introduction

3.1.1 Background of the Study

The Pearl River Delta and adjoining Hong Kong metropolitan area, like virtually all other major urban-industrialized regions of the world, suffers from photochemical smog and the unhealthful concentrations of ozone and fine particles that it engenders. The characteristic of smog that is readily apparent to the unaided observer is the low visibility or haziness caused by the fine particulate matter (PM) suspended within the smog. Less readily apparent but equally ubiquitous in smog is the high concentration of ground level ozone (O_3) generated from photochemical reactions between gaseous pollutants. Both particulate matter and O_3 are toxic and their presence in photochemical smog represents a health risk to a significant segment of the exposed population, especially the elderly, the young, and the infirm.

To protect the health and to continue to improve the quality of life of its citizens and visitors, officials from the Pearl River Delta region recognize that it must improve its air quality by reducing the severity of photochemical smog. However, the control of photochemical smog is complex and depends on a multitude of factors including meteorological conditions that foster smog formation (sea-breeze effects, winter monsoon circulations) and the transport and co-mingling of pollutants from distant and local sources.

This chapter summarizes the results and findings of a research study implemented to better elucidate the emissions and processes responsible for the formation and

accumulation of ground-level O_3 in Hong Kong. The research study represented Project 1 of the "*Pilot Study on the Use of Atmospheric Measurements to Manage Air Quality in Hong Kong and Pearl River Delta*." (Project 2 focused on fine particles in the Pearl River Delta) The Pilot Study, which was initiated in May 2002 and implemented over a 2-year period, built upon the work already done by the Hong Kong Environmental Protection Department (EPD), the universities in Hong Kong, and their counterparts in South China. It was specifically designed to explore and demonstrate the utility, for both extending scientific understanding and informing policy-makers, of observation-based methods: analyses, and models based upon new measurements of NO_x, VOC, O_3 (this project) and the chemical composition of the atmospheric fine particulate matter (project 2).

3.1.2 Objective of This Study

This Study was aimed at: (i) demonstrating how ground-based air quality measurements could be used in diagnostic analyses and observation-based modeling to elucidate the relative roles of emission sources of volatile organic compounds (VOC), carbon monoxide (CO), and nitrogen oxides (NO_x) in the formation of ground-level ozone (O_3) pollution in Hong Kong and the Pearl River Delta; and (ii) using these analyses and modeling to address policy-relevant issues related to the formation and mitigation of ozone pollution in the Hong Kong metropolitan area.

Four specific policy-relevant issues were to be addressed:

1. Assess the accuracy of pollutant emission inventories for Hong Kong and the PRD region;
2. Identify those specific VOC and VOC-sources that contribute most to the formation of photochemical smog;

3. Quantify the relative contributions of local production and pollutant import from other locations to the presence of photochemical smog; and
4. Assess, in a preliminary fashion, the relative benefits of various emission-control strategies (e.g. one based on VOC controls vs. one based on NO_x controls) for reducing the severity of photochemical smog.

In the sections that follow, I first provide a brief overview of the processes responsible for ground-level ozone accumulation and why observation-based approaches and models are useful for elucidating these processes in a given area or region (Section 3.2). I then summarize the field measurements that were carried out during the Study that provided the data upon which my analyses are based (Section 3.3). In Sections 3.4, 3.5, and 3.6 I present the results of various observation-based analyses that were carried out to address the issues listed above. Section 3.7 provides a summary of the project findings and recommendations for future studies. I also include Appendix B, where I discuss a newly-derived speciated VOC inventory for Hong Kong and Guangdong Province.

In reading this chapter, an important caveat should be noted: *The data that form the basis for my analyses and findings are spatially and temporally limited – they were gathered as part of a pilot study to demonstrate the feasibility and utility of the observation-based method. The general applicability of the findings to the area for all types of air pollution episodes has not been assessed.*

3.2 Ground Level O_3 Accumulation and the Use of Observation-Based Methods

Ground level O_3 is generated by a complex series of chemical reactions involving the oxidation of volatile organic compounds (VOC) in the presence of nitrogen oxides

(NO_x) and sunlight (North American Research Strategy for Tropospheric Ozone (NARSTO), 2000). For this reason, VOC and NO_x are often called O_3 precursors. Human-induced NO_x is produced in high-temperature combustion and human-induced VOC arises from the incomplete combustion of fossil fuels and the evaporation of solvents. VOC is also emitted into the atmosphere naturally by trees and other vegetation. Both VOC and NO_x are required to generate O_3, but the effect of changes in their emission on O_3 concentrations can vary considerably depending upon local conditions. For these reasons, it is necessary to find out which is more effective in a given area. One way to determine the best strategy is to apply sophisticated air quality simulation models.

As mentioned in Chapter 1, traditionally, the design of smog-control strategies has depended upon the use of Emission Based Models (EBMs). However, there are significant uncertainties in many aspects of EBMs; e.g., the emission inventories used to define the sources of O_3 precursors and the meteorological fields and parameterizations used to simulate boundary layer dynamics. Also pointed out in Chapter 1, a complementary approach to the use of EBMs is the application of Observation-Based Analyses and/or Models. These observation-based approaches use measurements of ambient concentrations of O_3 and precursors along with appropriate analytical techniques and photochemical algorithms to evaluate the accuracy of existing emissions inventories and for assessing the relative benefits of various proposed emission control strategies. Since the observation-based approaches do not use emission inventories and do not require the simulation of boundary layer dynamics, it avoids some of the uncertainties inherent in EBMs and thus provides a useful independent verification on the results obtained using EBMs. In this chapter, a variety of observation-based analyses and models

are used to evaluate emission inventories, identify the VOC species that are most critical in ozone formation, and assess the relative benefits of various proposed emission control strategies in Hong Kong.

3.3 Field Measurements

Our conclusions are primarily based on analyses of data collected over the period from October 1, 2002 to December 31, 2002 at five sites in Hong Kong: Central Western (CW), Tung Chung (TC), Tai O (TO), Tap Mun (TM), and Yuen Long (YL). Data collected during an earlier EPD study on the Pearl River Delta at two other sites, Tsing Yi (TY) and Tai Po (TP) were also used. (A detailed discussion of this study and its findings is provided by the project's final report [CH2M HILL (China) Limited, 2002; also found at the Hong Kong Environment Protection Department website http://www.epd.gov.hk/epd/english/environmentinhk/air/studyrpts/study_pearl.html]. In the discussions that follow I will refer to this study as the "earlier PRD study.") A map of Hong Kong showing the locations of each of the sites is provided in Figure 3.3.1. Discussions of the site characteristics and the measurements made at each site are provided in subsequent sections.

3.3.1 Meteorological Conditions during the Field Study as Compared to Climatology of Hong Kong

In this section I summarize the meteorological conditions encountered during the field-sampling period (October through December, 2002) and compare them to the meteorological conditions typical of the area during the fall. This discussion is based on weather summaries from the Hong Kong Observatory [http://www.hko.gov.hk] and data from the National Centers for Environmental Prediction [http://www.ncep.noaa.gov/].

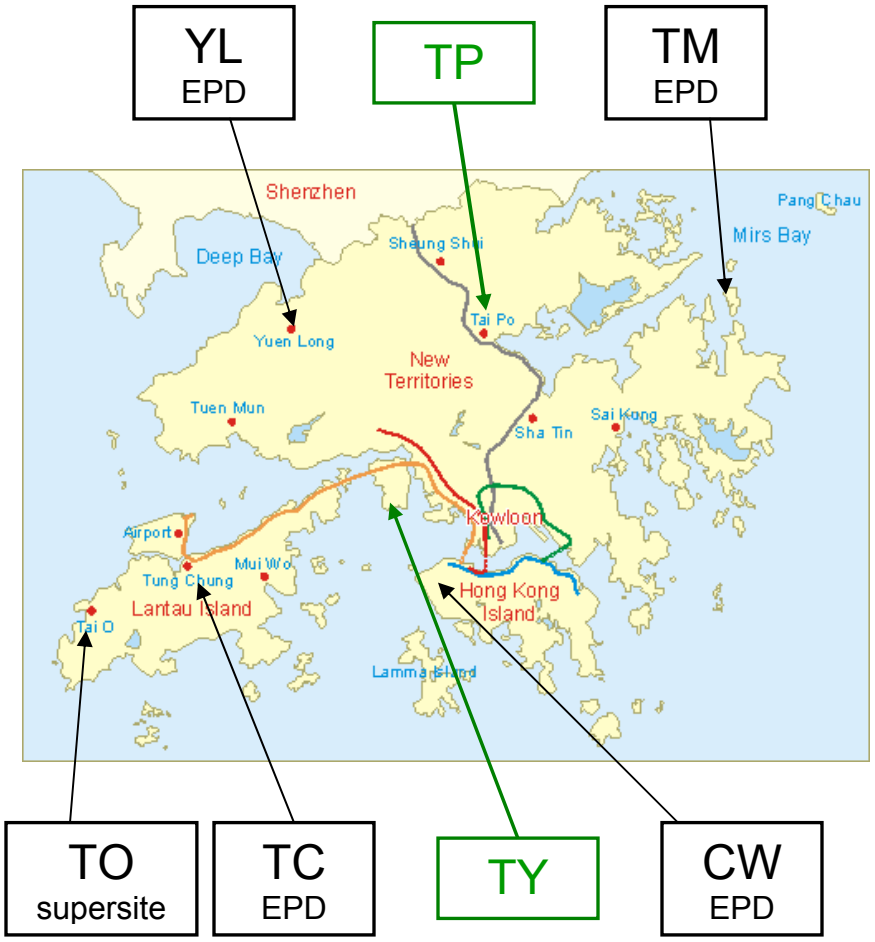

Figure 3.3.1 Map of Hong Kong area showing the location of sampling sites (TO = Tai O, TC = Tung Chung, CW = Central Western, YL = Yuen Long, TM = Tap Mun, TY = Tsing Yi, TP = Tai Po). A description of the site characteristics is presented in Section 3.3.2.

Hong Kong is situated on the South China coast and has a sub-tropical climate. The fall is characterized by moderate temperatures, light winds out of the northeast and little precipitation. These conditions favor the transport of polluted air from the Asian continent to Hong Kong, as well as the accumulation in Hong Kong of locally emitted pollutants.

3.3.1.1 October: Figures 3.3.2 and 3.3.3 compare the synoptic distributions of relative humidity and pressure for October 2002 with the 1968-1996 October average, and Table 3.3.1 lists the daily rainfall amounts for the territory during the month. While average pressure distribution in October 2002, with a depression over the South China Sea, was typical for the month, October 2002 was cloudier and wetter than usual. The relative humidity was 87% compared to the longer-term mean of 83%, and the total bright sunshine duration of 136.8 hours was 58.2 hours below normal.

There were two thunderstorms and one heavy rain, as well as several small rain patches during October 2002. It was cloudy with northeastern monsoon established gradually on the first few days of October. On 6 October a cold front crossed the South China coast. The drier air behind the cold front dispersed the clouds on 8 October and brought on a multiple-day period conducive to the accumulation of air pollution in Hong Kong. Figure 3.3.4 shows the pressure at the surface and geopotential height at 850 mb level in South China during the period from October 8 to 12, 2002. It can be seen that there was a depression behind a high-pressure system over southern China. The sunny and stagnant conditions associated with such high-pressure systems are favorable to the occurrence of photochemical smog (St. John and Chameides, 1997), and as will be shown

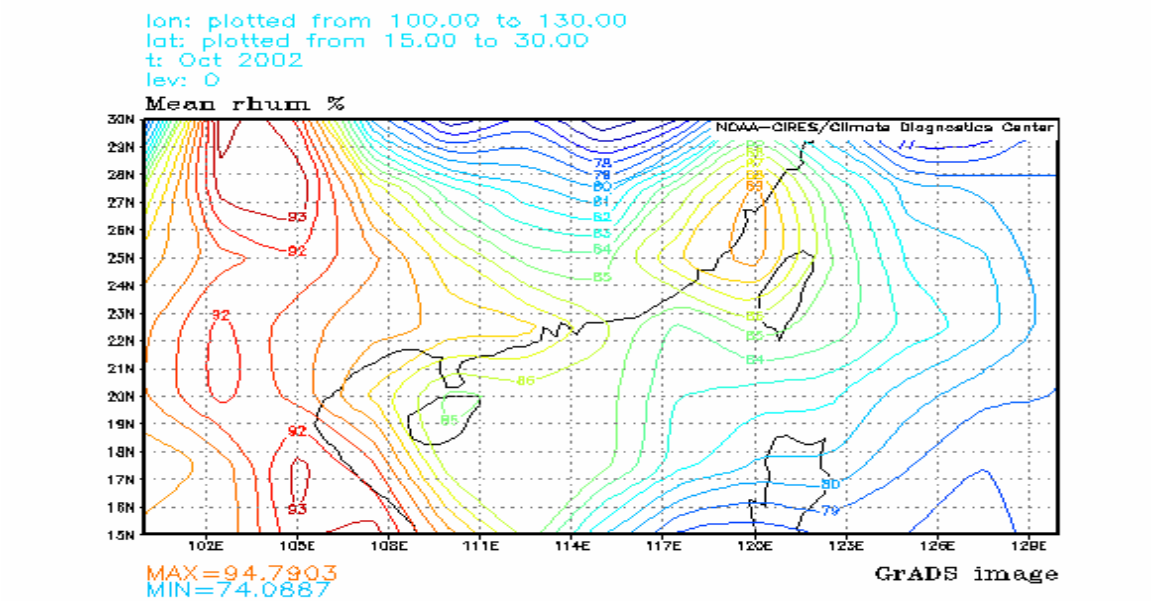

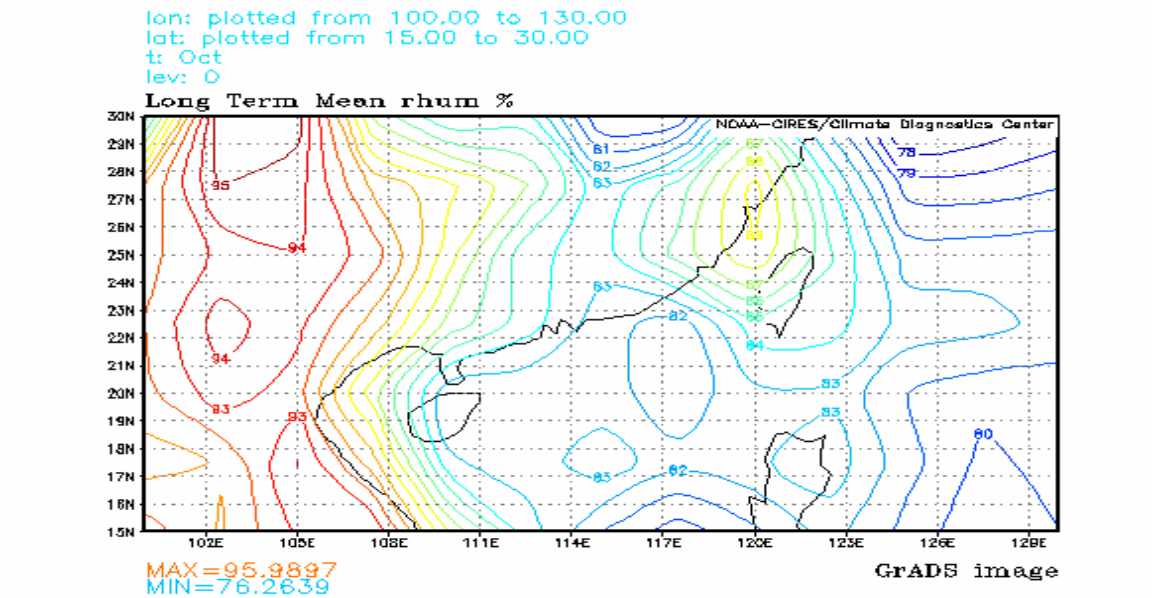

Figure 3.3.2 Distribution of monthly mean relative humidity in South China for October 2002 (upper) and for October 1968-1996 (lower).

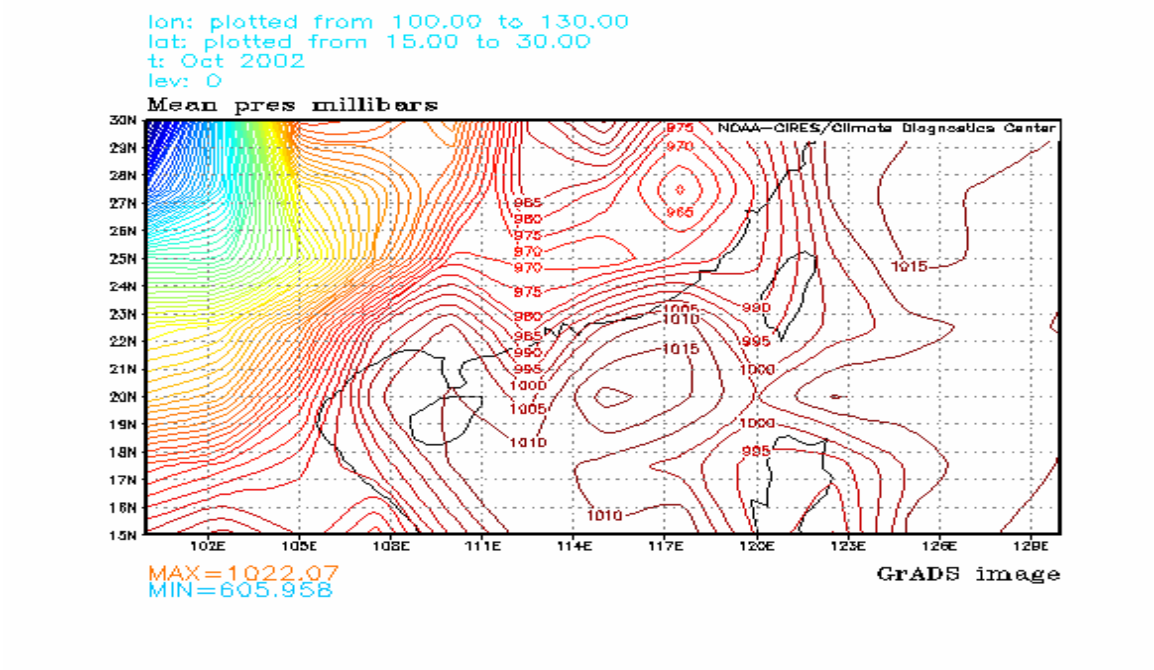

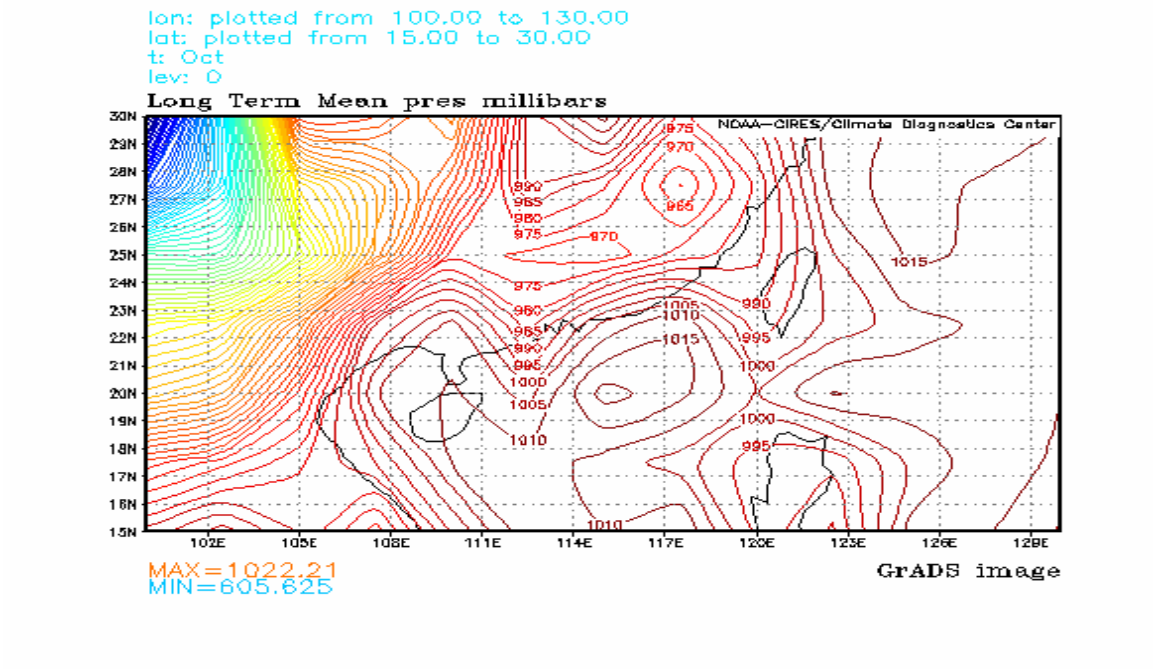

Figure 3.3.3 Distribution of monthly mean pressure in South China for October 2002 (upper) and for October 1968-1996 (lower).

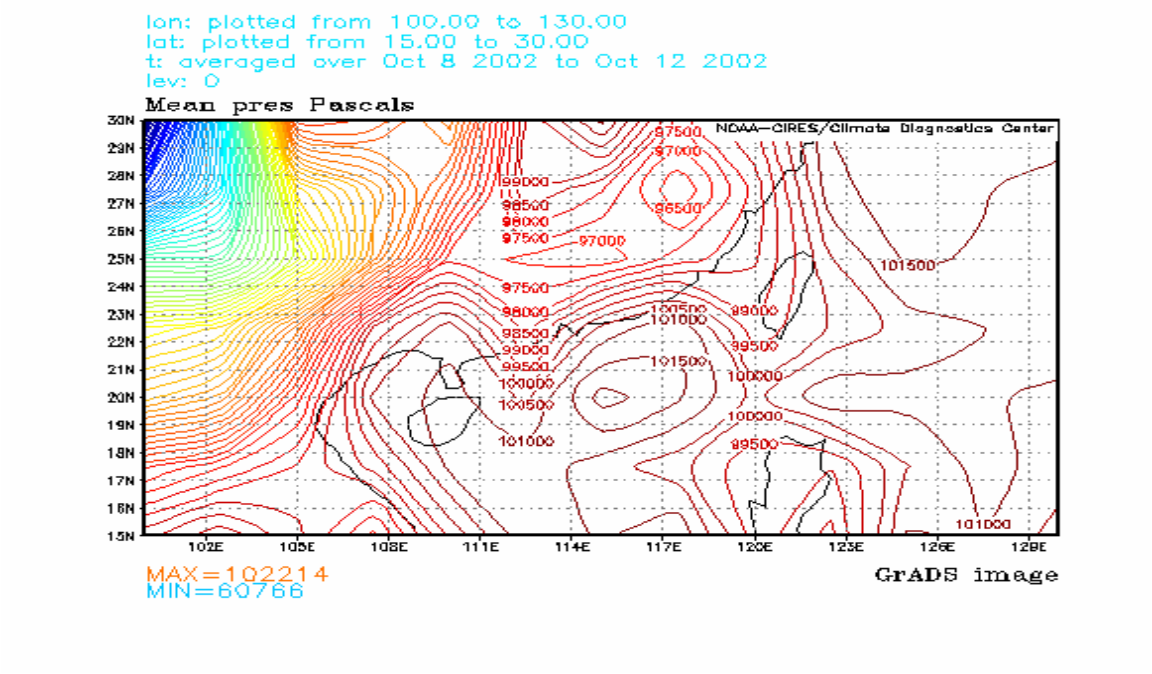

Figure 3.3.4 Pressure at surface (upper) and geopotential height at 850mb level (lower) over South China during the period of Oct. 8 to 12, 2002.

later, October 9 – 12, 2002 turned out to be O_3 episode days in Hong Kong (with the hourly-averaged peak O_3 at TO > 100 ppbv).

On 18 and 21 October two thunderstorms arrived in Hong Kong with fine weather in between. The weather improved on 25 October with long periods of sunshine for 2 days. On 25 October, the pressure system at surface and the geopotential height at 850 mb level are very similar to those for the period of Oct 8 to 12, and, as it turned out, October 25 was another O_3 episode day. It was overcast or rainy on the last days of this month with a heavy rain on 30 October.

3.3.1.2 November: Figures 3.3.5 and 3.3.6 compare the synoptic distributions of relative humidity and pressure for November 2002 with the 1968-1996 November average, and Table 3.3.1 lists the daily rainfall amounts for the territory during the month. November 2002 was drier than usual. The monthly rainfall of 23.3 mm was 34% below normal. The monthly average temperature for November 2002 was 20.5^{o}C and the long-term mean temperature for November from 1968 to 1996 was 20.2^{o}C. Similar to the previous month, there was a depression behind a high-pressure system over the South China Sea, which is favorable to the occurrence and accumulation of photochemical smog.

During the first two weeks of November the weather was fine with occasional strengthening of the northeast monsoon. Figure 3.3.7 shows the pressure at the surface and 850 mb level over the South China during the period of Nov. 5 to 8, 2002. These two panels show that a high-pressure system existed over South China area, bringing stagnant conditions and giving rise to the second multiple-day O_3 pollution episode encountered during the field measurement campaign.

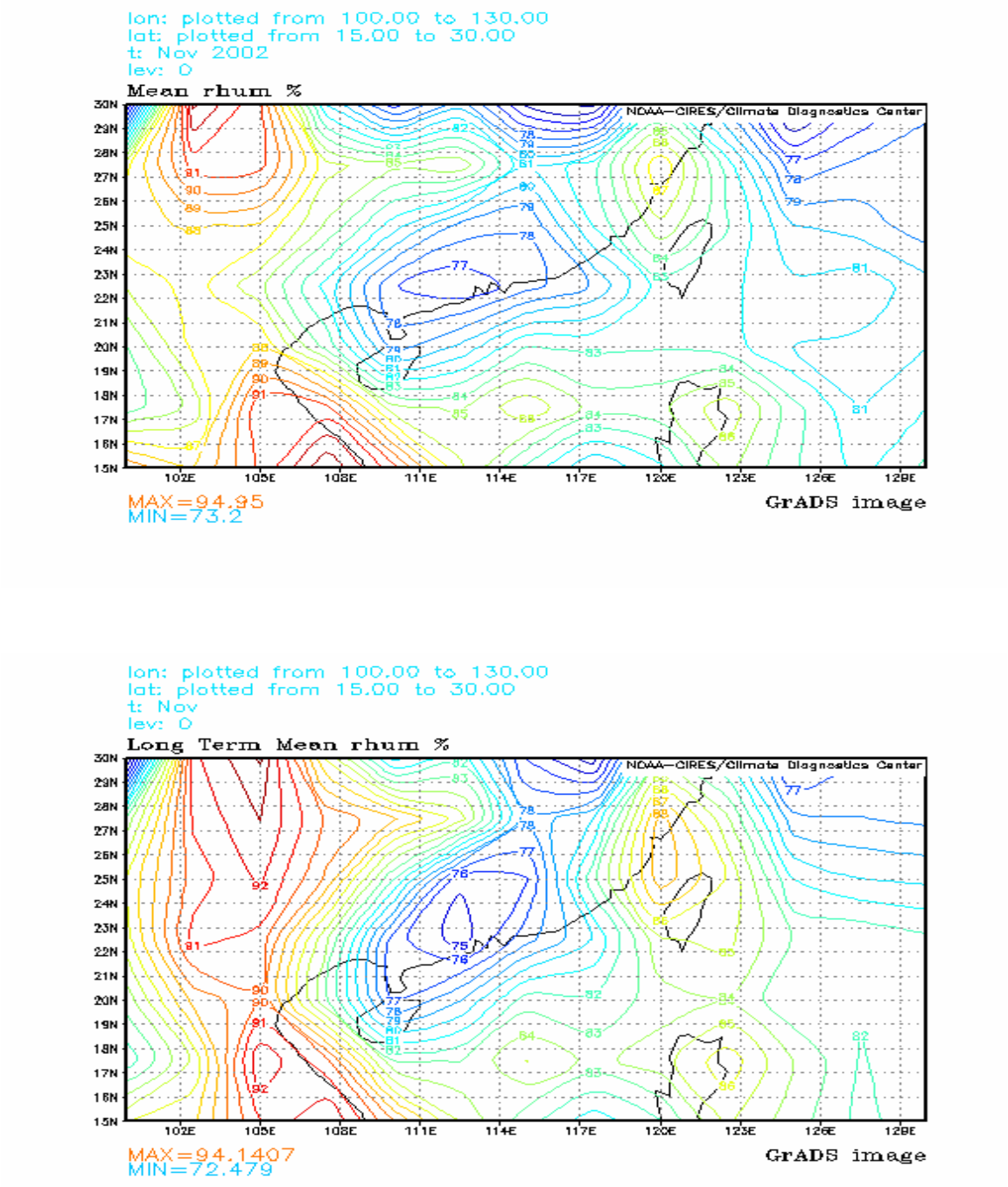

Figure 3.3.5 Distribution of monthly mean relative humidity in South China for November 2002 (upper) and for October 1968-1996 (lower).

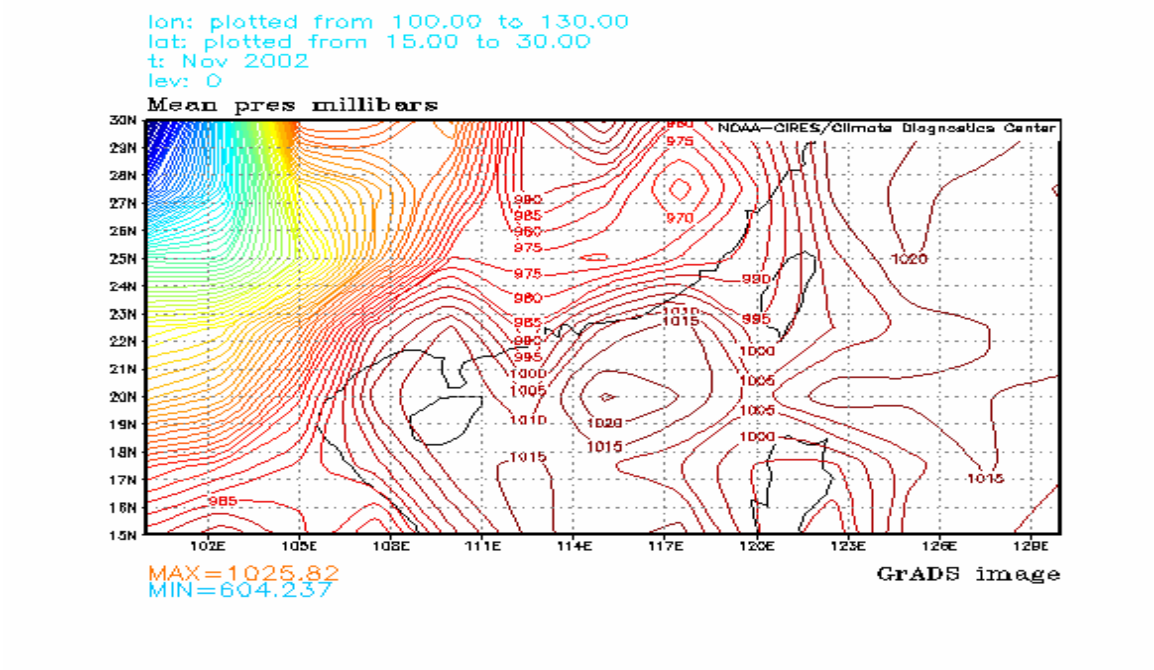

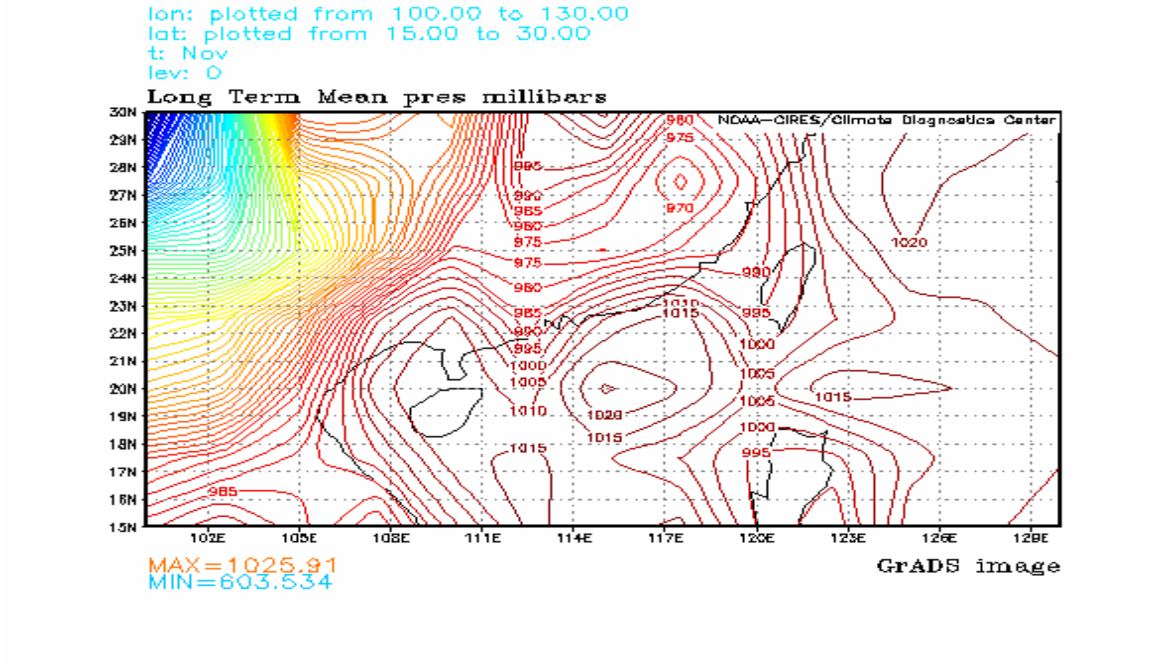

Figure 3.3.6 Distribution of monthly mean pressure in South China for November 2002 (upper) and for November 1968-1996 (lower).

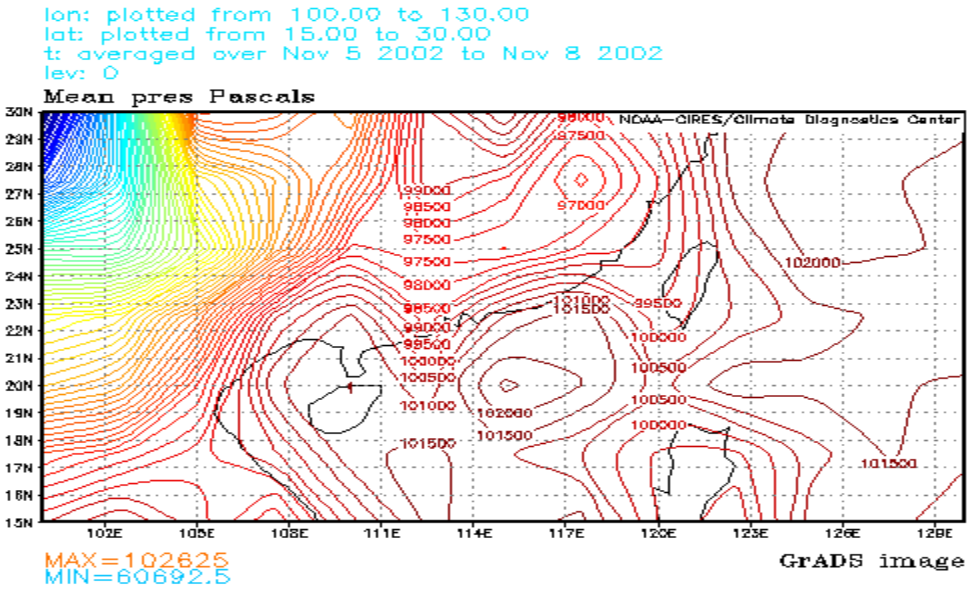

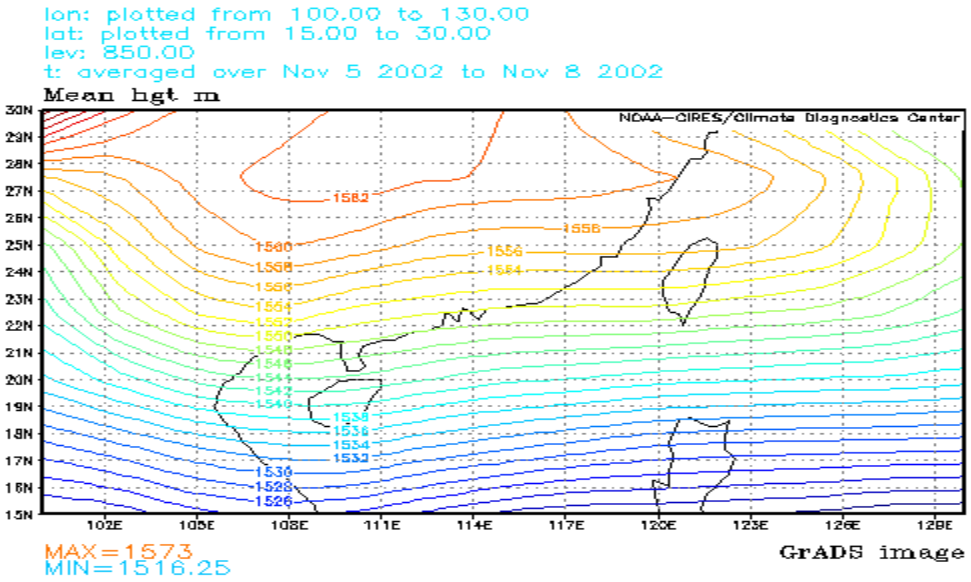

Figure 3.3.7 Pressure at surface and geopotential height at 850mb level over South China during the period of Nov. 5 to 8, 2002.

On 12 November, the pressure system at surface and the geopotential height at 850 mb level are very similar to those for the period of Nov. 5 to 8, and, as it turned out, November 12 was another O_3 episode day.

The territory was cloudy for the most time of the last two weeks of this month, with several small rain patches happened occasionally. The exception was on 20 November when the weather improved, followed by long periods of sunshine in the next 2 days.

3.3.1.3 December: Figures 3.3.8 and 3.3.9 compare the synoptic distributions of relative humidity and pressure for December 2002 with the 1968-1996 December average, and Table 3.3.1 lists the daily rainfall amounts for the territory during the month. December 2002 was cloudier and wetter than usual and there were no major O_3 episode days recorded during the month. The total bright sunshine duration of 125.8 hours was 30% below normal. The monthly rainfall was 64.1 mm, 2.3 times the normal amount. The monthly average relative humidity 84% was higher than the long-term monthly average of 76% from 1968-1996. But the monthly temperature 17.6^{o}C was still higher than the long-term monthly average of 16.8^{o}C from 1968-1996. The pressure system in this month was similar to the previous two months with a typical depression behind a high-pressure system over the South China Sea.

It was cloudy for the most time of this month with some long periods of sunshine between rainy days.

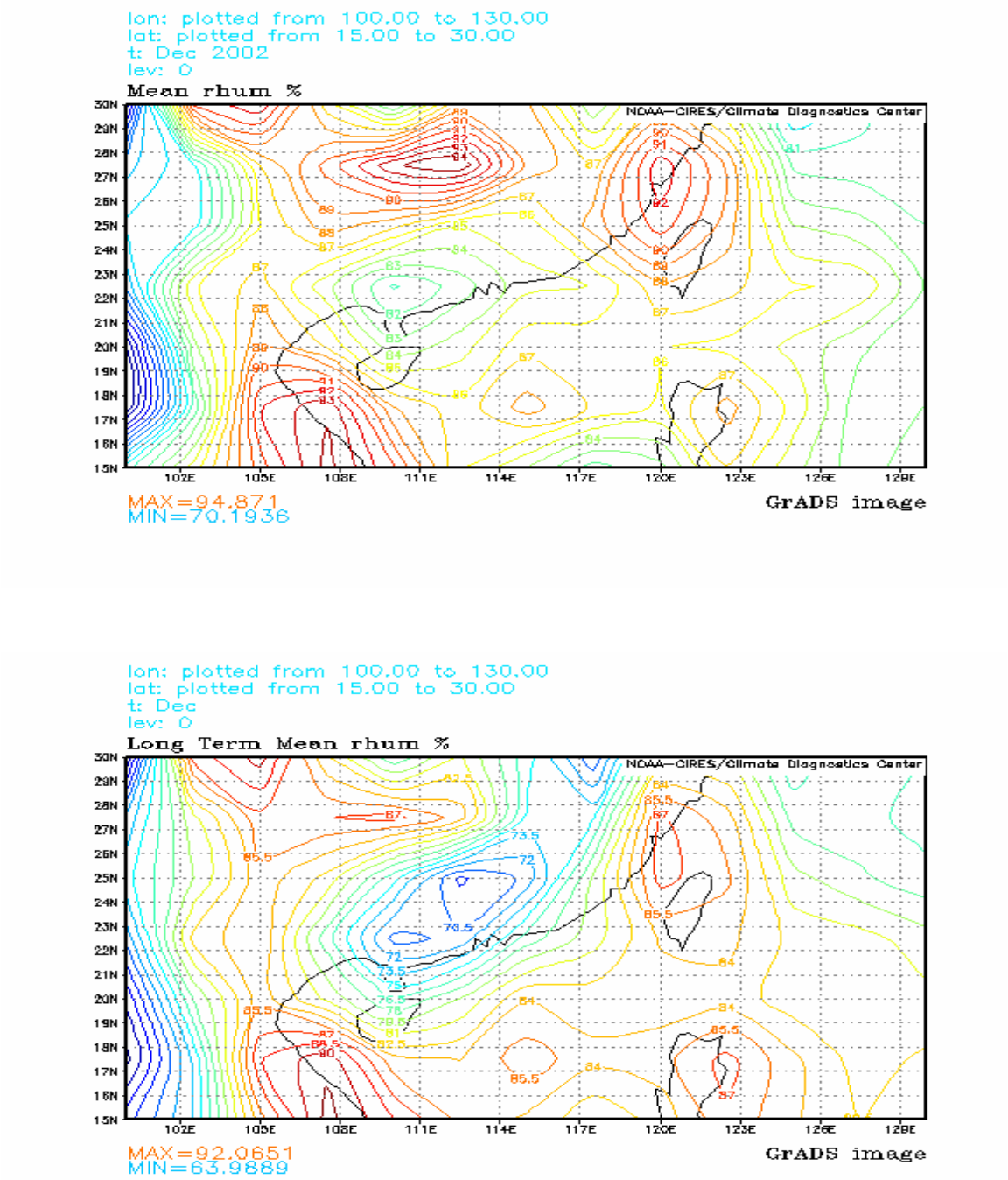

Figure 3.3.8 Distribution of monthly mean relative humidity in South China for December 2002 (upper) and for December 1968-1996 (lower).

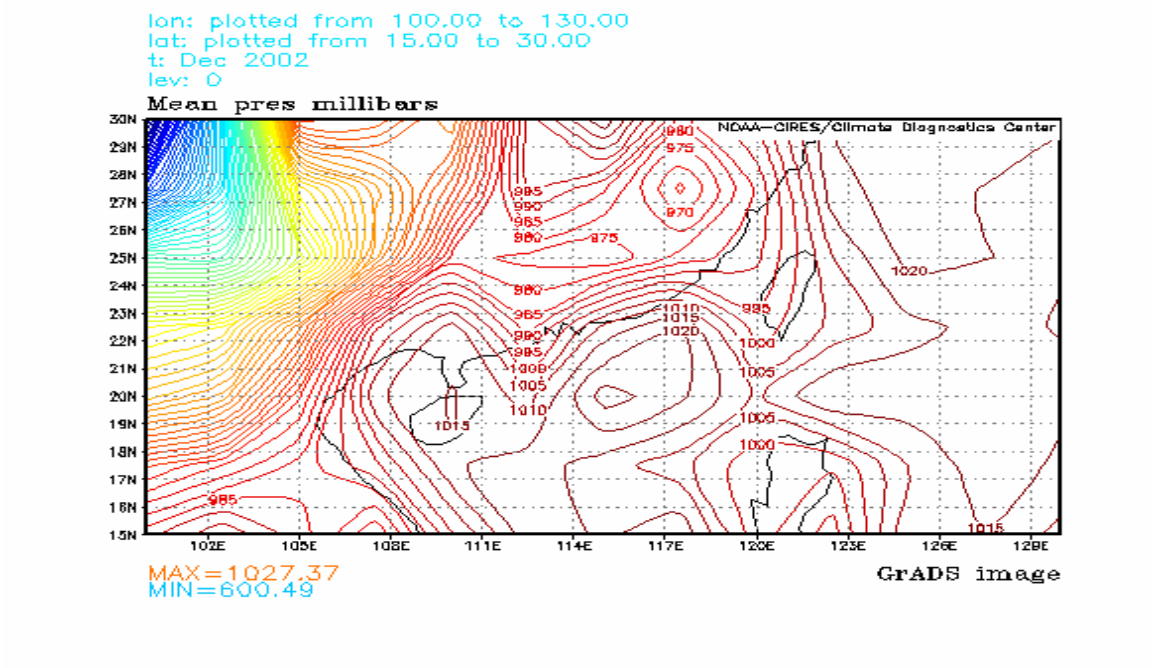

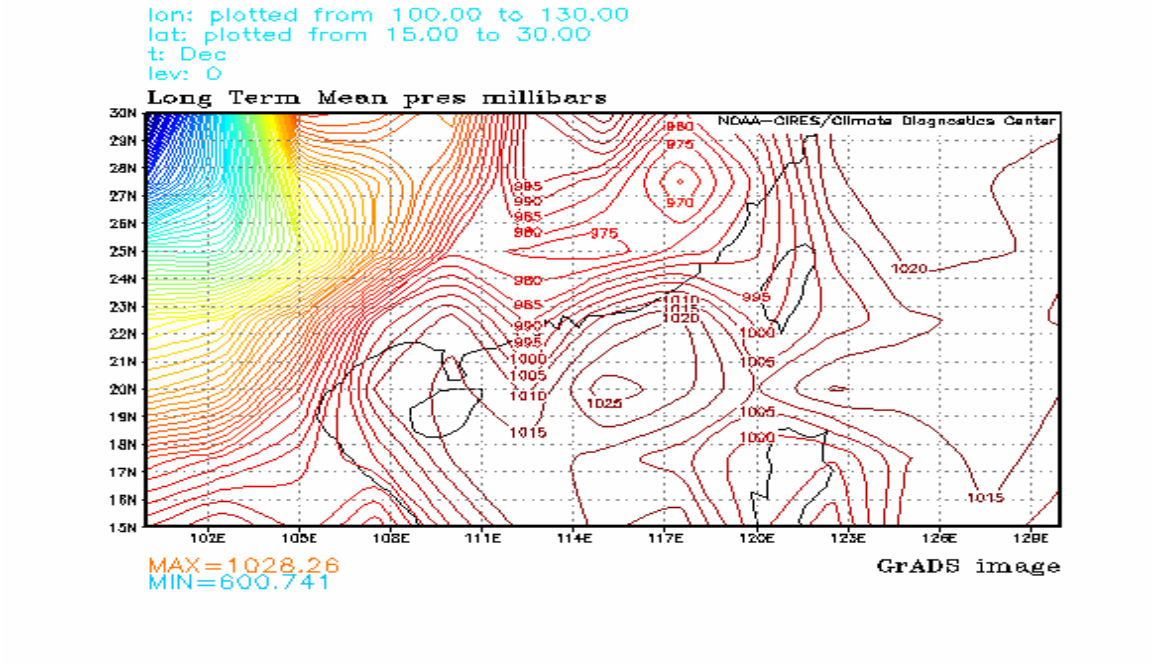

Figure 3.3.9 Distribution of monthly mean pressure in South China for December 2002 (upper) and for December 1968-1996 (lower).

Table 3.3.1 Daily total rainfall in October-December 2002 (mm).

October	1	2	3	4	5	6	7	8	9	10	
	7.6	-	-	-	-	trace	trace	-	-	-	
	11	12	13	14	15	16	17	18	19	20	
	-	-	-	-	-	-	0.1	54.9	-	-	
	21	22	23	24	25	26	27	28	29	30	31
	50.1	trace	9.2	trace	trace	0.5	0.1	1.0	4.1	66.2	5.2
November	1	2	3	4	5	6	7	8	9	10	
	-	-	-	-	-	-	-	-	-	-	
	11	12	13	14	15	16	17	18	19	20	
	-	-	-	-	trace	5.4	trace	trace	5.0	-	
	21	22	23	24	25	26	27	28	29	30	
	-	-	-	trace	-	-	trace	3.0	0.7	9.2	
December	1	2	3	4	5	6	7	8	9	10	
	2.3	0.6	-	-	0.2	trace	-	4.3	trace	-	
	11	12	13	14	15	16	17	18	19	20	
	8.0	8.0	-	-	trace	0.2	trace	trace	trace	23.0	
	21	22	23	24	25	26	27	28	29	30	31
	0.7	-	-	-	-	8.9	7.4	trace	-	-	0.5

Source: Hong Kong Observatory (http://www.hko.gov.hk).

3.3.2 Sites Description

In this section, I provide a brief overview of the characteristics of the sites where the measurements were made that form of the basis for my analysis.

3.3.2.1 Tai O (latitude 22^{o}15'11" N, longitude 113^{o}51'12" E): TO, the Supersite for the study, was operated during the field measurement campaign by Hong Kong Polytechnic University. Because the TO site was operated by the Science Team and more intensive observation was done at this Supersite, I present a more detailed description of this site than I do for the other sites (which were operated by the Hong Kong EPD).

TO is located in a sparsely populated coastal area in northwestern Lantau Island (see Figure 3.3.1). It is situated roughly in the north-south centerline of the Pearl Estuary with Hong Kong's urban center of 32 km to the east and Macau/Zhuhai to the west at

about the same distance. The measurement site is located inside an inactive Barracks, with elevation ~80 meters above the sea level. TO was selected as the location for the Supersite because: (i) available air quality data revealed that highest ozone concentrations during air pollution episodes are generally found in the western part of Hong Kong (Kok et al, 1997; Wang et al, 2001a); (ii) the area is surrounded by major urban centers in the PRD region, making it a good location to characterize emission and photochemical evolution of urban plumes; (iii) it is the westernmost land site in Hong Kong with sparse population and light emissions, thus air sampled here is not expected to be significantly contaminated by local sources of emission; and (iv) the property has a shelter, is fenced and watched by onsite security guards, and has access to electricity.

The instrumentation at TO were housed in a watch-tower situated on a cliff overlooking the bay (Figure 3.3.10). Ambient air was drawn through a sample inlet erected at 3 m above the rooftop of the premises. The other end of sample tube was connected to a PFA-made manifold with a bypass pump drawing air at a rate of 15 liters per minute. The intake of the analyzers for O_3, NO, CO, SO_2 were connected to the manifold, while the NO_y channel used a separate ¼" (outside diameter) Teflon line which was connected to an enclosure placed outside at about 1.5m above the rooftop. Filter samples for fine particle ($PM_{2.5}$) analysis were collected using a sampler independently mounted on the roof. A separate intake was also used for measurements of aerosol scattering and absorption.

The measurement instruments and their detection limits are shown in Table 3.3.2. The analyzers for NO, CO, SO_2 and NO_y were checked by zero and span gas which was generated using TEI model 111 Zero Air and an Environics model 6100 dynamic

Figure 3.3.10 Pictures showing the location and roof sampling-inlets at Tai O Supersite.

calibrator, respectively. A NIST traceable standard cylinder was used for the span test. The zero and span tests were performed on a daily basis at a fixed time each day (normally at mid-night) by the data logger. The efficiency of the NO_y catalytic converter was checked using a NIST traceable N-propy nitrate (NPN) standard (5ppm +/-5%) on a daily basis and periodically by a NO_2 standard, generated using the gas phase titration method. The O_3 analyzer was checked against a transfer standard and the zero air.

3.3.2.2 Central-Western (latitude 22°16'N, longitude 114°08'E): CW is an air monitoring site operated by Hong Kong EPD and is located in a residential area on the northern western part of the Hong Kong Island and near Hong Kong's busy "downtown" area (see Figure 3.3.1 and Figure 3.3.11).

3.3.2.3 Yuen Long (latitude 22°27'N, longitude 114°01'E): YL is an air monitoring site operated by Hong Kong EPD and is located in a new town in the northwestern part of New Territory Island in Hong Kong SAR (see Figure 3.3.11). It is about 15 km southwest to Shenzhen, a large and developing industrial city in Guangdong Province in South China. The site is situated in a residential area that is rapidly developing. There is a

Table 3.3.2 Measurement instruments used at TO and their detection limits.

Species/ Parameters	Sampling Frequency	Detection Method	Model	Detection Limit
O_3	Continuous	UV photometry	TEI 49	2 ppbv
NO	Continuous	Chemiluminescence	TEI	10 pptv
NO_y	Continuous	Mo conversion/ Chemiluminescence (with external converter module)	Modified TEI 42S with External Mo converter Analyzer	50 pptv
CO	Continuous	NDIR (with internal zero correction)	API Model 300	50 ppbv
SO_2	Continuous	Pulsed UV fluorescence	TEI Model 43 S	0.1 ppbv
Non-methane hydrocarbons	6/day on episode days	Canisters sampling GC/FID/MSD analyses	Hewlett Packard 5890 Series II Gas chromatograph with 5972 mass selective detector	5pptv
Total UV	Continuous	Eppley	Eppley total UV	Sensitivity:1. 97 W/m^2
Aerosol absorption	Continuous	Particle Soot Absorption Photometer	Radiance Research	10^{-6} m^{-1}
Aerosol scattering	Continuous	Integrating Nephelometer	Radiance Research	10^{-6} m^{-1}

Note: Wind speed and direction were measured by YOUNG model 05305V Wind Monitor-AQ and temperature & relative humidity are measured by YOUNG model 41372VC/VF Temp/RH Probe

nearby 67-hectare industrial estate (the Hong Kong Science and Technology Parks), with plants associated with petrochemicals, steel, papermaking and printing, and pharmaceuticals. These plants may utilize supplies of raw materials from Mainland China. For example, Hong Kong Petrochemical Co. Ltd. has its own jetty and storage in Tuen Mun (which is at the southwestern coast of New Territory Island), where there is also a fuel-storage facility for the Hong Kong International Airport.

Figure 3.3.11 Pictures showing the roof sampling-inlets at Central-Western (left) and the location at Yuen Long (right).

3.3.2.4 Tung Chung (latitude 22^{o}18'N, longitude 113^{o}56'E): TC is an air monitoring site operated by Hong Kong EPD and is located in North Lantau Island just to the east of TO and south of Hong Kong International airport on Chek Lap Kok (see Figure 3.3.1 and Figure 3.3.12). It is located in a relatively new town within a residential area, but adjacent to the highway and railway lines that connect the airport and to the other islands of Hong Kong SAR.

3.3.2.5 Tap Mun (latitude 22^{o}28'N, longitude 114^{o}20'): TM is an air monitoring site operated by Hong Kong EPD and is located in the police station on a remote island just

off the northeast coast of Hong Kong (see Figure 3.3.1 and Figure 3.3.12). The surrounding area is rural and sparsely populated.

Figure 3.3.12 Pictures showing the roof sampling-inlets at Tung Chung site (left) and the location of Tap Mun site (right upper) and Tap Mun Island (right lower).

3.3.3 Continuous Measurements

Table 3.3.3 lists the trace gases that were measured continuously at each of the sites. Among these species/parameters, O_3, NO, CO, and temperature are the critical inputs, together with organic compounds, to the Observation Based Model (OBM) discussed in Section 3.5 and used to assess the sensitivity of local O_3 photochemical production to decreases in the concentrations/emissions of NO_x and VOC. The data CO, SO_2 and NO_y can be used as tracers of specific types of pollution and thus can provide

valuable insights into the specific sources of pollutants that contributed to concentrations measured at the site (e.g. pollution from Hong Kong versus pollution from Guangdong).

Table 3.3.3 Trace gases monitored continuously at the five sites for this study from October to December 2002.

	O_3	SO_2	CO	NO	NO_2	NO_y
Tai O	yes	yes	yes	yes		yes
CW	yes	yes		yes	yes	
YL	yes	yes			yes	
TC	yes	yes	yes[(1)]	yes	yes	
TM	yes	yes	yes[(1)]	yes	yes	

1. CO measurements at these sites were made with instruments designed to monitor for compliance with the Hong Kong ambient air quality standard for CO (8-hr average of 8600ppbv) designed to protect human health and thus do not have the sensitivity to accurately quantify CO concentrations when these concentrations are relatively low (i.e., < 1000 pbbv).

Inspection of Table 3.3.3 reveals that of the species needed for the OBM, CO was not measured at CW and YL, and NO was not measured at YL, and CO measurements at TC and TM were made using instrumentation that lacked sensitivity to quantify CO concentrations when these concentrations are relatively low (i.e., < ppmv). (As noted in Table 3.3.3, the EPD CO instruments were designed to monitor for compliance with the Hong Kong ambient air quality standard for CO (8-hr average of 8600ppbv) designed to protect human health and thus do not have the sensitivity to accurately quantify CO concentrations when these concentrations are very low). In order to carry out the OBM analysis for these sites, these data were extrapolated from related measurements as described below. In the case of CO, it turns out that sufficiently sensitive determinations of the 24-hour averaged CO concentrations at CW, YL, TC, and TM were made along with speciated VOC concentrations by analyses of ambient air samples collected from

these sites (see Section 3.3.4 below). These 24-hour averaged CO measurements were used to set the magnitude of the CO concentrations input into the OBM with the local continuous CO measurements used to establish the diurnal variations. At CW, where local, continuous CO measurements were not available, continuous CO measurements made at a neighboring site (Central) were used to set the diurnal variation. For YL, the continuous CO measurements made at Twuen Wan (located about 10 km to the south of from YL) were used for the diurnal variation. Sensitivity calculations using constant CO concentrations at each of these sites throughout the diurnal cycle based on the grab sample analysis indicate that the results of the OBM analyses are not significantly affected by these approximations.

In the case of the NO concentrations used in the OBM for YL, these were estimated from the NO_2 and related data obtained for YL using the chemical mechanism and iterative algorithms already contained in the OBM. Here again sensitivity calculations where the NO concentrations input into the OBM for YL were allowed to vary within reasonable limits indicate that the conclusions reached here on the basis of the model calculations are not substantively affected by these approximations either.

In addition, aerosol optical properties were measured during most of the measurement period: these included monitoring of light scattering and light absorption. These measurements were used to identify if significant statistical correlations existed between ozone and particulate matter pollution.

3.3.4 Collection of Ambient Air Samples and Analysis for VOC and CO

The ambient concentrations at each of the sites of selected VOC-species, CO, and C1-C2 halons were determined on selected days through the collection of air samples in

canisters and their subsequent analysis using gas chromatography. For each sample, ambient air was pressurized by a metal bellows pump through ¼" stainless steel tubing to a 2-liter canister at a pressure of around 22psi. The canisters were then shipped to the University of California – Irvine and analyzed in the laboratory of Dr. Donald Blake. Table 3.3.4 lists the dates when the air samples were collected at each of the sites and Table 3.3.5 lists the species that were analyzed for and quantified from the air samples for each of the sites. As can be seen in Table 3.3.5, the list of species for TO is somewhat different than that of the EPD sites. However, the lists are quite similar and, as it turned out, the species that were measured at all of the sites were the most important in terms of ozone photochemistry (accounting for 95 – 96% of the total VOC reactivity at each site), and thus the inconsistencies between the lists did not substantively affect my analyses.

As noted above speciated VOC concentrations (as well as CO) as a function of time of day (e.g., hourly) is needed as input to run the OBM for a given site. However, the VOC analyses made for the 4 EPD sites were based on ambient air samples gathered over a 24-hour period and thus their use in the OBM required that estimates of hourly VOC concentrations at each site be derived. This was done through an iterative process within the OBM that demanded internal consistency between model-calculated OH and VOC concentrations while constraining the hourly CO, O_3 and NO concentrations along with 24-hour averaged VOC concentrations to their respective observed values. In the case of the VOC concentrations at TO, while individual canister samples were generally collected at several times during the day, the frequency of collection was not hourly. For this site, hourly VOC concentrations were estimated through a simple linear interpolation. Once again, it should be noted that sensitivity calculations with the OBM

Table 3.3.4 Dates when ambient air samples were gathered at the five sites and subsequently analyzed for VOC and CO.

October	1	2	3	4	5	6	7	8	**9**	**10**	
Tai O EPD sites		Y(1)						Y(1)	Y(4)	Y(1)	
	11	**12**	13	14	15	16	17	18	19	20	
Tai O EPD sites	Y(7)			Y(1)						Y(1)	
	21	22	23	24	**25**	26	27	28	29	30	31
Tai O EPD sites					Y(6)	Y(1)					
November	1	2	3	4	**5**	**6**	**7**	**8**	9	10	
Tai O EPD sites	Y(1)				Y(1)	Y(6)	Y(7) Y(1)	Y(6)			
	11	**12**	13	14	15	16	17	18	19	20	
Tai O EPD sites		Y(7)	Y(1)		Y(1)				Y(1)		
	21	22	23	24	25	26	27	28	29	30	
Tai O EPD sites					Y(1)		Y(1)	Y(1)	Y(1)	Y(1)	
December	1	2	3	4	5	6	7	8	9	10	
Tai O EPD sites	Y(1)	Y(1)		Y(1)	Y(1)	Y(1)	Y(1)		Y(1)	Y(1)	
	11	12	13	14	15	16	17	18	19	20	
Tai O EPD sites	Y(1)	Y(1)	Y(1)	Y(1)		Y(1)	Y(1)	Y(1)	Y(1)	Y(1)	
	21	22	23	24	25	26	27	28	29	30	31
Tai O EPD sites	Y(1)		Y(1)	Y(4)	Y(1)		Y(1)	Y(1)		Y(1)	Y(1) Y(1)

Note: a) 'EPD sites' denote CW, YL, TC, TM.

b) 'Y(#)' means that air samples were collected at that site on that day, and "#"represents the number of samples collected at that site on that day.

c) Air samples from TO were generally gathered in a few minutes, while the samples at the EPD sites were continuously pumped into the canister over 24 hours.

d) Dates underlined and in bold are "episode days" subjected to detailed analysis. See below.

Table 3.3.5 Species quantified from analysis of ambient air samples gathered from the different sites.

Species	Tai O	EPD sites
Methane	Y	Y
Ethane	Y	Y
Propane	Y	Y
n-butane	Y	Y
i-butane	Y	Y
n-pentane	Y	Y
i-pentane	Y	Y
n-hexane	Y	Y
2,2-dimethybutane	Y	
2,3-dimethybutane	Y	Y
2-methylpentane	Y	Y
3-methylpentane	Y	Y
n-heptane	Y	Y
n-octane	Y	Y
2,2,4-trimethylpentane	Y	Y
n-nonane	Y	
n-decane	Y	
Ethene	Y	Y
Propene	Y	Y
i-butene	Y	Y
1-butene	Y	Y
cis-2-butene	Y	Y
trans-2-butene	Y	Y
1,3-butadiene	Y	Y
Isoprene	Y	Y
Ethyne	Y	Y
Benzene	Y	Y
Toluene	Y	Y
o-xylene	Y	Y
m-xylene	Y	Y
p-xylene	Y	Y
Ethylbenzene	Y	Y
Isopropylbenzene	Y	Y
Propylbenzene	Y	Y
3-ethyltoluene	Y	Y
4-ethyltoluene	Y	Y
Methylcyclopentane	Y	
Cyclohexane	Y	
1,3,5-trimethylbenzene	Y	Y
2-ethyltoluene	Y	Y
1,2,4-trimethylbenzene	Y	Y
α-pinene	Y	
β-pinene	Y	
1-pentene		Y
2-methylhexane		Y
3-methylhexane		Y
1,2,3-trimethylbenzene		Y
CO	Y	Y

Note: a) 'EPD sites' represents CW, YL, TC, TM.

b) 'Y' means that species of HCs was measured at that site.

c) Halons are not included in this table.

(in this case using constant, 24-hour concentrations throughout the day) indicated that the approximations involved in estimating the diurnal variation in the VOC concentrations did not substantively affect my results.

3.4 Data and Diagnostic Analyses

3.4.1 O_3 Pollution Episodes

Figure 3.4.1 illustrates the time series of measurements made at TO during the field measurement period. For the purposes of the analyses discussed here, I define an O_3 episode day as a day when the peak one-hour averaged O_3 concentration at TO (the site where O_3 was generally the highest) exceeded 100 ppbv. (There were not any days during the measurement campaign when O_3 exceeded 100 ppbv at one of the other four sites but did not exceed 100 ppbv at TO, so this definition is inclusive.) Inspection of Figure 3.4.1 reveals that during the campaign, 9 O_3 episode days were encountered. Of these 9, 4 occurred during a multiple-day episode spanning Oct. 9-Oct.12 (O_3 maximum = 149ppbv), 3 occurred during a multiple-day episode spanning Nov.5-Nov.7 (O_3 maximum = 203ppbv). The Nov. 7^{th} episode day was especially interesting as the peak O_3 on that day of 203ppbv is the highest O_3 concentration ever reported for the HK/PRD region to date. The two other individual O_3 episode days occurred on Oct. 25 and Nov. 12.

Further inspection of Figure 3.4.1 reveals that the O_3 episode days occurred when the total UV was high, the wind speed was low, and the wind direction was generally from north /eastern north /western north. (A more detailed discussion of the synoptic conditions on the O_3 episode days is provided in Section 3.2.) On some of the episode days the SO_2 or NO_y was high, but not on others. CO was generally high on episode days,

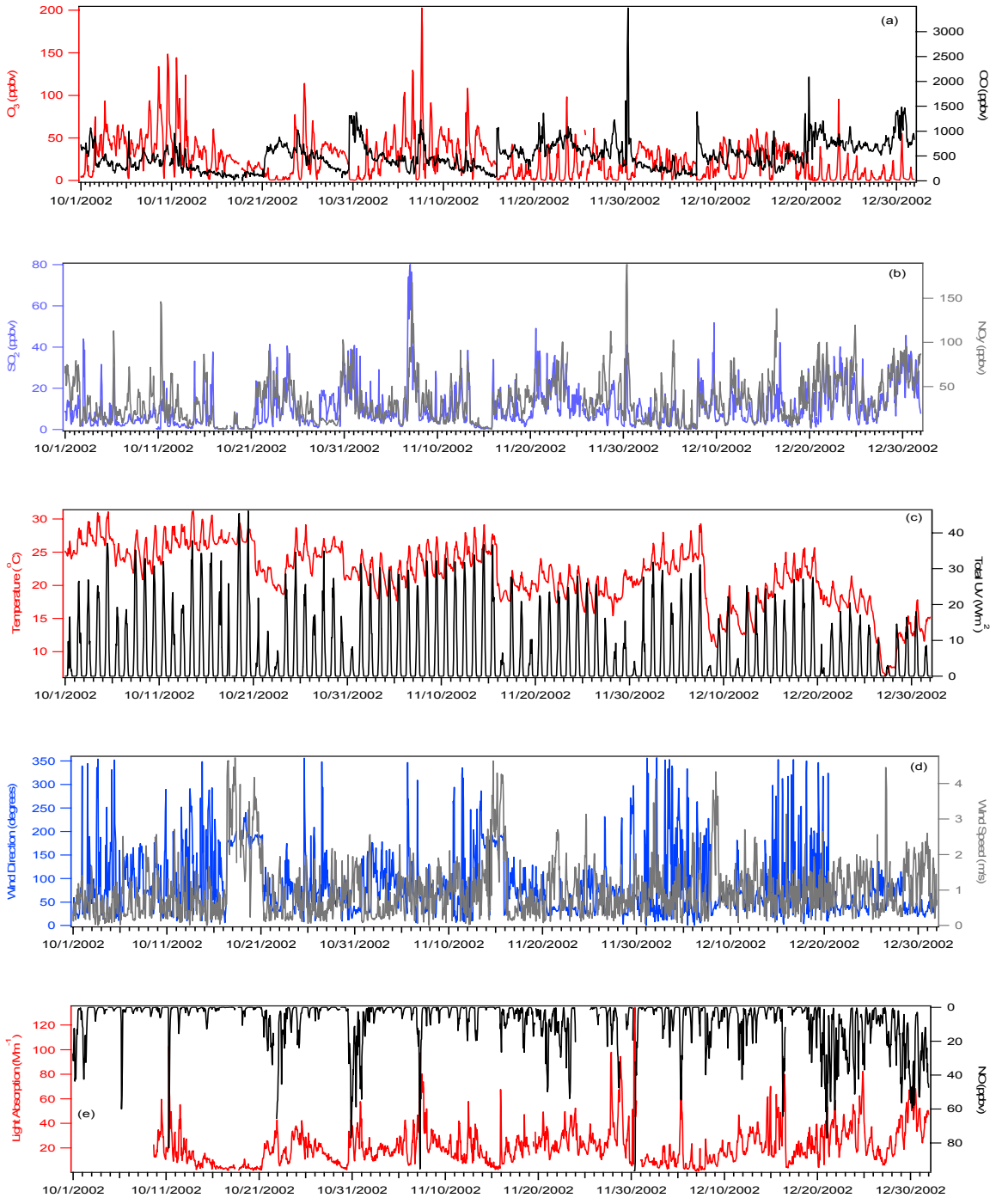

Figure 3.4.1 Time series of measured O_3, CO, NO, NO_y, SO_2, temperature, total UV, wind direction and speed, and light absorption during the period of Oct. 1 to Dec. 31, 2002.

especially on Oct 9-Oct 11, Oct 25, Nov 5-Nov 7. Aerosol absorption was high on Oct 10-Oct 11, and Nov 7. On Nov. 7, when O_3 reached its record high of 203 ppbv, SO_2, NO_y, CO, TUV and light absorption were all relatively high. By contrast, note that on Nov. 30, CO, SO_2, NO_y, and aerosol absorption were all high and the wind direction was favorable for the import of O_3 precursors into the Hong Kong area, and yet, probably because of low temperatures and overcast conditions (i.e., low total UV), an O_3 episode did not occur.

In the analyses presented here, I will focus on the aforementioned 9 O_3 episode days as well as an additional near-O_3 episode day (Nov. 8) when O_3 peaked at 91 ppbv to see if there are any striking differences in this day as compared to the actual episode days. Each of these days, along with the peak 1-hour O_3 observed at TO on that day and other relevant characteristics are listed in Table 3.4.1. Inspection of the Table reveals that on all days but Oct. 12, VOC data were obtained at TO. However, Nov. 7 was the only

Table 3.4.1 Days during the field campaign that are subjected to my analyses.

Date[1]	Daily maximum 1-hr O_3 (ppbv) at TO	Categorization[2]	Comment
9 October	134	L	VOC at TO
10 October	149	L, r	VOC at TO
11 October	144	L, r	VOC at TO
12 October	124	L, r	No VOC data
25 October	114	L	VOC at TO
5 November	104	L	VOC at TO
6 November	129	L	VOC at TO
7 November	203	R	VOC @ all sites
8 November	91	L, r	VOC at TO
12 November	108	L	VOC at TO

(1) All days except Nov 8 are O_3 pollution episode days when the 1-hour averaged O_3 at TO exceeded 100 ppbv.
(2) L = local episode
L, r = Local episode with some impact from mainland
R = Regional episode with significant impact from mainland

day when VOC data was obtained at the EPD-operated sites as well as at TO. For this reason, and because the O_3 recorded on this day was the highest on record for the area, the data gathered on this day are subjected to the most comprehensive analysis.

3.4.1.1 Summary: The 3-month measurement campaign provided several O_3 pollution episode days – some part of multi-day episodes and some not – that can form the basis for analyses to address the questions and objectives identified for the project.

3.4.2 Diurnal Variation of O_3 and Related Species at TO

Figure 3.4.2 shows the diurnal O_3 variation on the episode days at Tai O. As is typical of urban areas, O_3 is low at night and in the morning (presumably due to NO titration and dry deposition), and peaks during the afternoon (as a result of downward mixing of ozone from above the boundary layer and photochemical production). There are some notable features of the O_3 variation at TO. In the first place, O_3 does not begin to increase until relatively late in the morning, and secondly, O_3 appears to peak relatively early and begin to decline relatively early in the afternoon. There are two likely reasons for this behavior: (i) high concentrations of NO (see later discussion); and (ii) a short period of intense sunlight (the episodes are occurring well after the fall equinox).

Figure 3.4.3 illustrates the diurnal variation in other primary and secondary pollutants at TO on the O_3 episode days. There are two aspects of Figure 3.4.3 that bear noting. The first is the generally large concentrations of NO that were encountered; daytime NO concentrations of several ppbv were the norm. Similarly high NO concentrations were also encountered at the other sites. As later discussion and analyses will show, these high NO concentrations directly lead to two important conclusions: (1) HONO concentrations in the early morning hours may be quite high and may

significantly enhance O_3 production; and (2) O_3 photochemical production in the area during the episode days considered was strongly VOC-limited.

The second feature of note is the anomalously high early morning concentrations of NO, VOC, CO, and aerosol absorption in Oct. 11 and Nov. 7. These high concentrations suggest that TO was subject to an unusually large amount of pollution during the early morning on these two days. There are two possible explanations: the presence of transient local emissions and/or unusual nighttime transport patterns that brought urban emissions to TO in the early morning hours of those two days. As discussed later, an analysis of the speciated VOC data suggests the later explanation. It is also interesting to note that the high VOC concentrations on the mornings of these two days were dominated by xylenes. The source of these xylenes is discussed in Section 3.4.8.2.

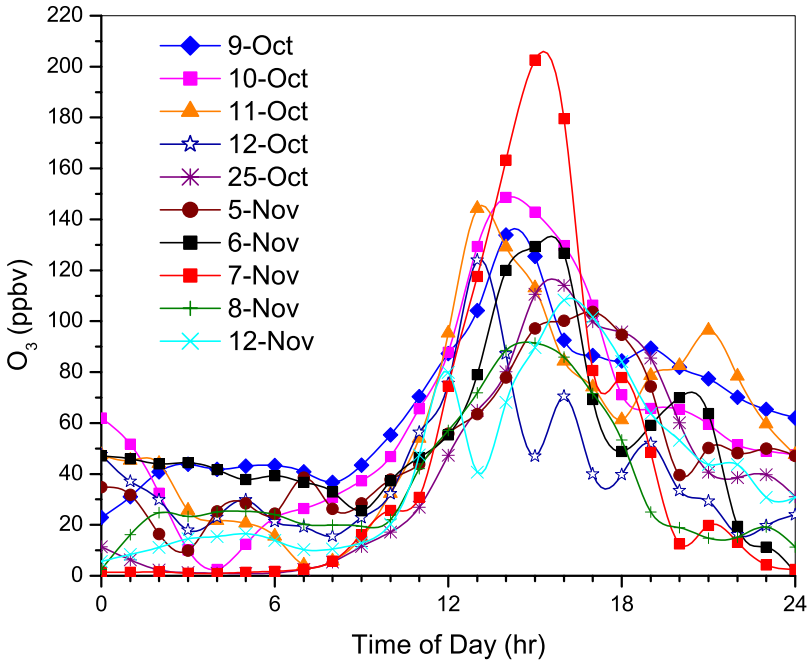

Figure 3.4.2 Diurnal variation of O_3 observed at TO during episode days.

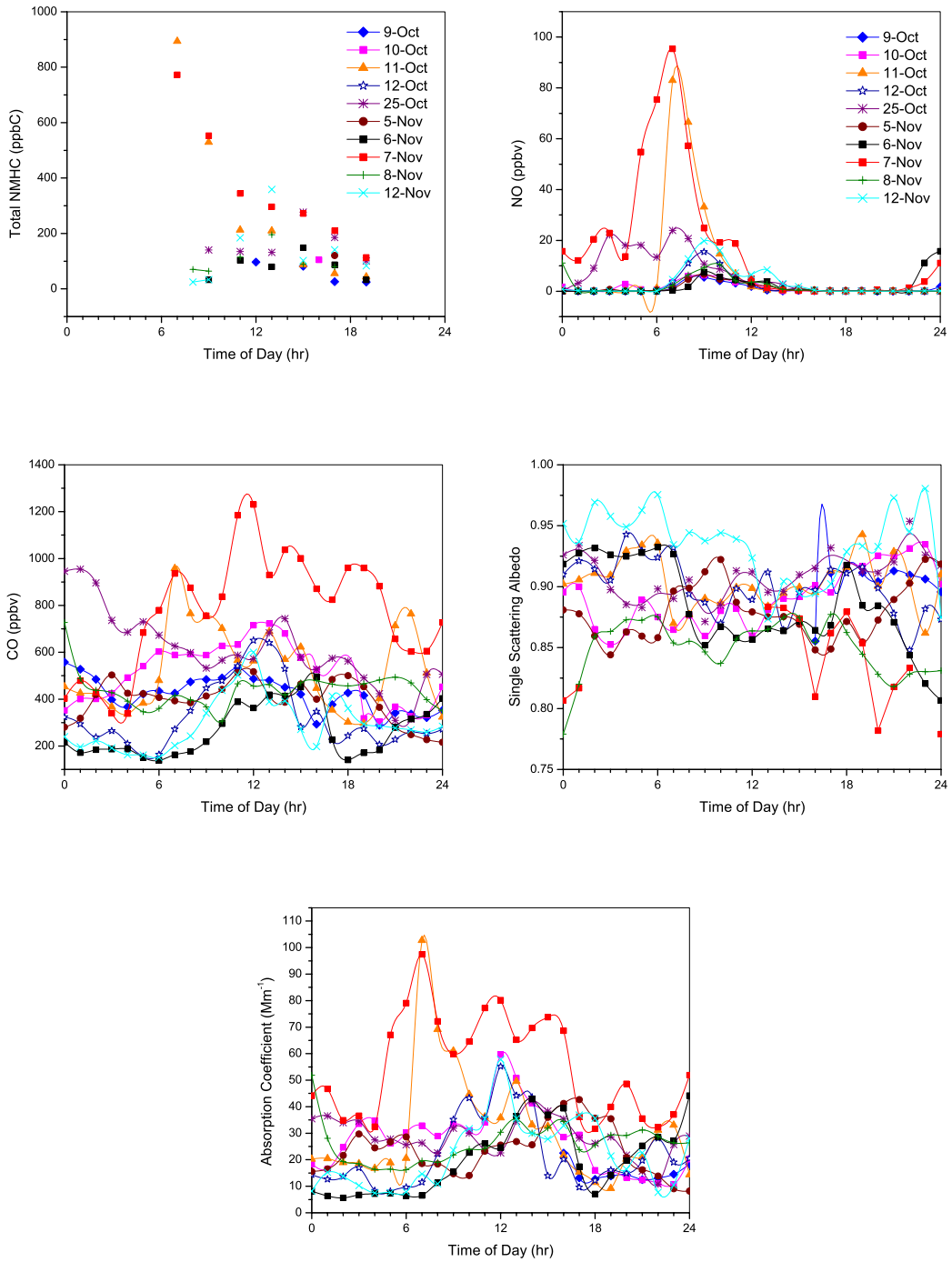

Figure 3.4.3 Diurnal variation of nonmethane hydrocarbons (i.e., VOC - CH_4), NO, CO, scattering albedo, and light absorption coefficient observed at TO on the episode days.

3.4.2.1 Summary: The diurnal variation of O_3 at TO was similar for all ozone episode days, although the magnitude of the peak concentration did vary. The peak on the most severe episode, 203 ppbv on November 7, was the highest on record in the Hong Kong area. In general, O_3 concentrations on the episode days were observed to begin their rise relatively late in the morning and peak relatively early in the afternoon (i.e., ~ 1600 hours).

3.4.3 Diurnal Variation of O_3 at EPD-Operated Sites

Figure 3.4.4 shows the O_3 concentrations at all the five sites on Nov. 7. As is typical of the area and typical of all episodes encountered during the field campaign, O_3 was highest on Lantau Island (TC, TO), and of the two sites on Lantau Island, highest at TO. Also note that the diurnal variation of O_3 observed at the EPD-operated sites is quite similar to that observed at TO; i.e., O_3 increase begins relatively late in the morning and the O_3 peak occurs relatively early in the afternoon.

3.4.3.1 Summary: On O_3 episode days, the recorded O_3 peak concentrations were highest on Lantau Island and, on Lantau Island, highest at TO. The diurnal variation of O_3 at the other sites were generally similar to that of TO with a rise in O_3 beginning relatively late in the morning and the peak occurring relatively early in the afternoon.

3.4.4 Transport Characteristics of O_3 Episode Days

One of the key questions to be addressed in this chapter relates to the relative roles of local emissions and emissions transported from Guangdong Province in fostering O_3 pollution in Hong Kong. To address this question, I attempted to characterize the degree to which the air masses encountered in Hong Kong on the O_3 episode days was impacted by air transported from Guangdong Province. Each day was assigned one of

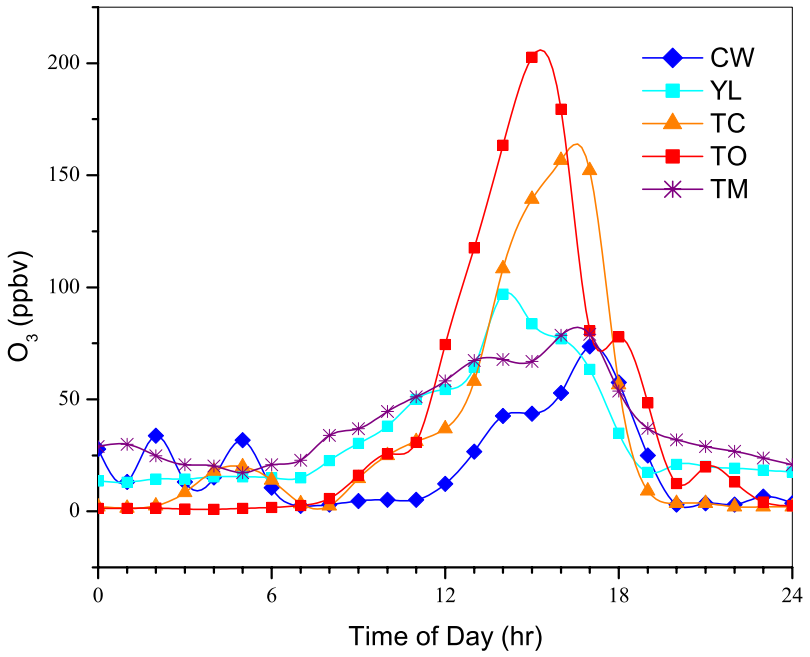

Figure 3.4.4 Diurnal variation in O_3 concentrations at all five sites on Nov. 7, 2002.

three possible categories: (i) "L," indicating that the episode was largely local in character; "L, r," indicating a local episode with some impact from Guangdong Province; and "R," indicated an episode with significant impact from Guangdong Province. As described below, two independent analyses were carried out to determine the appropriate category for each day. The results are summarized in Table 3.4.1. Inspection of the table reveals that only one of the episode days (i.e., Nov. 7, the most severe episode) received an "R" categorization; 4 days (Oct. 10, 11, 12, and Nov. 8) received an "L, r" categorization; and the remaining 5 days received an "L" categorization. Thus it would appear that both local and transported pollutants can act independently or in concert to bring about O_3 pollution in the Hong Kong area.

3.4.4.1 Chemical Tracers: The ratio of the increment of CO to the increment of NO_y (i.e., dCO/dNO_y) in an air mass is a useful diagnostic of the relative influence of pollution from South Mainland China and from Hong Kong (Wang et al., 2001a), since the emission ratio of CO-to-NO_x from Guangdong and Hong Kong are so different; i.e., ~15 in Guangdong and ~ 1 in Hong Kong (Streets et al, 2003). High values in the ratio are generally indicative of air masses from Mainland China and low ratios of air masses impacted by local Hong Kong emissions (Kok et al, 1997; Wang et al, 2001a).

In the analysis presented here, dCO/dNO_y was calculated from the 1-hour averaged CO and NO_y measurements recorded at TO, subtracting the "background" CO and NO_y concentrations from the observed concentrations, and then forming the ratio. The background CO and NO_y concentrations were estimated in two ways. A "seasonal" dCO/dNO_y was calculated using constant background CO and NO_y concentrations of 211 and 3.37 ppbv, respectively. These concentrations are the mean values observed for marine air advecting over Hong Kong in the fall season (Wang et al, 2001b). A "24 hourly" dCO/dNO_y was calculated using the minimum CO and NO_y concentrations observed on that day. Figure 3.4.5 illustrates the diurnal variation in the two sets of ratios for each O_3 episode day. Note that Nov 7 is the only day with consistently high ratios during the late morning and early afternoon (consistent with its "R" categorization). Oct 10, Oct 11, Oct 12 and Nov 8 have transient spikes of high ratios and thus have "L, r" categorizations. On the other episode days, the ratios remained low throughout the photochemically important period and thus have "L" categorizations.

3.4.4.2 Isentropic Back Trajectories: As an independent check on the results obtained from the dCO/dNO_y ratios, isentropic back trajectories for air masses at TO during each

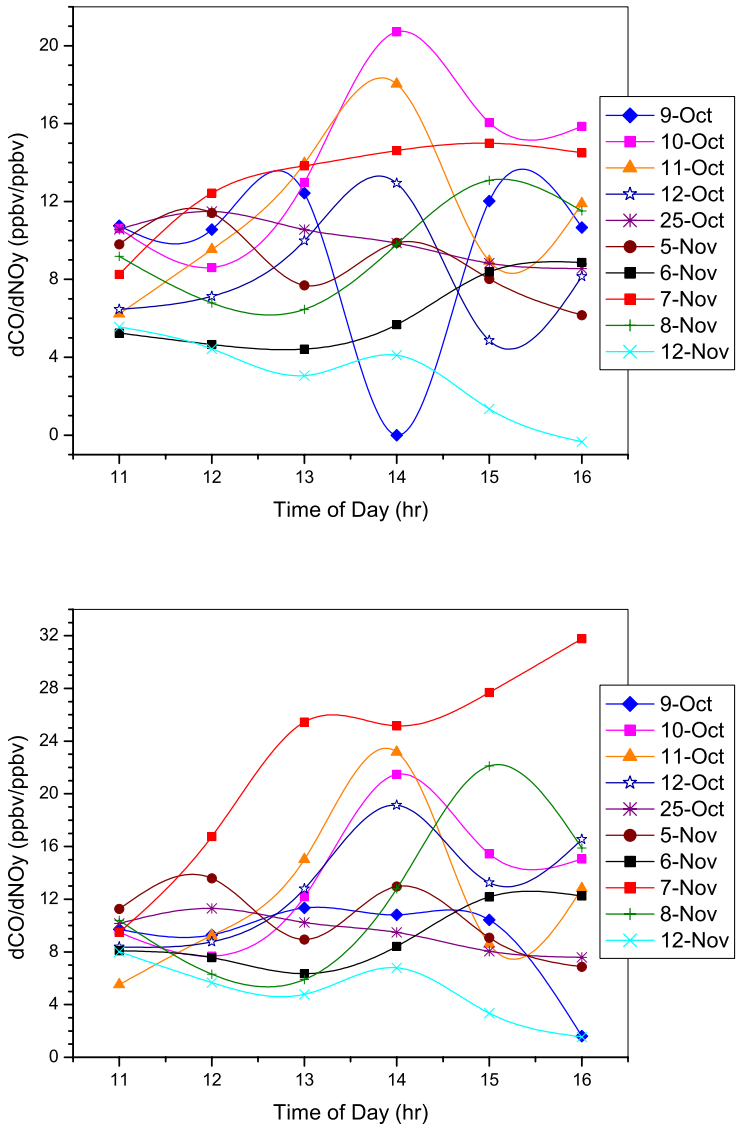

Figure 3.4.5 Ratio dCO/dNO_y at Tai O on episode days. Upper panel: 'seasonal', lower panel: '24 hourly'.

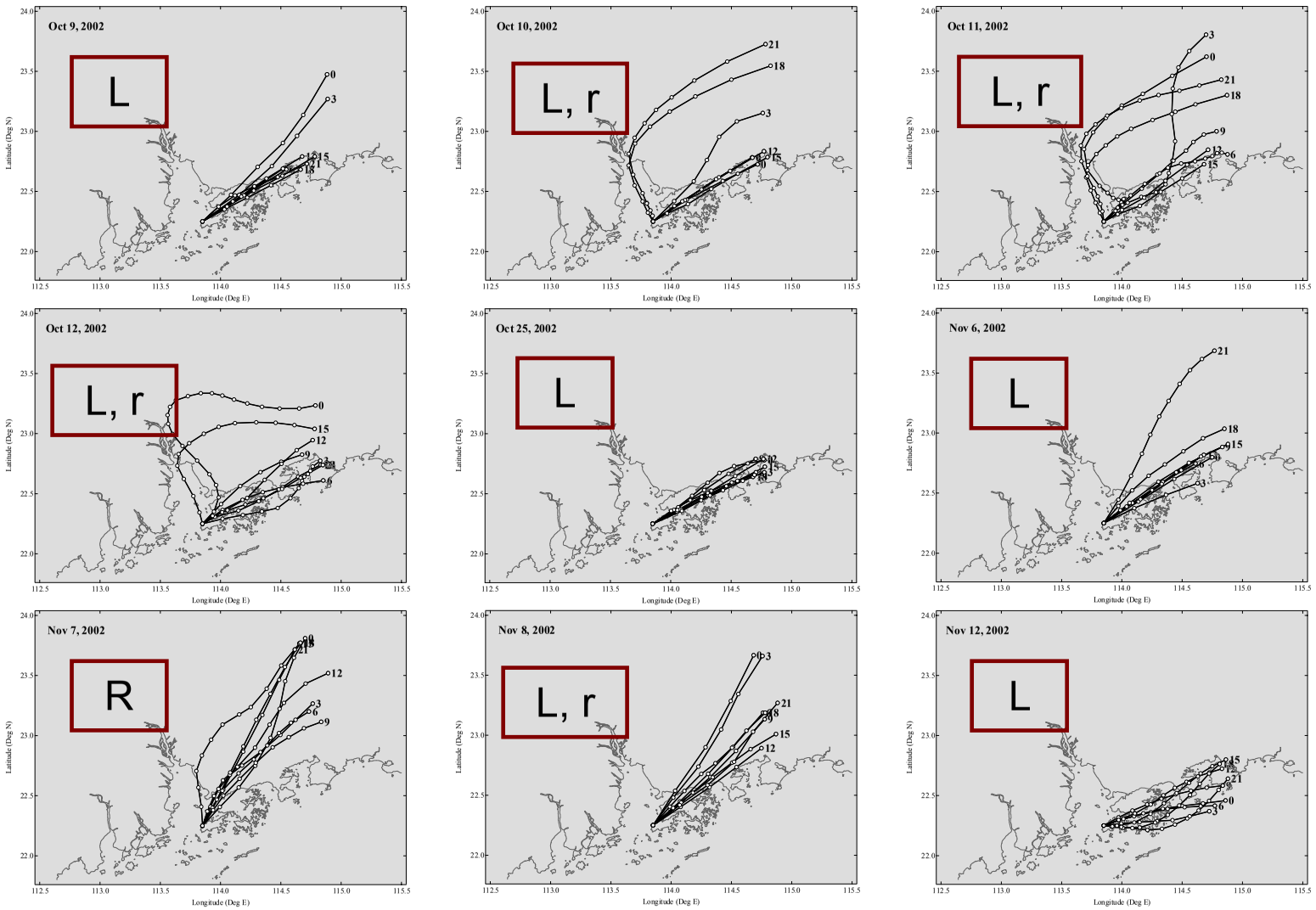

Figure 3.4.6 Back trajectory clusters of air masses arriving at TO at different times on each of the O_3 episode days. (T. Wang, private communication, 2004)

of the O_3 episode days were calculated (Figure 3.4.6, T. Wang, private communication, 2004). These plots generally corroborate the results from the ratio dCO/dNO_y. For example, Nov. 7 is the only day with air masses consistently arriving at the site from the mainland during the late morning and early afternoon hours.

3.4.4.3 Summary: Both local and transported pollutants from the Guangdong Province appear to have contributed to the high O_3 concentrations observed on the O_3 episode days. Of the 10 episode days studied, 5 were local in character, 4 have local and regional characteristics, and one appeared to be consistently impacted by regional transport. It would appear, therefore, that both local and transported pollutants can act independently or in concert to bring about O_3 pollution in the Hong Kong area.

3.4.5 Distribution and Speciation of VOC on Nov. 7th Episode

In this section I discuss the distribution and speciation of VOC observed at the various sites during the Nov. 7th O_3 pollution episode. (Recall that Nov. 7th was the only day during the field measurement campaign when VOC was measured at all sites.) To facilitate the analysis and discussion, I have grouped the 40+ species measured at each site into three major types: anthropogenic hydrocarbons (AHC), biogenic hydrocarbons (NHC) and CO, with NHC defined as isoprene and the pinenes. AHC are further divided into five sub-types according to their structure and reactivity in the atmosphere: reactive aromatics (R-AROM) encompassing all aromatics except benzene; reactive olefins (R-OLE), comprised of all olefins except ethylene; alkanes higher than C4 (>=C4); ethylene (ETH); and the low reactivity hydrocarbons (LR) which include methane, ethane, propane, acetylene and benzene.

Figure 3.4.7a and 3.4.7b illustrate the 24-hour averaged concentrations of the major VOC groups and AHC subgroups at the sites on Nov. 7. It can be seen that AHC dominates over NHC at all sites. AHC is highest at YL. Although TC and TO are in the downwind direction of CW and YL, AHC at these two sites are higher than at CW, and comparable to YL. This suggests that there must be some other significant source of VOC at TC and TO other than simply transport from the urban/industrial areas surrounding CW/YL. In AHC, R-AROM is the dominant species group; this group is, in turn, richest in xylenes and toluene, and to a lesser extent tri-methylbenzenes and ethyl-benzene. R-AROM is highest at YL and TO, following these two are TC, CW and TM in sequence. As discussed below, the high concentration of R-AROM at TO relative to that of YL and CW suggests the influence of a source of these VOCs to TO other than transport from YL and CW.

R-AROM tend to be highly reactive. For example, xylenes have lifetimes on the order of 2-4 hours if OH radical concentration is 5.5 x 10^6 molec/cm^3 which is typical of the values in autumn. It follows therefore that the reactive aromatics at TO, which are higher or essentially the same as the concentrations measured at CW and YL, cannot have come solely from CW and YL. The concentrations of CO at different sites also show that CW could not have been the only source of CO at TC and TO.

3.4.5.1 Summary: AHC dominated over NHC at all sites, and, of the AHC, R-AROMs were the most abundant. The relative concentrations of AHC's, R-AROM, and CO at the various sites suggest that there must be a source of AHC's (and especially R-AROM) impacting TC and TO from a locale other than that of CW and YL, and also there might be a source of CO impacting TC and TO from an area other than that of CW and YL. (In

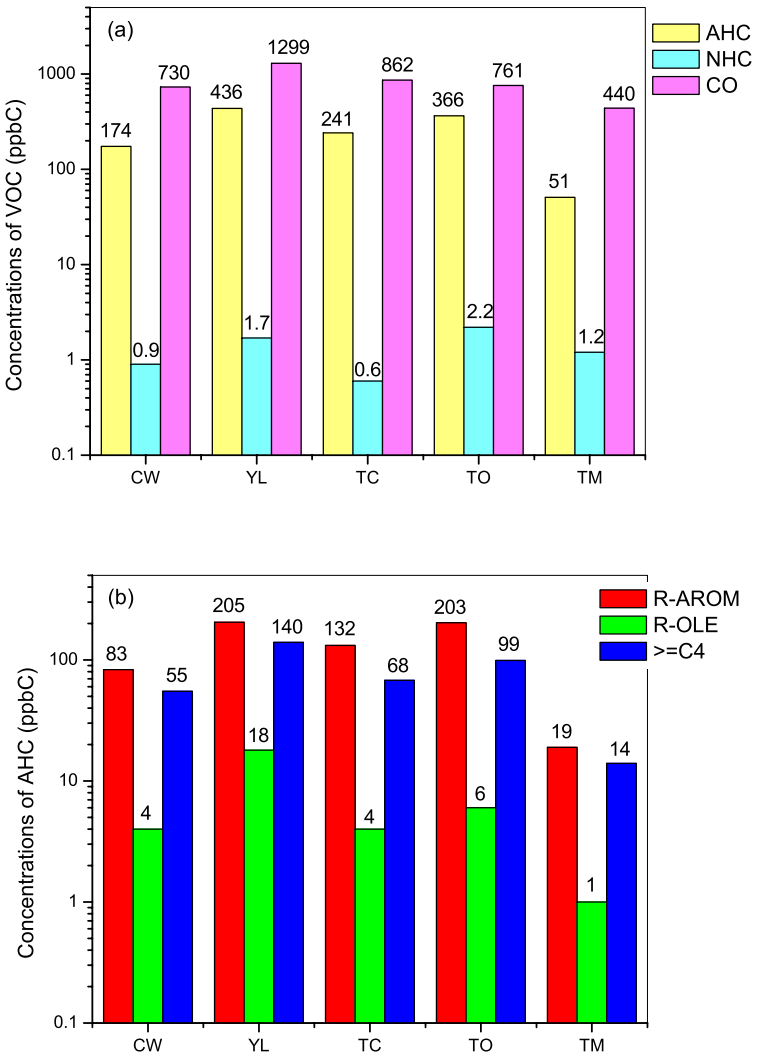

Figure 3.4.7 VOC distribution (in unit of ppbC) at all five sites on Nov. 7, 2002: (a) Total VOCs grouped into AHC, NHC, and CO; (b) AHCs sub-groups R-AROM, R-OLE, and >=C4.

the discussion that follows, I will refer to this apparent source of VOCs that impact TC and TO but not CW and YL as the "additional source of VOCs.") On the basis of this data alone, it is not possible to determine if this additional source is local to TC and TO or a distant source that is not downwind of CW and YL. Subsequent analyses presented below will address this issue.

3.4.6 VOC Reactivity

Not all VOCs react at the same rate, some react more quickly and some more slowly. In general the rate of reactivity among VOC species can vary by as much as or even more than the concentrations of the VOCs in the atmosphere. For this reason, the relative concentration of VOC species is not necessarily indicative of their relative importance in generating O_3 pollution. Reactivity analysis attempts to place all VOCs on equal footing by taking into account both concentration and reactivity of each VOC. Here I use a reactivity scale called propy-equivalents (Chameides et al, 1992):

$$C_i \text{ (propy-equiv)} = C_i \text{ (observed)} * \{k_{OH}(i)/k_{OH}(C_3H_6)\} \qquad (3.1)$$

where 'i' stands for any VOC species. In this formulation, the concentration of each VOC species is re-normalized by a factor that is proportional to its reactivity with OH. The resulting reactivity is referred to as propy-equivalents because the normalization factor used is the rate constant for propylene with OH. The choice of propylene is arbitrary and another normalization factor could be used with the same results.

3.4.6.1 Distribution of Reactivities on Nov. 7: Figure 3.4.8a and 3.4.8b show the propy-equivalents of different species groups at the five sites on Nov. 7, and Figure 3.4.9 a-f shows the relative contributions of various groups of VOCs to the total reactivity. For the most part the reactivity analyses illustrated in these figures tend to reinforce the

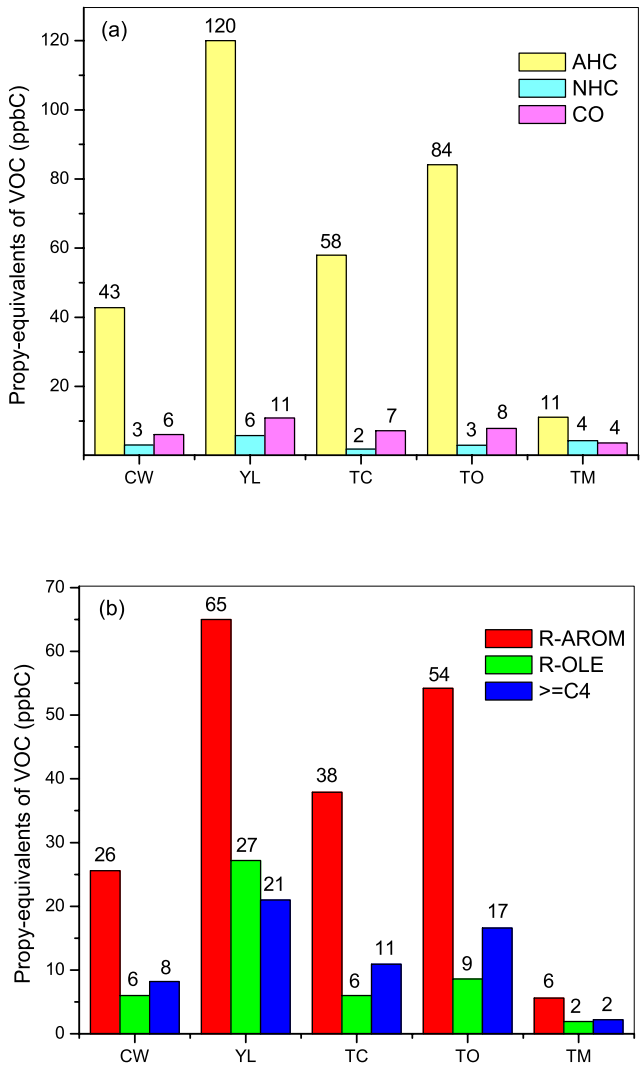

Figure 3.4.8 Propy-equivalents (in unit of ppbC) of different VOC groups at all five sites on Nov. 7, 2002: (a) Total VOCs grouped into AHC, NHC, and CO; (b) AHCs sub-groups R-AROM, R-OLE, and >=C4.

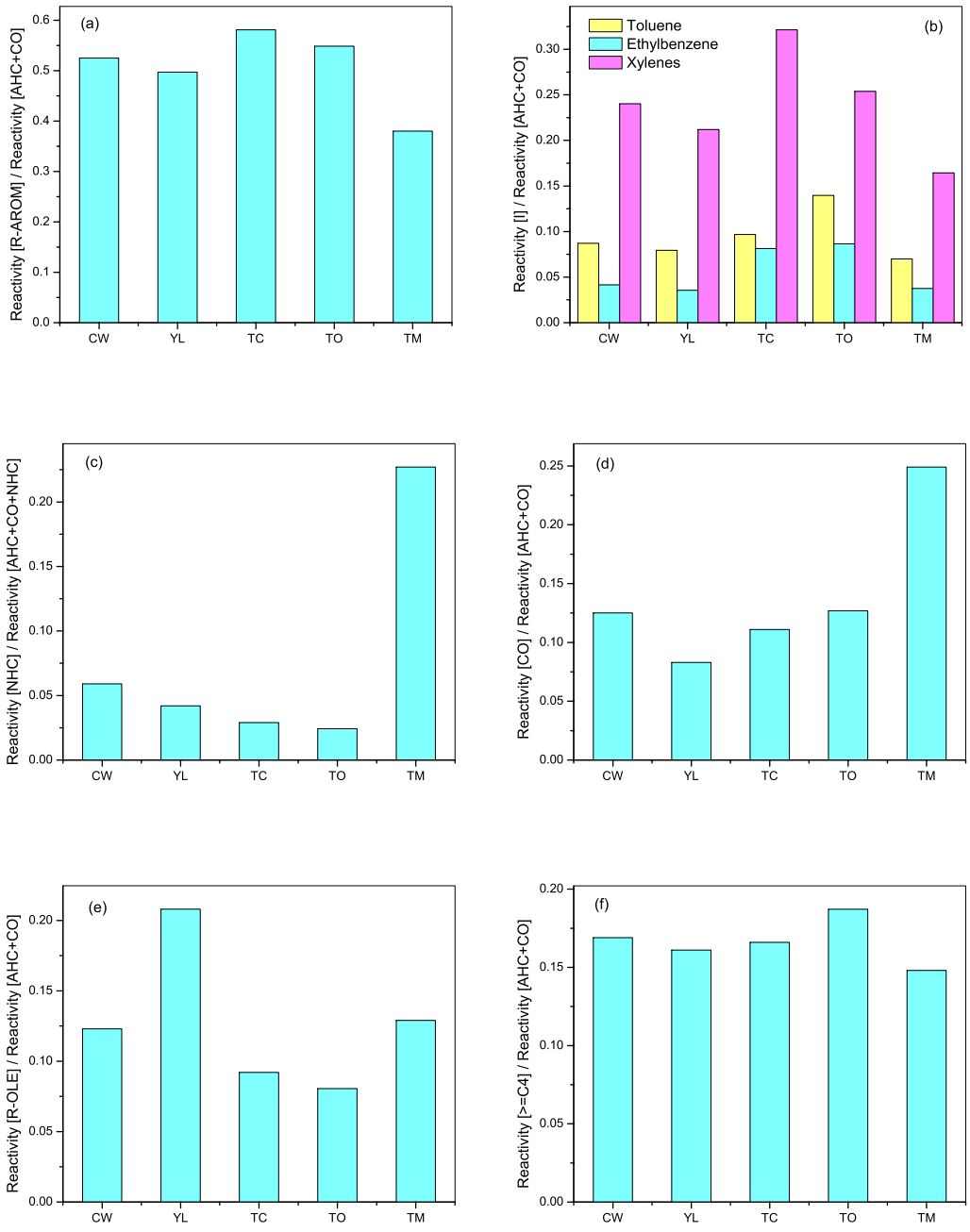

Figure 3.4.9 Propy-equivalent reactivity fractions of different species or species groups in the total reactivity of anthropogenic VOCs and CO.

conclusions reached earlier on the basis of the VOC concentrations; i.e., AHC dominated over NHC and of the AHC species, R-AROM species were most important. However, there are a number of additional insights that can be garnered. For example, even though the concentrations of CO were greater than the total VOC concentrations at all sites, the total AHC reactivity was greater than that of CO at all sites. This suggests that AHC played a greater role in generating O_3 than CO. This issue is examined in more detail in the section on the application of the OBM (Section 3.5.4).

A comparison of the ratio of AHC reactivity-to-AHC concentration at the different sites shows that the ratios at TC and TO were reduced relative to that of CW and YL. This occurred primarily because some of the more reactive VOCs (especially R-OLE's) were relatively depleted at TC and TO. A likely explanation for the depletion of these reactive VOCs at TC and TO relative to that of CW and YL is that the AHC's at TC and TO were not local, but, at least for the most part, had been transported from sources upwind of the two sites, while the AHC's at CW and YL were in fact mostly of local origin. This would in turn suggest that the additional VOC source believed to be impacting TC and TO was not local as well. On the other hand, while most reactive VOCs were relatively depleted at TC and TO, R-AROM's were not, and were actually enhanced in their relative reactivity. This suggests that if TC and TO were in fact impacted by upwind VOC sources, these sources must have been relatively rich in R-AROM species. These issues will be examined in more detail in Sections 3.4.7 and 3.4.8.

As noted above, R-AROM contributed most to the total reactivity at all sites, accounting for over 50% at CW, YL, TC and TO and close to 50% at TM (49%). Of the species included in the R-AROM group, xylenes dominated, accounting for over 25% of

the total reactivity of anthropogenic VOCs at TC and TO and over 20% of that at CW and YL. At YL, R-OLE also made a significant contribution to the total reactivity from anthropogenic compounds (i.e., ~ 20%).

The results from TM are of interest because even though TM is a rural site, the influence of anthropogenic compounds appears to have been significant. While the contribution of NHC to the total reactivity was largest at TM (~ 23%), AHC and CO still dominated. The fraction of CO reactivity to the total anthropogenic reactivity was highest at TM; i.e., ~25% as compared to about 10-15% at CW, TC and TO, and 10% at YL. The reason for this may be that CO has a lifetime about 1~2 months, much longer than most VOCs. As more reactive VOCs are consumed by photochemistry, CO's relative importance will tend to rise. Since TM is a rural site, one might expect CO would account for a higher fraction than at other sites. On the other hand, the contribution from R-OLE was relatively high at TM (~ 13%), and, given R-OLE's relative short lifetimes, this would appear to suggest that TM is directly influenced by local anthropogenic emissions.

3.4.6.2 Reactivity at Tai O: Figure 3.4.10 shows the total propy-equivalent reactivity at Tai O on all episode days with VOC data. It can be seen that Oct. 11 and Nov. 7 are similar in that in the early morning the total propy-equivalent reactivity is much higher than that observed during the daytime. As the morning progresses, however, the total propy-equivalent reactivity decreases rapidly and at noon the total reactivity on these two days was close to that on other episode days. As noted earlier, the anomalous behavior on Oct. 11 and Nov. 7 may reflect the presence of a transient VOC sources close to the TO site on these days and/or unusual meteorological conditions that caused

the early-morning accumulation of pollutants at the TO site on these days. This issue is discussed further in Section 3.4.8.

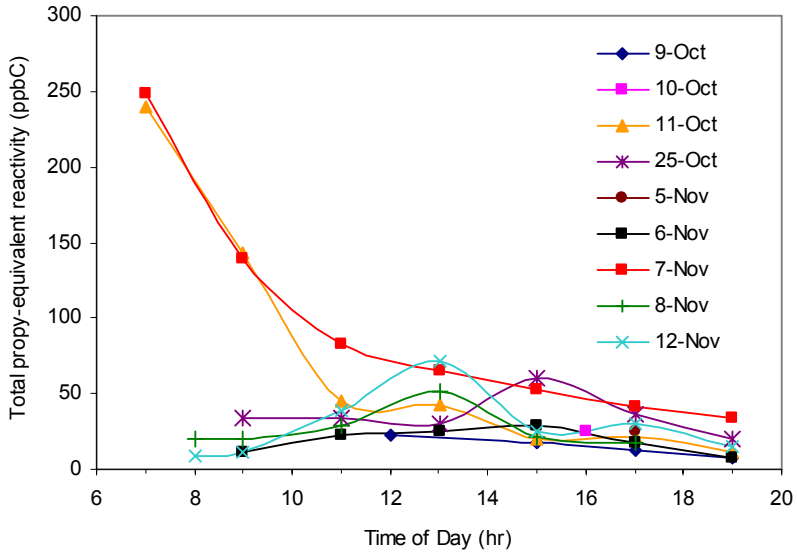

Figure 3.4.10 Total propy-equivalent reactivity at TO on all episode days with VOC data.

Figure 3.4.11 a-e shows the fractions of different species groups to the total propy-equivalent reactivity at TO on the various episode days. It can be seen that R-AROM dominated on all episode days. Alkanes higher than C4 and CO were also major contributors to the total propy-equivalent reactivity. Examining R-AROM, it can be seen that the high concentrations of AHC in early morning of Oct. 11 and Nov. 7 are due in part to high concentrations of xylenes. However, as the day progressed on Oct. 11 and Nov. 7, the reactivity fraction from xylenes decreased while that of toluene increased (see Figure 3.4.12). At midday the reactivity fractions of xylenes and toluene were roughly equivalent, and at later hours, the reactivity fraction of toluene was larger than that of xylenes. On the days other than Oct. 11 and Nov. 7, on the other hand, the diurnal variations of xylenes and toluene at TO were more similar, with toluene still tending to

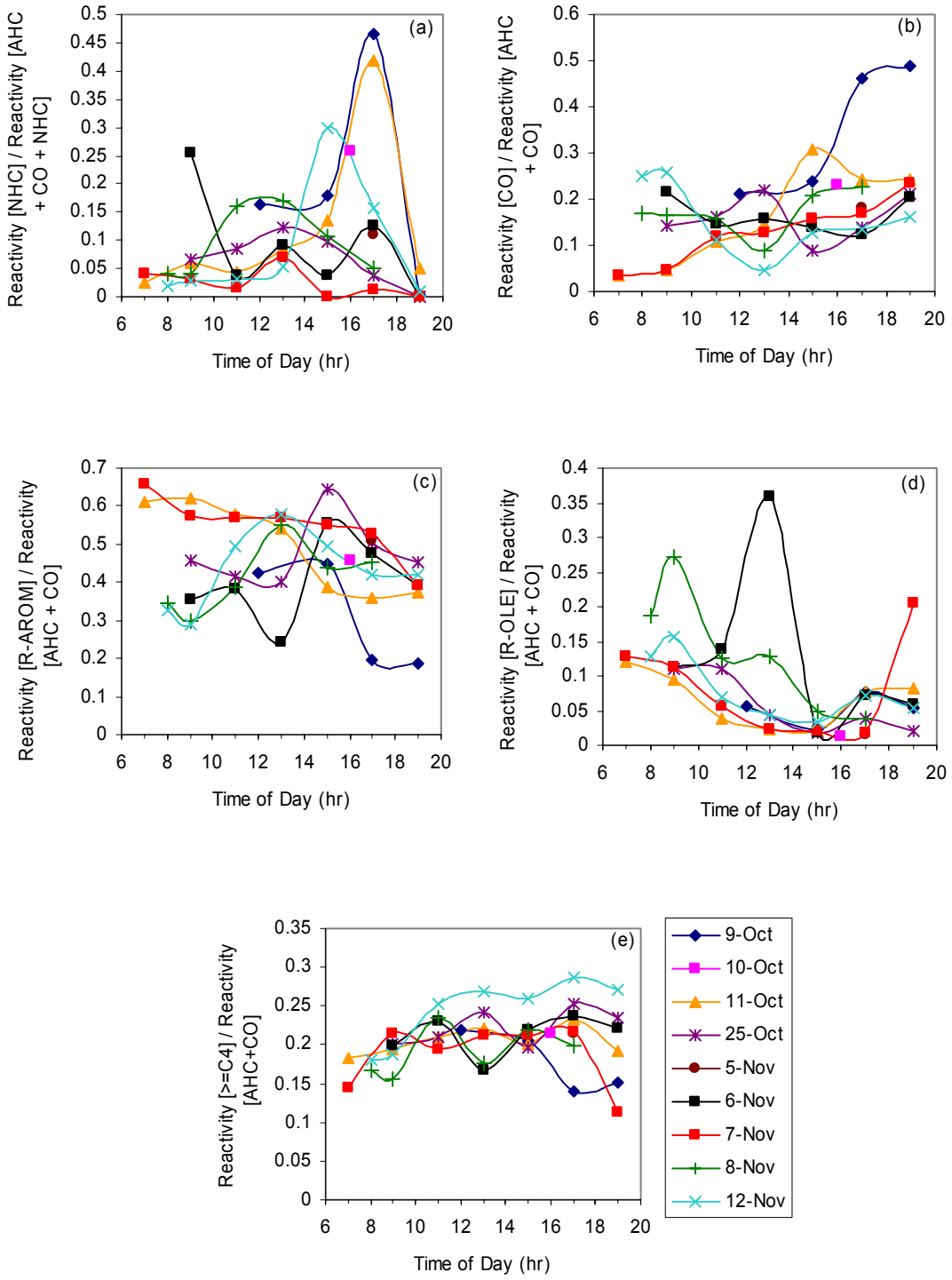

Figure 3.4.11 Fractions of different species groups to the total propy-equivalent reactivity at Tai O on all episode days with VOC data.

increase in importance relative to that of xylenes but less so. This modest increase in the reactivity of toluene relative to that of xylenes is to be expected, since xylenes are more reactive than toluene. The large increase in Oct. 11 and Nov. 7 is more difficult to rationalize on the basis of photochemistry. This suggests that the source that caused the high concentration of pollutants at TO on Oct. 11 and Nov. 7 was relatively rich in xylenes relative to that of toluene and that the influence of this source tended to decline with time as these days progressed. This issue will be addressed in more detail in Section 3.4.8.

3.4.6.3 Summary: AHC made the major contribution to the total (VOC + CO) reactivity at all five sites included in my analysis on all episode days with VOC data. Of the AHC's, R-AROM dominated the reactivity, and, of the R-AROM's, xylenes and toluene were most important. Data collected at TO suggest that toluene tended to grow in importance as the day progressed. On days when xylenes dominated over toluene, this generally occurred in the morning. The data also suggest that AHC's at TO and TC are more strongly impacted by upwind sources of VOCs than those of CW and YL, and that these upwind sources tend to be enriched in R-AROM's.

3.4.7 Sources of VOC: Local Emissions vs. Transport from Distant Sources

Further insights into the nature of the VOC sources impacting the various sites can be obtained by examining the ratios of VOC species with different photochemical lifetimes (or reactivities) as a measure of the so-called "photochemical age" of the VOC's (Nelson and Quigley, 1983). For example, imagine two VOC species: X and Y. Suppose X is more reactive (has a shorter lifetime) than Y. As these species are processed in the atmosphere by photochemical processes, the ratio of X to Y will tend to decrease.

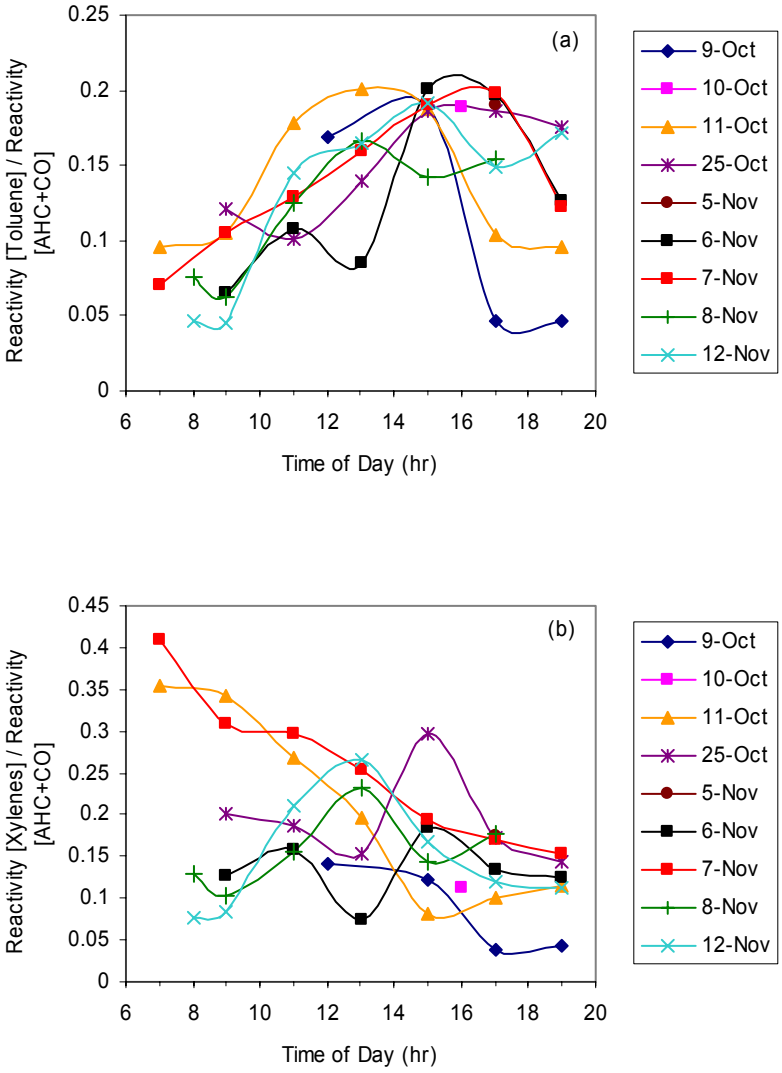

Figure 3.4.12 Fractions of toluene and xylenes to the total propy-equivalent reactivity at Tai O on all episode days with VOC data.

Thus, air masses with relatively high ratios of X to Y have undergone relatively little photochemical processing and are said to have a low photochemical age. For this reason, monitoring sites with air masses with consistently low photochemical ages are indicative of sites with VOCs that have undergone little or no photochemical processing and are thus relatively close to the sources of the VOC's. On the other hand, sites that have lower ratios of X to Y are reflective of more aged VOC mixes and thus presumably VOCs that were emitted from more distant sources.

In the analysis presented here, I use the ratio of m,p-xylenes to ethylbenzene as a metric of photochemical age. I have chosen these two species because their lifetimes are appropriate for distinguishing source contributions between the various sites considered here; the transport time between the various sites on a typical episode day is a few hours while, for an OH concentration of 5 x 10^6 molec/cm^3, the xylene lifetimes is about 3 hours and the ethylbenzene lifetime is about 8 hours. Additionally, both species fall into the R-AROM group, and thus their ratio will be most relevant to this most dominant group. Another reason to choose this ratio is that various sources of these two species tend to have a similar ratio of about 3.6 (Nelson and Quigley, 1983), so the difference of the ratios can be attributed to photochemistry and not emissions. It is worth noting that from the speciated version of emission inventory from the earlier PRD study discussed in Section 3.3, this ratio is 4.4 at Hong Kong and 4.0 at Pearl River Delta Region, respectively, which is consistent with the value of 3.6. Figure 3.4.13 shows the relation between the ratio of m,p-xylenes to ethylbenzene and O_3 at Tai O. Generally, higher O_3 concentrations are indicative of greater photochemical age and so the strong negative

correlation between O_3 and the m,p-xylenes-to-ethylbenzene ratio suggests that the ratio can in fact be used to assess photochemical age.

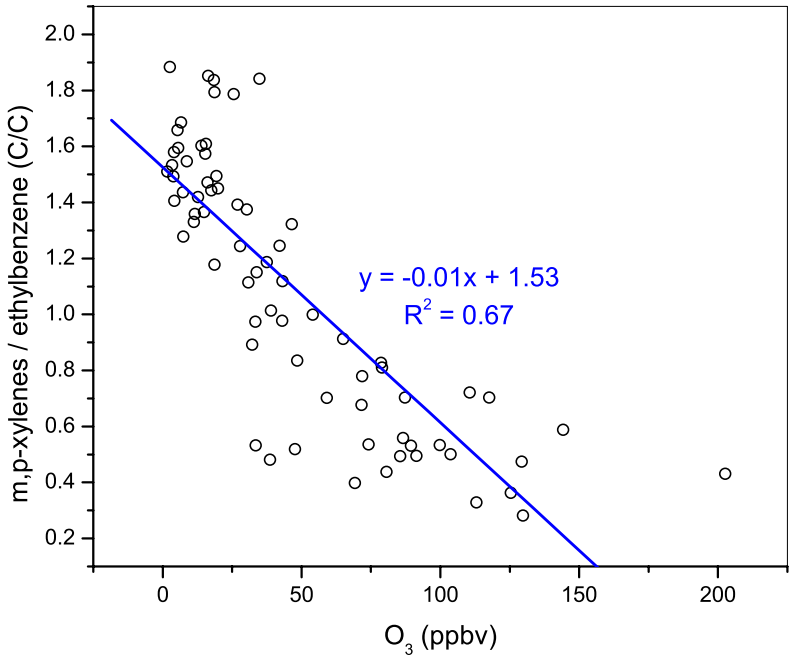

Figure 3.4.13 Scatterplot of simultaneous measurements of O_3 and the ratio of xylenes to ethylbenzene at Tai O.

Figure 3.4.14 illustrates the averaged m,p-xylenes-to-ethylbenzene ratio observed at each of the five sites during the measurement campaign. CW and YL have relatively high ratios, while TC, TO, and TM have lower ratios. These results are generally consistent with what might be expected in the basis of the characteristics of each of the sites. CW is the most urban site and YL is close to a number of industrial facilities and thus we would expect the VOC mix at these sites to reflect their close proximity to sources. TC, TO and TM, being more rural sites would be expected to have a more photochemically-aged mix of VOCs reflecting their greater distance from VOC sources. These results also suggest that the additional source of VOCs that impacted TC and TO

(but not CW and YL) were most likely not local but from source located upwind of the TC and TO but downwind of CW and YL.

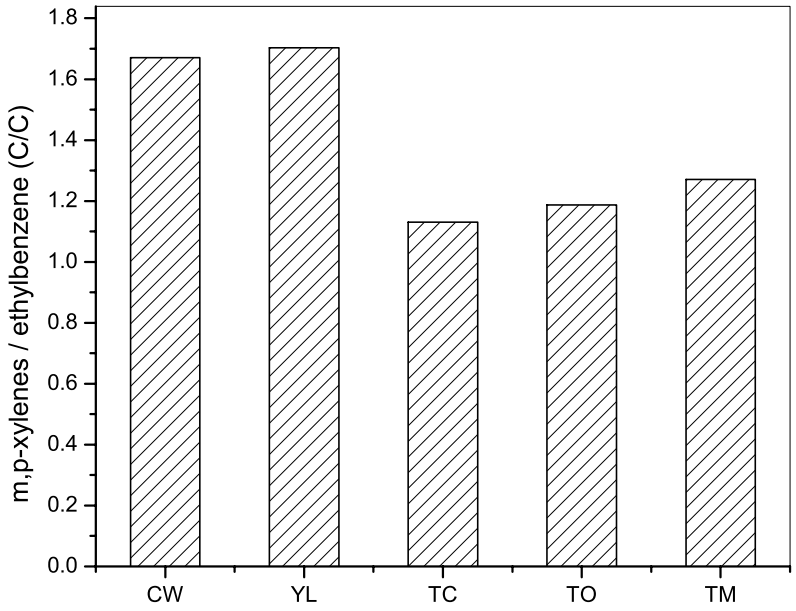

Figure 3.4.14 Average ratio of the observed 24-hour averaged concentrations of m,p-xylenes to that of ethylbenzene at all five sites during the measurement campaign.

3.4.7.1 Summary: The VOC mix at CW and YL reflected a relatively low photochemical age, indicative of sites that are impacted primarily by local/nearby sources. The mix at TO, TC, and TM reflected a greater photochemical age suggesting that these sites were impacted by VOCs that had been emitted elsewhere and transported to the sites.

3.4.8 What is the Nature of Additional VOC Source at TO and TC?

Toluene and xylenes were found to be the most reactive VOCs during episode days and their concentrations were relatively enhanced at TC and TO, indicating the existence of an additional source of VOCs to these sites. The anomalous diurnal variations of toluene and xylenes on Oct. 11 and Nov. 7 further suggest that these two R-

AROMs may have differing sources. In this section I examine the speciated VOC observations in more detail to gain insight into the sources of toluene and xylenes.

3.4.8.1 Ratio of butanes-to-toluene: While ratios of the concentrations of VOCs with ***different*** photochemical lifetimes can be used to assess the photochemical age of the VOCs, the ratios of the concentrations of VOCs with ***similar*** photochemical lifetimes can be used to identify the relative influence of different source types to the VOCs observed at a given site. In the later case, since the VOCs have the same lifetime, variations in the ratios of the two species must reflect the influence of different source types that emit the species at differing relative amounts.

To gain insight into the kinds of sources that were responsible for the high concentrations of toluene at TO and TC, I considered the ratio of butanes-to-toluene. These species have lifetimes of about 1 day. In general, the major source of butane is mobile; while the major sources of toluene are industrial and fuel storage as well as mobile (see Figure 3.4.15). Thus, one might expect relatively high butanes-to-toluene ratios for mobile sources and lower ratios for more industrial sources and sources that reflect evaporative losses and leakages from fuel depots.

This expectation is largely confirmed from examination of Figure 3.4.16 based on data collected at two sites in Hong Kong – Tsing Yi and Tai Po (see Figure 3.3.1) during the earlier PRD study discussed in Section 3.3. Tsing Yi is a roadway site located at the entrance to a tunnel and thus is generally dominated by mobile sources. The ratio of butanes-to-toluene is therefore generally high at Tsing Yi. The exception is when the VOC concentrations are extremely low, most likely reflecting extremely low-traffic conditions when the site was being impacted by more distant non-mobile sources. Tai Po

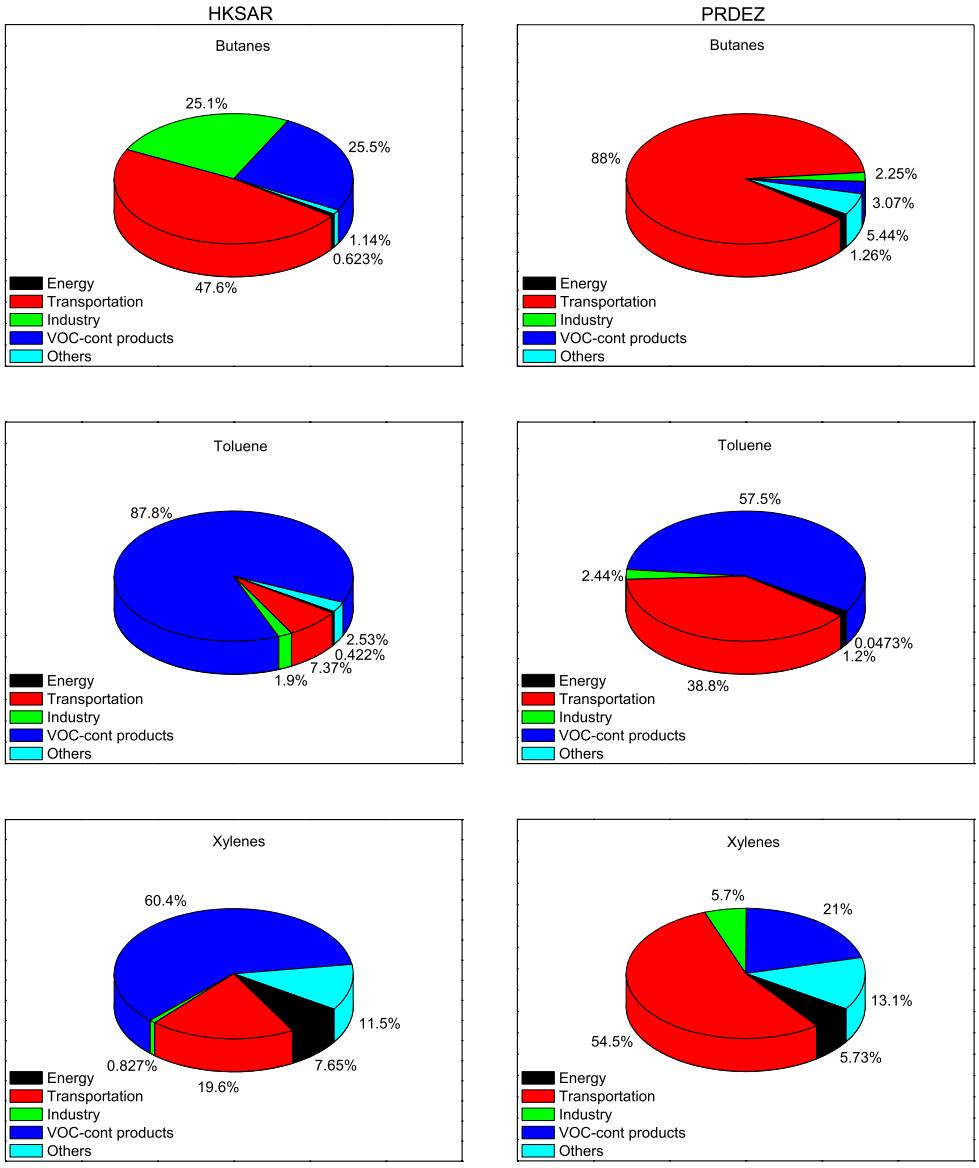

Figure 3.4.15 Emissions of butanes, toluene and xylenes by sector for Hong Kong SAR and Guangdong Province. Source: Earlier PRD Study [CH2M HILL (China) Limited, 2002].

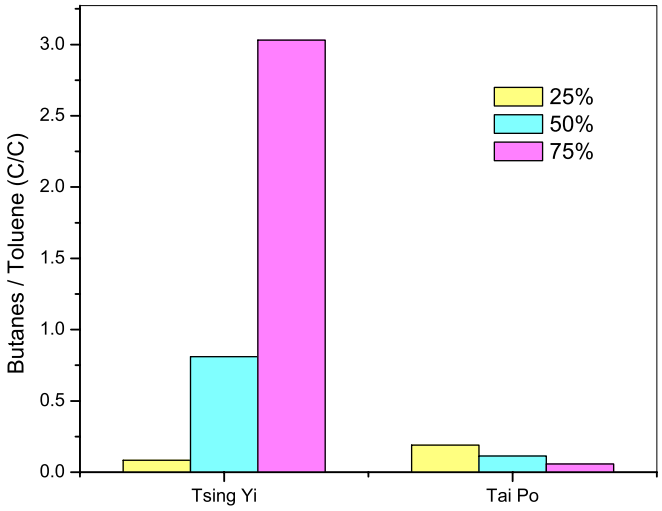

Figure 3.4.16 Ratio of butanes-to-toluene at Tsing Yi and Tai Po for the 25th, 50th, and 75th percentile in observed VOC concentrations from an earlier PRD study [CH2M HILL (China) Limited, 2002]

is situated in an industrial waterfront park, and here the butanes-to-toluene ratio was consistently low.

Figure 3.4.17 illustrates the butanes-to-toluene ratio observed at each of the sites on episode and non-episode days, and the diurnal variation in the ratio observed at TO on episode days. From Figure 3.4.17a we see that the ratio is depressed at TC and TO compared to other sites, especially on episode days (about 0.3). This suggests that the excess abundance of toluene (and perhaps the additional source of VOCs in general) at TC and TO is related to industrial, waterfront, and/or fuel-storage emissions as opposed to mobile emissions. Inspection of Figure 3.4.17b indicates that at TO the ratio tends to decrease in the early afternoon at the same time that O_3 tends to increase on episode days. This result is consistent with the growing contribution of toluene to the total reactivity at TO in the afternoons discussed earlier and suggests that the air masses contributing to the

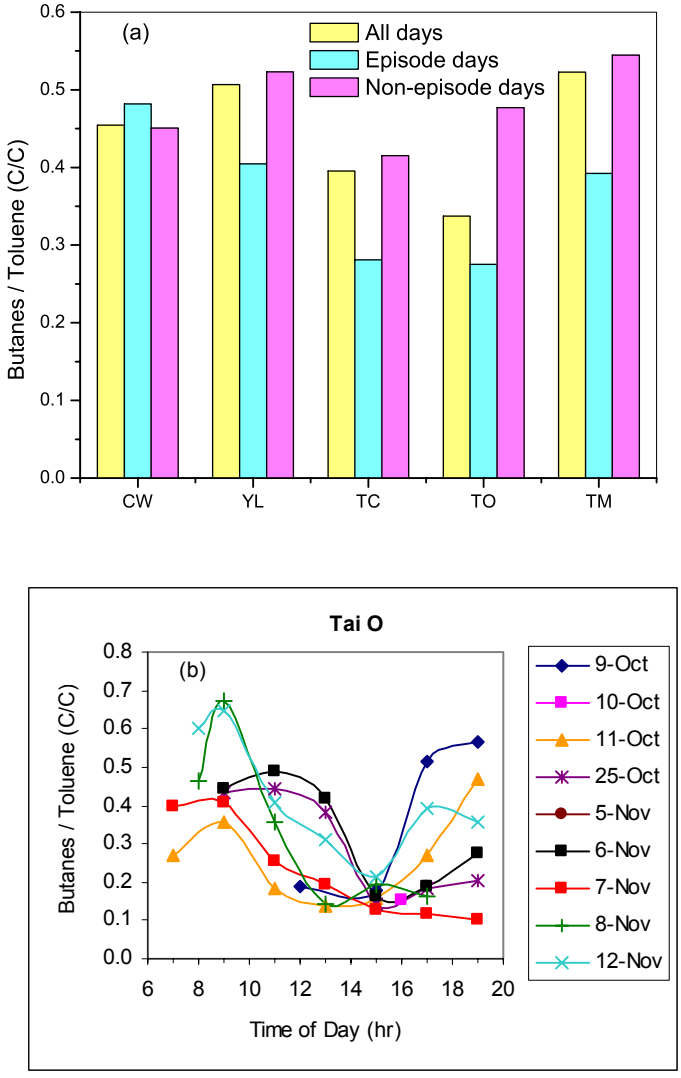

Figure 3.4.17 Observed. ratios of butanes-to-toluene: (a) 24 hour averaged ratios at all five sites on episode days, non-episode days and all days; (b) ratios at Tai O as a function of time of day on episode days.

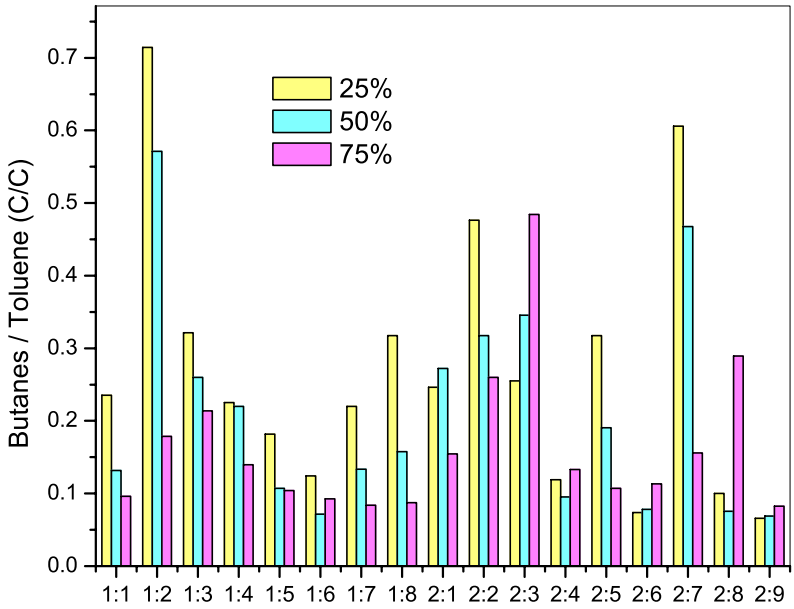

Figure 3.4.18 Ratio of butanes to toluene at various sites in Guangdong Province from a previous Hong Kong EPD study (see Section 3). The names of the sites are: 1:1, Dongguan City Changping Town; 1:2, Guangzhou City Conghua City; 1:3, Guangzhou City Guang-Shen Highway; 1:4, Guangzhou City Tianhe District; 1:5, Guangzhou City Huangpu District; 1:6, Jiangmen City Fengjiang District; 1:7, Shenzhen City Nanshan District; 1:8, Zhuhai/Zhongshan City Guang-zhu Highway; 2:1, Guangzhou City Baiyunshan; 2:2 Guangzhou City Conghua City; 2:3, Guangzhou City Yuexiu District; 2:4, Guangzhou City Huadu City; 2:5, Guangzhou City Baiyun District; 2:6, Guangzhou City Lianhuashan; 2:7, Guangzhou City Tianhe District; 2:8, Guangzhou City Xinken County; 2:9, Shenzhen City Baoan District.)

rise of O_3 at TO are more heavily influenced by emissions from industrial, waterfront, and/or fuel-storage than from mobile emissions.

The analyses discussed above and in the previous sections suggest that the additional toluene impacting TO and TC are not local and that they arise from industrial, waterfront, and/or fuel-storage activities. A related question is whether these sources are located in Hong Kong or in Guangdong Province. To address this question I first examined the butanes-to-toluene ratios observed at a number of sites throughout Guangdong Province during the aforementioned Hong Kong EPD study (Figure 3.4.18).

We can see that low ratios of butanes-to-toluene, similar to that observed at Tai Po (i.e., less than 0.1), were also observed at a number of sites in Guangdong Province. This suggests that Guangdong Province cannot be ruled out as a source of the additional toluene observed at TC and TO.

Further insight can be gained by examining a scatterplot between dCO/dNO_y (a tracer for distinguishing between pollution from Hong Kong and Guangdong) and the butanes-to-toluene ratio observed at TO. Two such scatterplots are illustrated in Figure 3.4.19: (a) using the 24-hour dCO/dNO_y ratio; and (b) using the seasonal dCO/dNO_y ratio. No matter which dCO/dNO_y ratio is used, I find a significant negative correlation between the butanes-to-toluene ratio and dCO/dNO_y. The plots suggest that over 30% of the variability in the butanes-to-toluene ratio observed at TO was correlated with a factor associated with pollution from Guangdong Province. This, in turn, implies that emissions from Guangdong Province are responsible, in part, for the high concentrations of toluene observed at TO. On the other hand, it should be noted that the regressions in Figure 3.4.19 were obtained by omitting two outlying data points that were obtained on Oct. 9

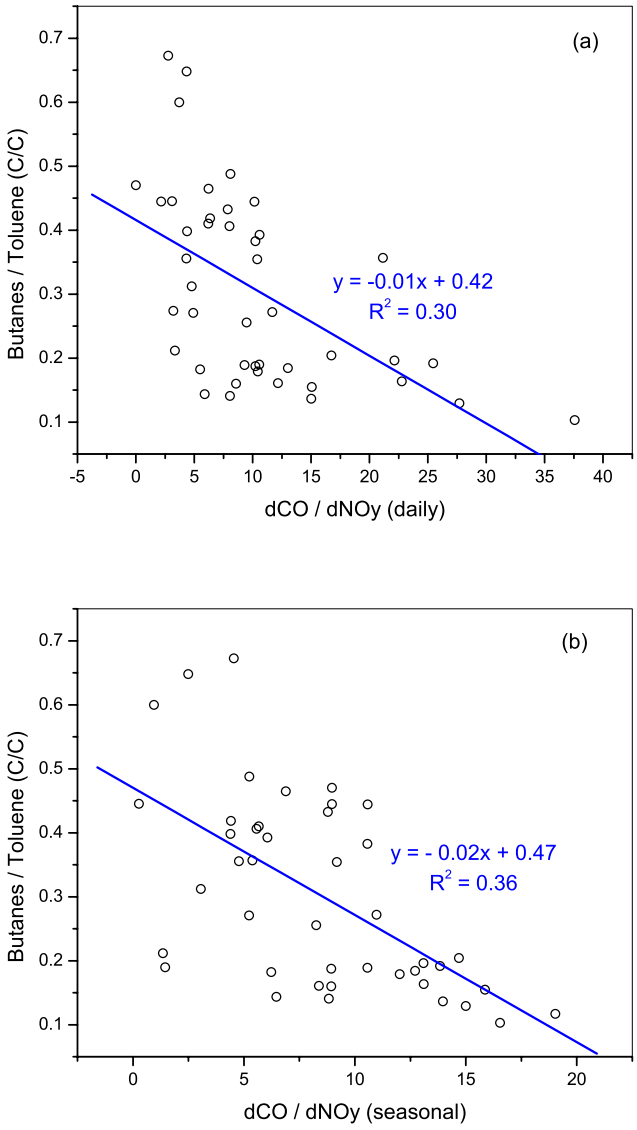

Figure 3.4.19 Scatterplots of the butanes-to-toluene ratio versus dCO/dNO_y observed at TO: (a) Using 24-hour dCO/dNO_y; (b) Using the seasonal dCO/dNO_y. Note: These scatterplots were obtained by omitting two outlying datapoints (see text).

that happened to have very high CO and very low toluene concentrations and were outside the upper 95% confidence interval of dCO/dNO_y. If these two points are included in the scatterplot (Figure 3.4.20), the statistical relationship between dCO/dNO_y and the butanes-to-toluene ratio at TO is lost.

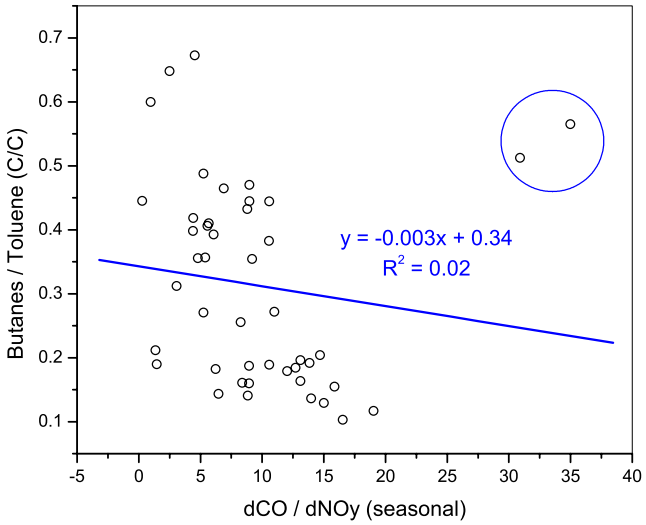

Figure 3.4.20 Scatterplots of the butanes-to-toluene ratio versus the seasonal dCO/dNO_y observed at TO when two outlying datapoints (circles) are included.

3.4.8.2 Xylene Ratios: I now turn my attention to xylenes, the other dominant VOC species observed in Hong Kong during the field campaign. Recall from my earlier discussion that the observed variations of xylenes in Hong Kong had some similarities to toluene and also some differences. On Nov. 7, the 24-hour averaged reactivity from xylenes was greater than that of toluene at all sites. The time-resolved data for TO indicated that on most episode days the reactivity contribution from toluene tended to increase somewhat as the days progressed, a tendency consistent with the fact that xylenes are more reactive than toluene. However, more anomalous behavior was observed at TO on Oct. 11 and Nov. 7 when xylenes dominated the reactivity in the early

morning but declined rapidly relative to that of toluene during the late morning and early afternoon. The rapid decline in xylenes' contribution on these two days could be indicative of xylenes and toluene having different sources. In fact, emission inventories for these two species generally indicate that they do indeed have different sources. Inspection of Figure 3.4.15 derived from the emissions inventory obtained from the earlier PRD study reveals that emissions from the transportation sector tend to be more important for xylenes than for toluene.

To investigate this possibility I analyzed the ratio of p-xylene to total xylenes as a function of the total xylene concentration (Figure 3.4.21). For most of the data gathered at the EPD sites, the ratio of p-xylene-to-total xylenes hovers around 0.2 - 0.3. Thermodynamic equilibrium in the reforming process used in gasoline and aromatics production tends to produce a ratio of p-xylenes-to-total xylenes of ~ 0.25 (J. Schauer, private communication, 2004). Thus, much of the xylene observed at the EPD sites can be rationalized in terms of emissions related to transportation; e.g., evaporation of gasoline. In the case of TO, however, most of the datapoints have p-xylene-to-total xylene ratios greater than 0.3. This suggests that, during most of the episode days, a major source of the xylenes at TO, like that of toluene, was non-mobile and related to industrial/petrochemical activities. This in turn implies that the "additional source" of VOCs I inferred earlier for TO and TC that was enriched in R-AROMs is also likely related industrial/petrochemical activities.

However, there is a notable exception to the above conclusion. Note in Figure 3.4.21 that there are five data points with extremely high total xylene concentrations (i.e., greater than 50 ppbC) and the p-xylene-to-total xylene ratio for these were all around 0.3,

a ratio consistent with a source related to transportation and close to that observed at the EPD sites. Interestingly, all the datapoints were observed in the early morning hours of Oct. 11 and Nov. 7 – the two days with anomalously high early morning concentrations of VOCs, NO, and CO at TO. This suggests that the anomalously high concentrations of pollutants at TO on Oct. 11 and Nov. 7 was most likely associated with transport of urban-type emissions typical of the other EPD sites and not due to emissions from a transient source near TO.

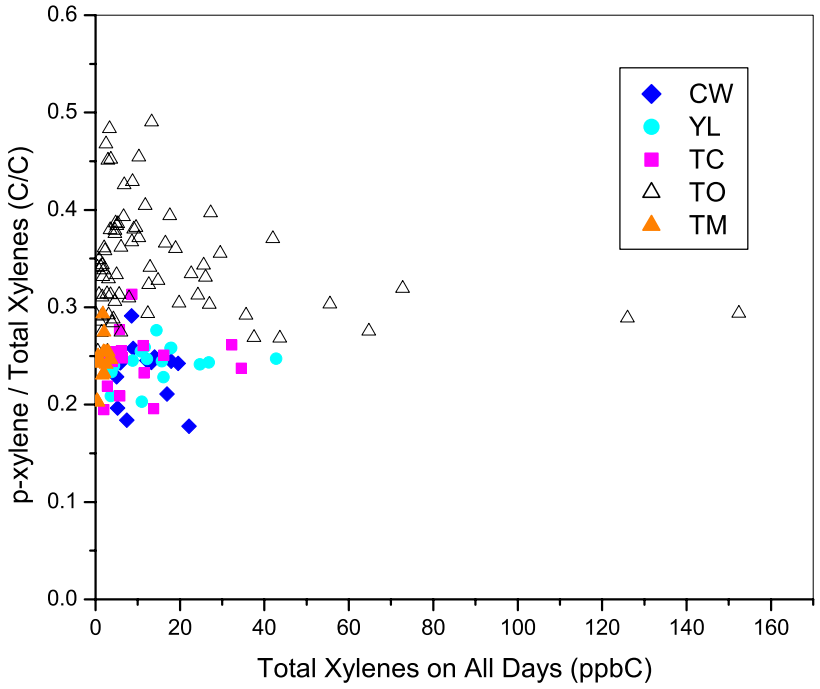

Figure 3.4.21 Observed ratios of p-xylenes-to-total xylenes as a function of total xylenes concentration at various sites.

3.4.8.3 Summary: Analyses of the speciated VOC data suggest that the xylenes observed at the EPD sites on Nov. 7 were dominated by sources related to the transportation sector. However, the additional sources of VOC impacting TO and TC were likely related to

petrochemical/industrial, waterfront, and/or fuel-storage activities. Anomalously high pollutant concentrations at TO in the early morning hours of two episode days, on the other hand, appear to have come from transport of emissions from sources similar to those impacting the EPD sites. Negative correlations between VOC ratios and dCO/dNO_y suggest that sources from the Guangdong Province are a significant, but not sole, contributor to the additional VOCs observed at TO and TC. By extension it appears likely that Guangdong Province is contributing significantly to the high concentrations of R-AROM species observed throughout Hong Kong.

3.5 O_3 production and Relative Incremental Reactivity

In this section I summarize the results of my application of the Observation Based Model (OBM) to the data collected at each of the five sites on the November 7th episode and at TO on all episode days. I begin with a brief overview of the OBM.

3.5.1 Introduction to OBM

The OBM (Cardelino and Chameides, 1995) uses the concentrations of hydrocarbons, nitric oxide, carbon oxide and ozone, as well as meteorological data measured as a function of time at a given location as input for a coupled set of photochemical box models that calculates the total amount of ozone photochemically produced during the daytime at each location. The models also calculate the sensitivity of the ozone production to changes in the concentrations of the precursor compounds. Because the concentrations of a given precursor compound are directly related to its emission rate, this model-calculated sensitivity can be used to determine the sensitivity of

ozone photochemical production to emissions of precursors in the area of measurements without a detailed knowledge of the emissions.

To calculate the ozone photochemical production, two base simulations of OBM are needed to be carried out. The first simulation uses the concentrations of O_3, NO, CO and the primary VOC functional groups specified as a function of time to calculate the concentrations of the unspecified species by solving equations of the following form,

$$\frac{\partial C_j}{\partial t} = P_j - L_j - D(t)(C_j - C_j^{FT}) \qquad (3.2)$$

where C_j is the concentration of the j^{th} unspecified species, and P_j and L_j are the photochemical production and destruction rates of species j respectively, C_j^{FT} is the free tropospheric concentration of species j (assumed to be zero for all unspecified species), and D(t) is related to the mixing height variation following the method described for the OZIPM4 model (Hogo and Gery, 1988). Also during the first simulation, the time-dependent source function $\Sigma_i(t)$ is calculated by solving equations of the following form,

$$\Sigma_i(t) = [\frac{\partial C_i}{\partial t}]_{obs} - P_i + L_i + D(t)(C_i - C_i^{FT}) \qquad (3.3)$$

where C_i is the concentration of the i^{th} specified species, and $[\partial C_i / \partial t]_{obs}$ is the observed local time derivative in C_i. This source function, $\Sigma_i(t)$ (in unit of ppb hr^{-1}), in fact represents the combined effects of emissions at the site, horizontal transport to the measurement site, and the horizontal transport away from the measurement site.

Once the source functions are determined, a second calculation is done following Equation 3.4,

$$\frac{\partial C_i}{\partial t} = P_i - L_i + \Sigma_i - D(t)(C_i - C_i^{FT}) \qquad (3.4)$$

In this second base simulation, all species are calculated. By integrating the coupled differential equations of the form 3.2, the unspecified species are again calculated, while by solving equations of the form 3.4, the species previously specified in the first base simulation are calculated. By the second base simulation, the ozone production potential ($P^s_{O3\text{-}NO}$, which is the integration of model-calculated rates of O_3 production and NO destruction) is calculated.

To assess the sensitivity of O_3 production at each site to variations in precursor concentrations, source reduction simulations are carried out by varying the input concentrations as well as the source functions. In the OBM calculations described here the input concentrations and source functions are changed by 10%. In the OBM, this sensitivity is calculated as the relative incremental reactivity (or RIR) (Cardelino and Chameides, 1995); i.e.

$RIR^s(X)$ = the % decrease in ozone production at site S per % decrease in the concentration of a given precursor compound or class of compounds X at site S.

Since the production of O_3 is related to the concentration of O_3 at a site, and the concentration of a precursor is essentially linearly related to its emissions, RIR can be used as a metric for the effect of a given emission reduction on O_3 concentrations at a site. To calculate the RIR function for a specific precursor or class of compounds over multiple sites, an area-averaged RIR function is used as follows:

$$\overline{RIR(X)} = \frac{\sum_{S}^{NS}[RIR^S(X)P^S_{O_3-NO}(HC_i, NO, O_3, CO)]}{\sum_{S}^{NS}P^S_{O_3-NO}(HC_i, NO, O_3, CO)} \qquad (3.5)$$

And the standard deviation for this area-averaged RIR function is defined by:

$$\sigma^2_{\overline{RIR(X)}} = \frac{\sum_{S}^{NS}[(RIR^S(X)^2 - \overline{RIR(X)}^2)P^S_{O_3-NO}(HC_i, NO, O_3, CO)]}{(NS)(\sum_{S}^{NS} P^S_{O_3-NO}(HC_i, NO, O_3, CO))} \quad (3.6)$$

The standard error of the mean for this area-averaged RIR function is given by:

$$\sigma = \frac{\sqrt{\sigma^2_{\overline{RIR(X)}}}}{\sqrt{NS}} \quad (3.7)$$

There are internal tests that can be carried out to confirm that the application of the OBM to a given dataset is appropriate. One test is to assess the consistency of the RIR's across multiple sites and/or multiple days; for example, if σ defined above is relatively small, the RIR's calculated are more likely to be robust. Another test is to consider the magnitude of the ozone production calculated by the OBM at each site and compare it to the increment of O_3 observed at the site during the episode. If the ozone production calculated is similar in magnitude to the observed increment, it suggests that the RIR pertains to a significant portion of the amount of O_3 that appeared at the site and is therefore relevant to policy-making decisions with regard to emission control strategies.

As noted earlier, because the OBM uses observed concentrations, it is an observation-based as opposed to an emission-based model. It complements emission-based model as part of a weight-of-evidence approach to air quality control.

3.5.2 Deduction of hourly profile of VOC

Since the VOC data at the four EPD sites are 24-hour averages, it is necessary to derive time-dependent concentrations from the averages for use in the OBM. In this section I discuss how this is accomplished within the general framework of the OBM technique.

The method is based on the entraining eulerian box model (Seinfeld and Pandis, 1997). Assuming the atmosphere in the area of interest is well-mixed, the concentrations of a species is determined by the factors of emission, chemical reaction, deposition (dry/wet), advection, and vertical entrainment. Equations 3.8a and 3.8b give the resulting time rate of change in the concentration of species "i":

$$\frac{dc_i}{dt} = \frac{q_i}{H(t)} + R_i - \frac{v_{d,i}}{H(t)} c_i + \frac{c_i^0 - c_i}{\tau_r} \qquad for \frac{dH}{dt} \le 0 \qquad (3.8a)$$

$$\frac{dc_i}{dt} = \frac{q_i}{H(t)} + R_i - \frac{v_{d,i}}{H(t)} c_i + \frac{c_i^0 - c_i}{\tau_r} + \frac{c_i^a - c_i}{H(t)} \frac{dH}{dt} \qquad for \frac{dH}{dt} > 0 \qquad (3.8b)$$

Here c_i is the concentration (mol m^{-3}) of species i, q_i is the emission rate (mol m^{-2} s^{-1}) of species i per unit area, R_i is its chemical production/destruction rate (mol m^{-3} s^{-1}), $v_{d,i}$ is its dry/wet deposition rate (m s^{-1}) (assumed to be zero for all the hydrocarbons), c_i^0 is the background concentration, τ_r is the residence time of air over the area (which is the ratio of the length of the box to the prevailing wind speed), c_i^a is the concentration (mol m^{-3}) of species i above the boundary layer (assumed to be zero for all the hydrocarbons), and H(t) is the mixing height (m) as a function of time (t). For my purposes, the advection term $(c_i^0 - c_i)/\tau_r$ in equations 3.8a and 3.8b is combined with the emission term $q_i / H(t)$. Equations 3.8a and b are solved using Gear's backward differentiation formula (see for example, Jacobson, 1999).

Since emission rates for the different VOCs and their chemical destruction rates are unknown, I therefore adopt an iterative approach to determine the hourly variations in the VOC species, along with their emission and destruction rates on the basis of their 24-hour averaged concentrations and other inputs. I begin by assuming an initial OH profile

and an emission rate for the VOCs, and then calculate the time variation in the VOC species. The resulting 24-hour averaged VOC concentrations thus calculated are compared to the observed 24-hour average concentrations, the emission rates are appropriately scaled to bring the calculated 24-hour averages in line with the observed averages, a new OH profile is calculated on the basis of the VOC concentrations, and the process is repeated until convergence is obtained. In the results presented 2% consistency is used as the basis for establishing consistency.

In addition to calculating the diurnal VOC profiles, this approach is also used to calculate the diurnal profiles in HONO, formaldehyde and higher aldehydes; species that were not observed during the field campaign but can impact the OBM results. These calculations and their implications are discussed in Section 3.5.3.1.

3.5.2.1 Emission Rates: The annual emissions of speciated anthropogenic VOC (Streets et al., 2003, also available at the website http://www.cgrer.uiowa.edu/EMISSION DATA/index_16.htm) from the TRACE-P project of NASA were used to set the initial VOC emission rates of the VOCs. The diurnal variations in the anthropogenic VOC emissions were estimated on the basis of the source type: industry and power generation were assumed to have no diurnal variation; domestic sources were kept constant during the daytime while at night (e.g. 9pm-5am) were set to 0; mobile emissions were allowed to have a diurnal variation that differed as a function of day of the week (Cardelino, 1998). The diurnal variations of biogenic VOC (isoprene, α-pinene and β-pinene) were estimated considering the temperature and solar radiation.

3.5.2.2 Mixing height profile: The estimation of mixing height is based on the principle that heat transferred to the atmosphere at the surface results in convection, vigorous

vertical mixing, and establishment of a dry-adiabatic lapse rate (Holzworth, 1967). Here upper air soundings and hourly temperature are used to compute the twice-daily mixing heights. The upper air soundings are reported by National Climate Data Center (NCDC) and available at the website of NOAA http://raob.fsl.noaa.gov/. To compute the morning mixing height, the minimum temperature at the surface from 2am local standard time (LST) to 6am LST, inclusive, is determined. To this value is added 2^{o}C to account for the temperature differences between the rural and urban environments and for some initial surface heating just after sunrise. While a 5 ^{o}C difference was adopted by Holzworth (1967), Hong Kong has latitude of 22.32^{o}N and the daily temperature difference of different areas is probably not as much as at mid-latitudes, and so a 2^{o}C difference seems more appropriate. To estimate the morning mixing height, this adjusted minimum surface temperature is assumed to follow the dry adiabatic lapse rate up to the intersection with the observed 0000 GMT temperature sounding; the mixing height is taken as the altitude of this intersection. For the afternoon mixing height, the maximum temperature at the surface from 12pm LST to 4pm LST, inclusive, and the 1200 GMT sounding are used, except that the surface temperature is not adjusted. With the morning and afternoon mixing heights, the hourly mixing height profile is obtained by interpolating between these two heights, considering that the mixing height increases rapidly after sunrise in early morning while it increases slowly in early afternoon until it reaches the afternoon mixing height.

3.5.2.3 Results: The calculated diurnal variations in the total VOC reactivity on Nov. 7 at the 4 EPD sites along with the observed diurnal profile at TO are illustrated in Figure

3.5.1. The similarity between the observed profile at YL and the observed profile at TO (two sites with similar average reactivities) is encouraging.

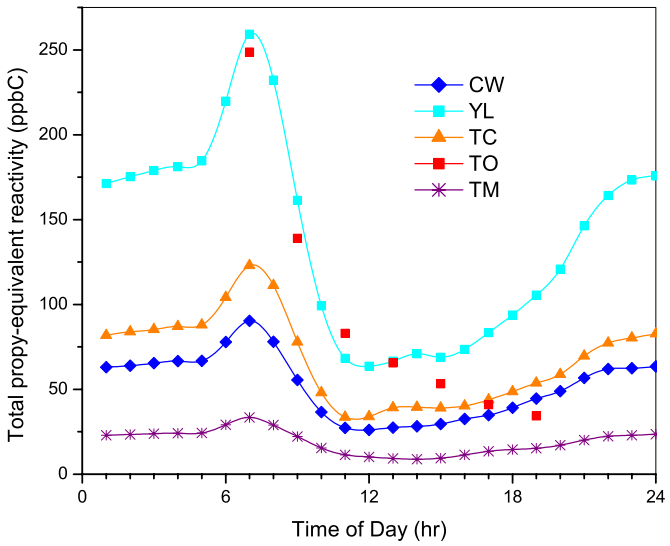

Figure 3.5.1 Inferred diurnal profile of total reactivity from VOCs at CW, YL, TC, and TM and the measured reactivity profile of VOC at TO.

3.5.3 OBM-Calculated Net O_3 Production

In principle, the O_3 that appears at a given site during an episode is due to local photochemical production plus the transport of O_3 that has been produced elsewhere. However, the OBM only calculates the O_3 produced locally and/or in air masses with similar chemical compositions as that found locally. As a result the RIR functions calculated by the OBM only pertain to the O_3 produced locally; i.e., they represent estimates of the sensitivity of the O_3 produced locally to changes in precursor concentration/emissions and not of the O_3 that had been transported to the site. If local production represents a significant portion of the total O_3 increase (or increment) experienced in the area then this feature of the OBM does not represent a significant

limitation; if local production is much smaller than the O_3 increment, then the RIR functions calculated by the OBM are of limited utility. In this section I examine this issue by comparing the net photochemical production O_3 calculated by the OBM at each site with the actual O_3 increment (or increase) observed at each site over the course of the episode day.

Figure 3.5.2a and 3.5.2b illustrates the model-calculated net O_3 production and observed O_3 increment at each of the sites on Nov. 7 and at TO for all episode days, respectively, with and without early morning HONO and aldehydes (see Section 3.5.3.1). Inspection of the figures suggests one of two conclusions: Either (i) early morning HONO and aldehyde concentrations at the sites during the episode days were not significant (and were much lower than those estimated by the OBM), and the photochemical production estimated by the OBM is only able to account for a small fraction of the O_3 increments observed at the sites during the field campaign; or (ii) early morning HONO and aldehydes concentrations were significant (as estimated by the OBM), and as a result of the OH produced by these compounds in the early morning, the OBM is able to account for most of the ozone increments observed during episode days. Exceptions to the latter conclusions are: TC on Nov 7th and TO on Oct. 9th, Nov.6th, and Nov. 12th when the calculated O_3 production was significantly less than the observed increment even with early morning HONO and aldehydes included.

3.5.3.1 The role of HONO and aldehydes in early morning chemistry: Previous investigators have found that the presence of HONO and/or aldehydes in the urban atmosphere in the early morning hours can significantly enhance the amount of O_3 produced over the course of the day (Jenkin et al., 988; Alicke et al., 2002, 2003;

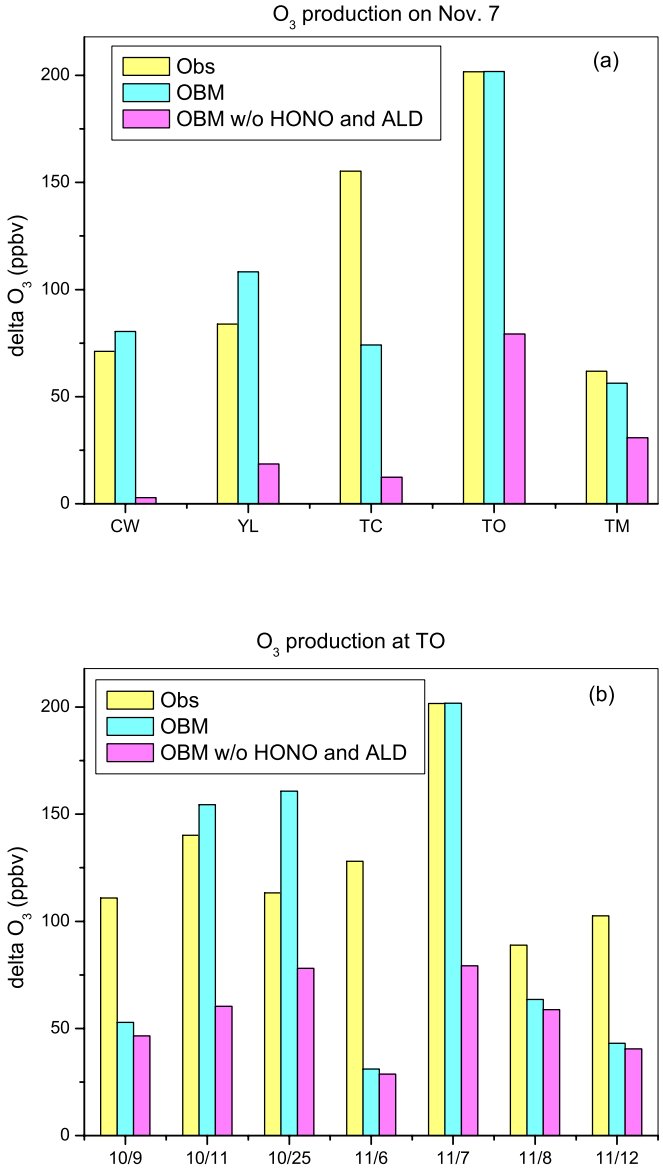

Figure 3.5.2 Comparison of net O_3 photochemical production calculated by the OBM and the observed O_3 increment: (a) at all sites on Nov. 7; and (b) at Tai O on episode days. Results are shown for OBM calculations with and without early morning HONO and aldehydes (see Section 3.5.3.1).

Finlayson-Pitts et al., 2003). HONO and aldehydes are fairly reactive and as a result their concentrations are usually fairly small during most of the daylight hours. However, at night, in the absence of sunlight and OH, their concentrations can accumulate if sufficient sources of these compounds are present. Then, in the early morning, when the sun first appears, they can be rapidly photolyzed; one product of this photolysis is OH. Because other sources of OH (e.g., O_3 photolysis) tend to be small in the early morning, HONO and aldehyde photolysis can represent a significant early-morning source of OH, and this source can jump-start the photochemical reactions that lead to O_3 production. The net result is more O_3 production over the entire course of the day.

HONO and aldehydes were not measured during the field campaign and thus could not be specified in the OBM. I therefore carried out two sets of OBM calculations: in the calculations labeled OBM w/o HONO and ALD I assumed that no HONO, H_2CO, and higher aldehydes were present in the morning; in the standard OBM calculations I allowed the OBM to estimate the early morning HONO, H_2CO, and ALD concentrations using the iterative process described in Section 3.5.2. In these calculations, I assumed that HONO was produced at night via a heterogeneous reaction involving NO_x

$$2NO_2 + H_2O \xrightarrow{surface} HONO + HNO_3 \qquad (3.9)$$

And further assumed a mixing height dependent rate constant following Harrison et al. (1996); e.g.

$$\text{Rate Constant for HONO Production} = \frac{3.36\times10^{-2}}{MixingHeight(m)}(\text{min}^{-1}) \qquad (3.10)$$

Nighttime losses of HONO included dry deposition (with a rate constant of 1.2/mixing height (m) in unit of min^{-1}).

Illustrative of my results are the diurnal variations in HONO, formaldehyde and higher aldehydes calculated by the OBM at TO on Nov. 7th in Figure 3.5.3a. Note the high HONO concentrations (of ~ 10 ppbv) just before sunrise. As the sun comes out, however, HONO starts to photolyze and its concentration rapidly drops to sub-ppbv levels. However, as illustrated in Figure 3.5.3b, the photolysis of HONO in the early morning represents the major source of OH in the OBM calculations, and, as a result, early morning OH concentrations are significantly enhanced (Figure 3.5.3c). Inspection of the figures reveals that, although the concentrations of formaldehyde and higher aldehydes are higher than HONO, their impact on OH production from these species is relatively small. Inspection of the figures also indicates that after ~1100 hours, HONO concentrations have fallen sufficiently and O_3 photolysis takes over as the dominant source of OH.

Figure 3.5.4 shows similar results at CW on Nov. 7th. The results at CW are even more pronounced than those discussed above for TO. At CW on Nov. 7th, the concentration of NO after sunset was in excess of 40ppbv and even reached 111ppbv at 8pm. This high level of NO led to extremely high HONO production rates and as a result the OBM predicted a peak HONO concentration of ~ 20 ppbv just before sunrise. As a result, the OH production rate from HONO at 0700 hours was calculated to be more than four orders of magnitude higher than that from O_3 and this, in turn, led to more than an order of magnitude increase in OH. Not surprisingly, the difference in the OBM-calculated net O_3 production at CW with and without HONO and aldehydes is quite substantial (see Figure 3.5.2). Figures 3.5.5 and 3.5.6 show the role of HONO and aldehydes in the early morning chemistry at YL and TC on Nov. 7th. Here again, the

OBM calculations suggest that HONO played an important role in the early morning chemistry provided that HONO was present at the concentrations derived from the OBM calculations.

3.5.3.2 Summary: The OBM is able to account for a significant fraction of the O_3 increment observed at the sites during episode days, but only by including a heterogeneous chemical mechanism for generating HONO in the nighttime hours from NO_x that results in pre-dawn HONO concentrations of several ppbv to as much as 20 ppbv. Future field experiments will be needed to determine if the OBM-based predictions of large HONO concentrations in the early morning hours in the Hong Kong area and the resultant enhancement in early morning OH production rates are appropriate.

3.5.4 Relative Incremental Reactivity

3.5.4.1 RIR's on Nov. 7: Figure 3.5.7 shows the calculated RIRs for AHC, NHC, CO and NO_x at each site on Nov 7, and Figure 3.5.8 shows the area averaged RIRs for each precursor group. Inspection of the figures reveals that AHC is the group with the highest RIR, meaning that AHC is the most important group in producing O_3. NHC has a significant RIR at TM, the most rural site, but even here AHC has a larger RIR. Not surprising in light of the reactivity analysis presented in Section 3.4, R-AROM have the largest RIR among the AHC sub-groups.

RIR for NO_x is negative at all the sites except TO where the RIR for NO_x is essentially zero, and the area-averaged RIR for NO_x is also negative. This negative RIR for NO_x is the result of the relatively high NO concentrations that were typically encountered at the sites during the field campaign and suggests that throughout the Hong Kong area O_3 photochemistry is strongly VOC-limited, and that initial reductions in NO_x

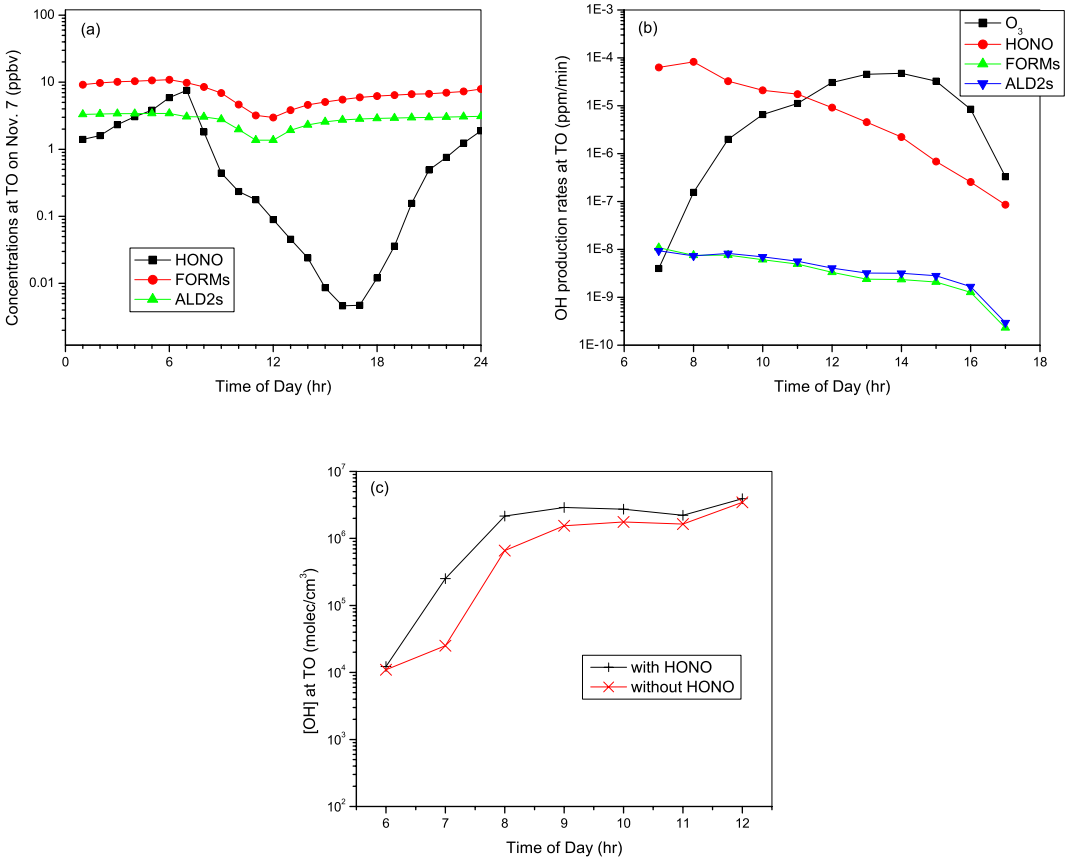

Figure 3.5.3 a): OMB-calculated concentrations of HONO, formaldehyde and higher aldehydes at Tai O on Nov. 7, 2002; b): OBM-calculated OH radical production rates from photolysis of O_3, HONO, formaldehyde and higher aldehydes at Tai O on Nov. 7, 2002; c): Comparison of OBM-calculated OH concentrations at TO on Nov. 7, 2002 with (black line) and without (red line) inclusion of early-morning HONO and aldehydes.

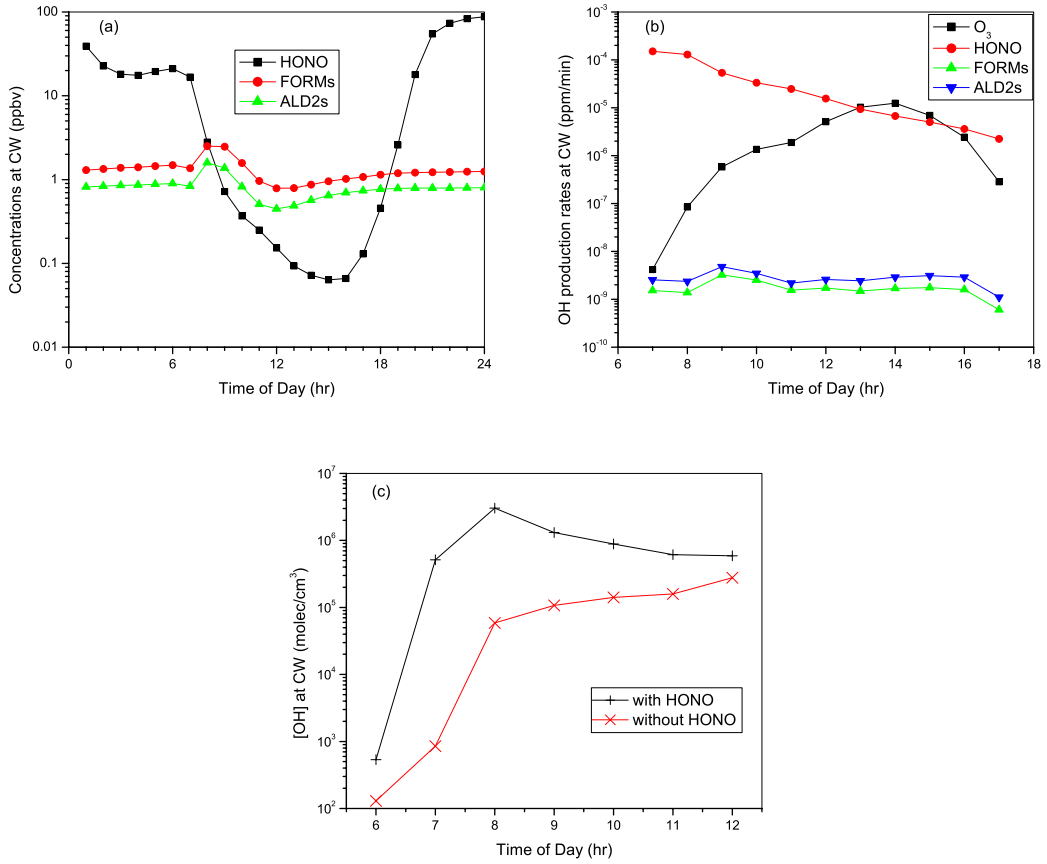

Figure 3.5.4 a): OMB-calculated concentrations of HONO, formaldehyde and higher aldehydes at CW on Nov. 7, 2002; b): OBM-calculated OH radical production rates from photolysis of O_3, HONO, formaldehyde and higher aldehydes at CW on Nov. 7, 2002; c): Comparison of OBM-calculated OH concentrations at CW on Nov. 7, 2002 with (black line) and without (red line) inclusion of early-morning HONO and aldehydes.

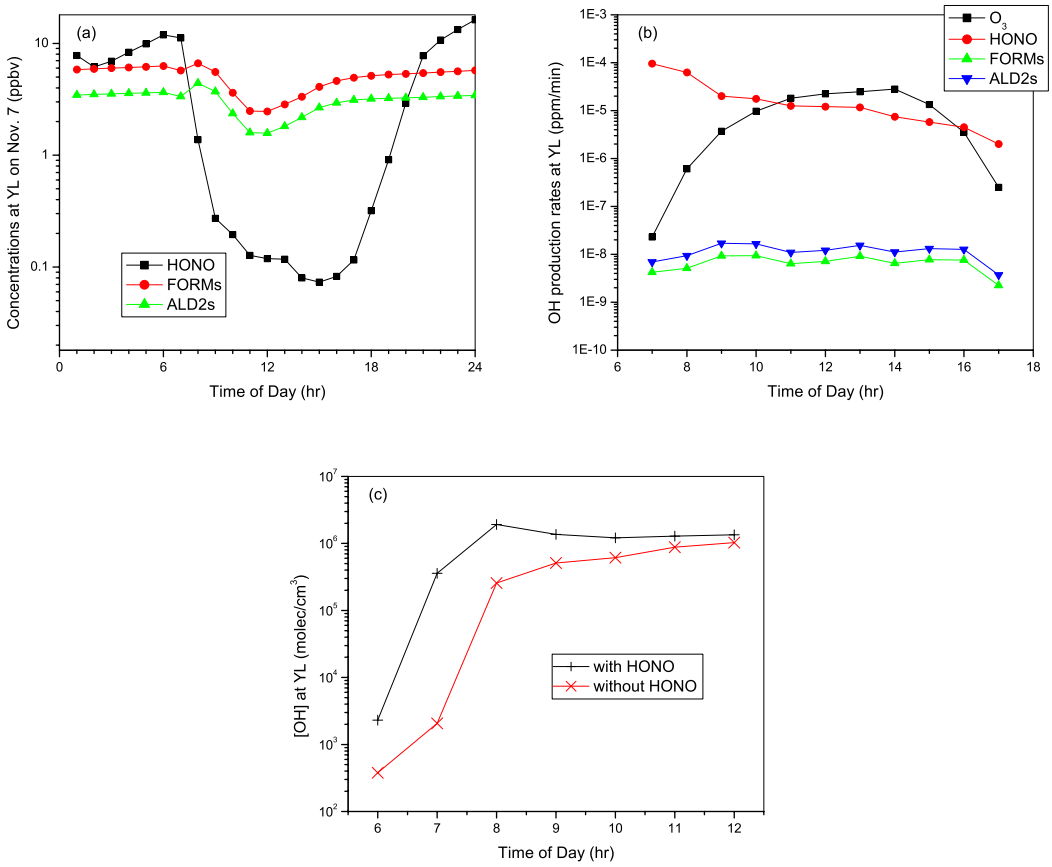

Figure 3.5.5 a): OMB-calculated concentrations of HONO, formaldehyde and higher aldehydes at YL on Nov. 7, 2002; b): OBM-calculated OH radical production rates from photolysis of O_3, HONO, formaldehyde and higher aldehydes at YL on Nov. 7, 2002; c): Comparison of OBM-calculated OH concentrations at YL on Nov. 7, 2002 with (black line) and without (red line) inclusion of early-morning HONO and aldehydes.

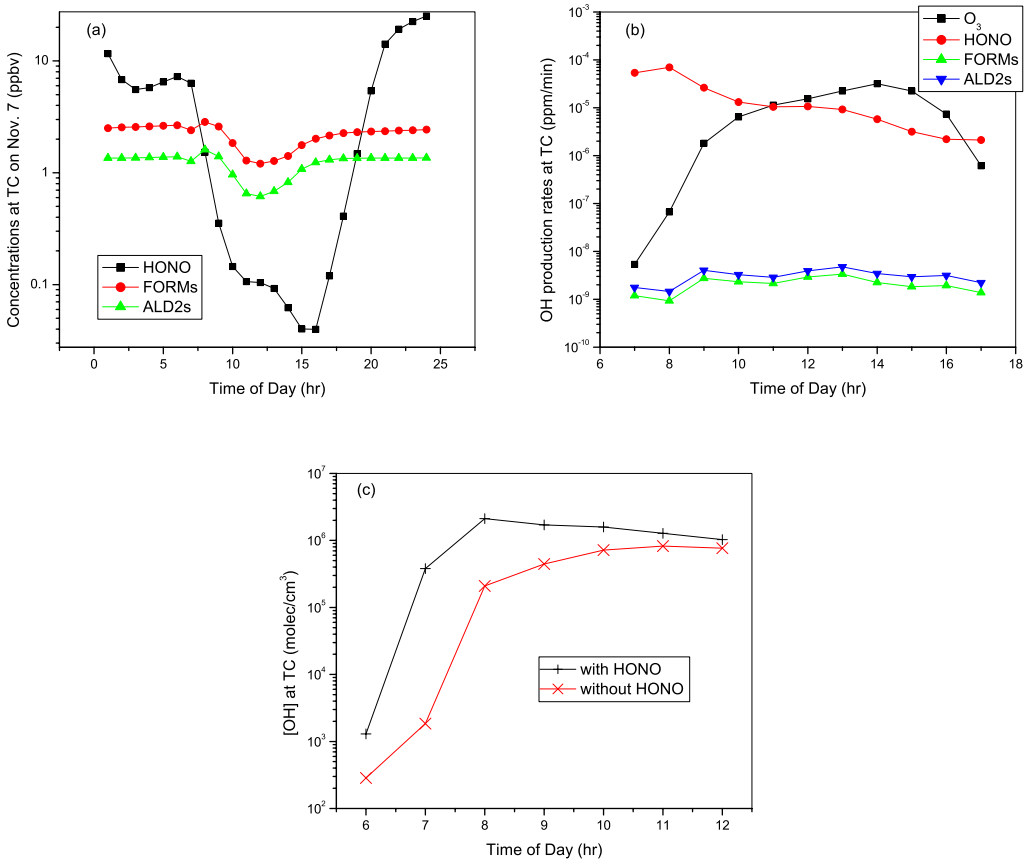

Figure 3.5.6 a): OMB-calculated concentrations of HONO, formaldehyde and higher aldehydes at TC on Nov. 7, 2002; b): OBM-calculated OH radical production rates from photolysis of O_3, HONO, formaldehyde and higher aldehydes at TC on Nov. 7, 2002; c): Comparison of OBM-calculated OH concentrations at TC on Nov. 7, 2002 with (black line) and without (red line) inclusion of early-morning HONO and aldehydes.

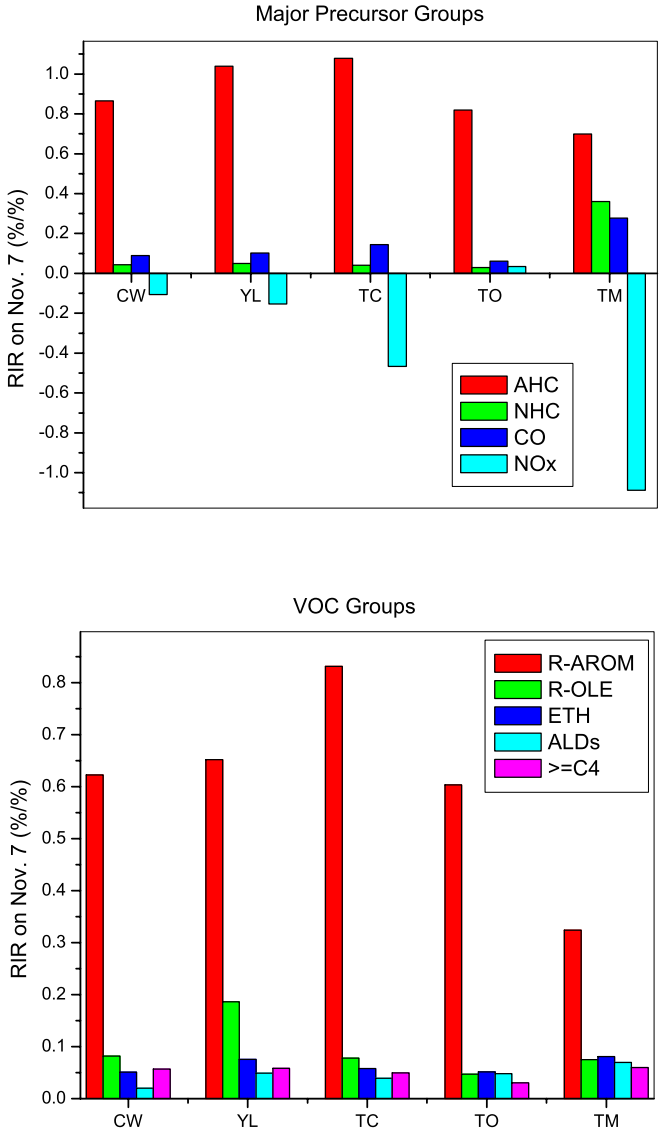

Figure 3.5.7 Calculated RIRs for various major O_3 precursor groups at all five sites on Nov. 7, 2002.

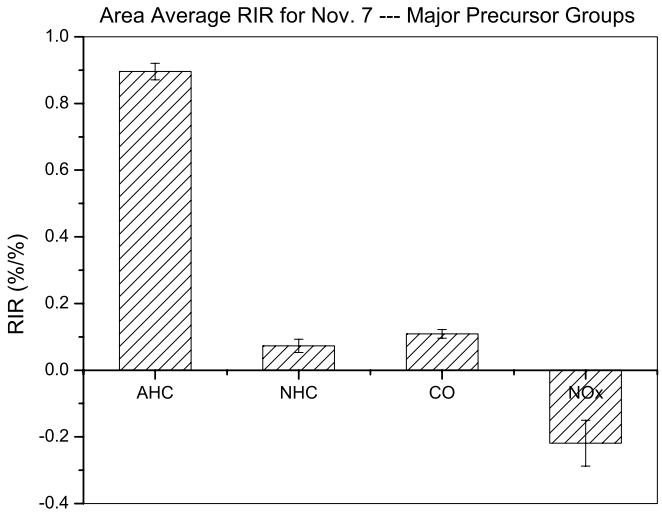

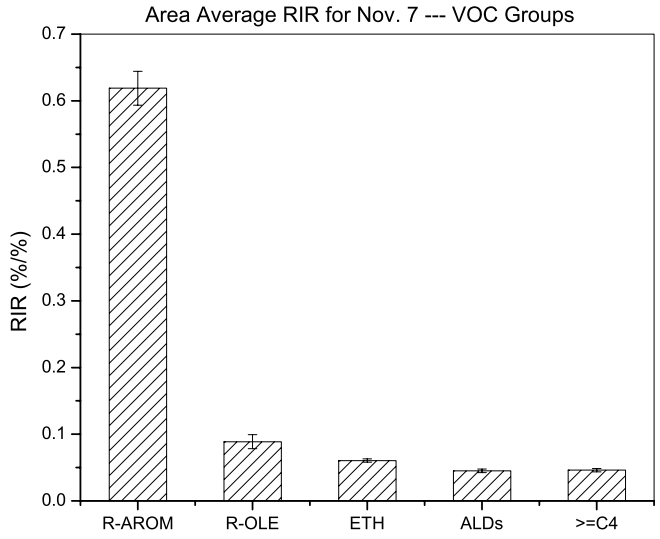

Figure 3.5.8 Calculated area-averaged RIR and σ, the standard error of the means for various major O_3 precursor groups on Nov. 7, 2002.

emissions in the area would actually lead to local O_3 enhancements.

Finally it should be noted that the standard error of the means in the area-averaged RIR's tend to be relatively small when compared to the RIR's themselves (see Figure 3.5.8). This suggests that, at least from a statistical point of view, the RIR functions calculated here are robust.

3.5.4.2 RIR's at TO: Figure 3.5.9 shows the calculated RIRs for the major O_3 precursor groups at TO on the episode days with VOC data. The results from TO generally confirm the results obtained from the other sites for the Nov 7th episode. AHC is the dominant precursor group with largest RIR's, and, among the AHC's, R-AROM dominate. NO_x tends to suppress O_3 production on most of the episode days except on Oct. 9th, and thus on all days except Oct. 9th the RIR for NO_x was negative. The anomalous result for Oct. 9th can be attributed to the fact that the NO concentrations on Oct 9th were significantly lower than the other episode days; the maximum NO concentration on Oct. 9th was only 5.5ppbv.

3.5.4.3 Sensitivity of RIRs to Model Uncertainties and Model Inputs: There are a large number of input parameters and model formulations in the OBM that are uncertain and add uncertainty to the RIR-functions calculated by the OBM. However, I have carried out a wide variety of sensitivity studies where I allowed input parameters and formulations to vary over reasonable ranges. In all cases, the results were essentially the same. For example, in Figure 3.5.10 I compare the RIR's obtained with the standard version of the OBM using diurnal profiles for VOC species as discussed in Section 3.5.2 with OBM results obtained with constant VOC concentrations as a function of time of day. While differences between the two calculations were obtained, the essential results are the same;

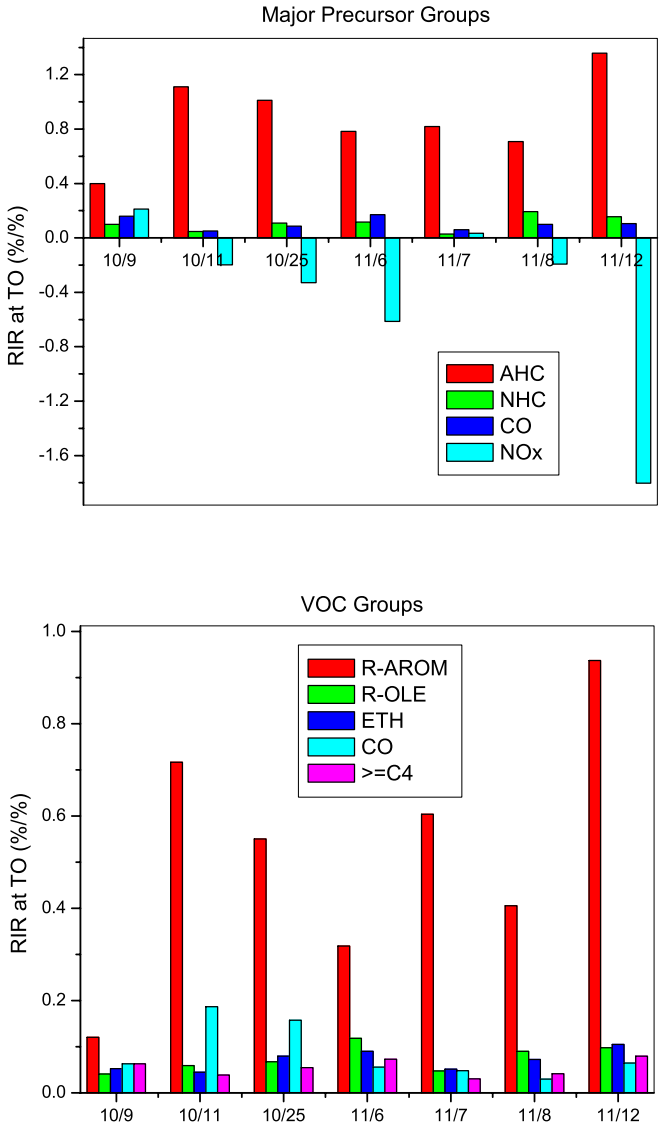

Figure 3.5.9 Calculated RIRs for various major O_3 precursor groups at TO on the episode days.

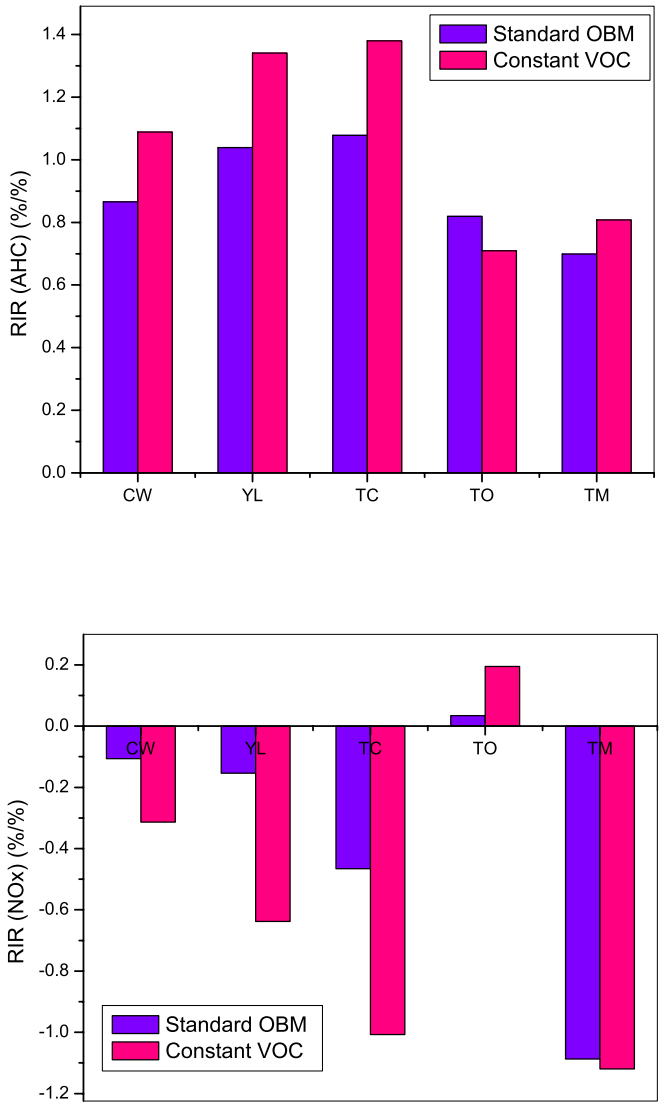

Figure 3.5.10 Sensitivity of OBM results to use of diurnally varying VOCs (Standard OBM) or constant VOCs. RIR's are illustrated for various sites on Nov. 7th for AHC (a) and NO_x (b).

i.e., the RIR's for AHC are large and positive and the RIR's for NO_x are negative at the four EPD sites or small at TO.

In Figure 3.5.11 I illustrate the sensitivity of the OBM results to method used to calculate the inputs into the OBM and method used to calculate the RIR functions. In the standard model, the hourly-averaged concentrations input into the model are arithmetic means of the high-resolution data collected at the sites. The RIRs are calculated from the difference in the net O_3 production for the observed concentrations and for a -10% of change in a precursor's concentrations. Figure 3.5.11 illustrates the effect on RIR's of using geometric means and of using a +10% change in a precursor's concentrations. Here again, the essential results of the OBM calculations are unchanged.

3.5.4.4 RIRs by sources: In addition to apportioning the RIRs by VOC functional group, the RIRs can be apportioned by source category. This approach requires the use of a speciated VOC inventory so that the RIRs associated with each species can be divided into their respective source-types. In the analysis presented here, I used the speciated VOC inventory described in Appendix B, which was in turn based on the general VOC inventory developed by the earlier PRD study [[CH2M HILL (China) Limited, 2002].

In Figure 3.5.12 I illustrate the calculated RIRs associated with the major VOC at all five sites on Nov. 7 (a) and the area average for Nov. 7 (b). Figure 3.5.13 shows the RIR's calculated for TO on the episode days with VOC data. The RIRs for stationary sources and mobile sources are found to be roughly equivalent with the RIR's for stationary sources tending to be, on average, somewhat larger than that for mobile sources.

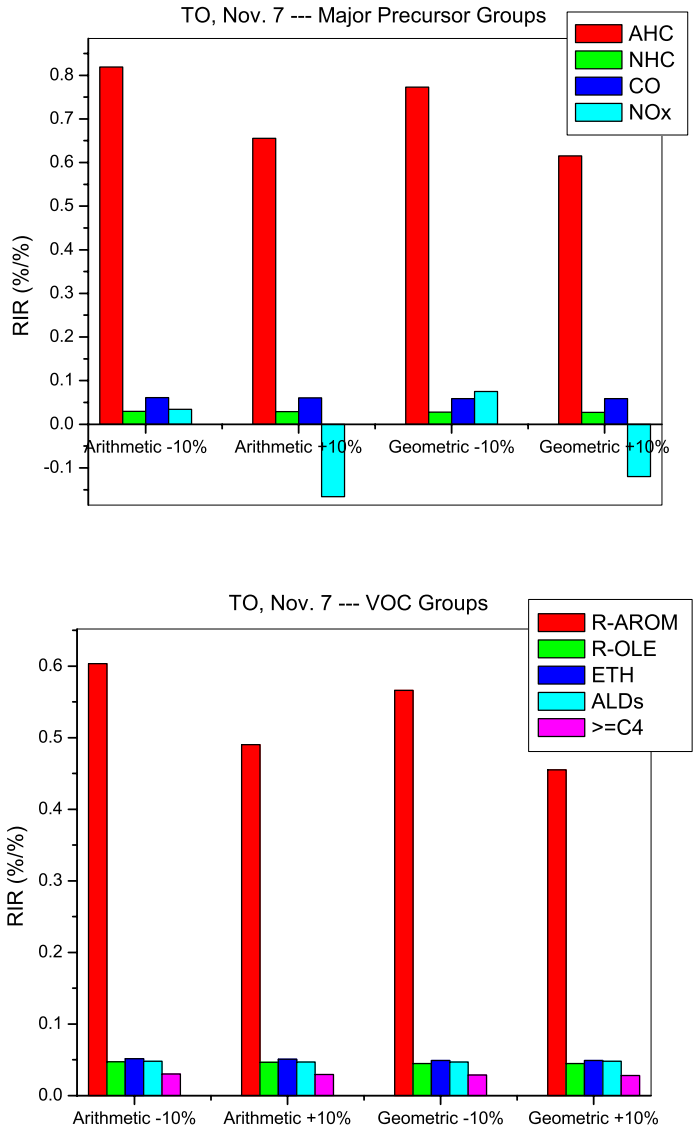

Figure 3.5.11 Comparison of RIRs calculated for TO on Nov. 7th with arithmetic and geometric means of NO and CO and using +10% and -10% changes in the precursor concentrations.

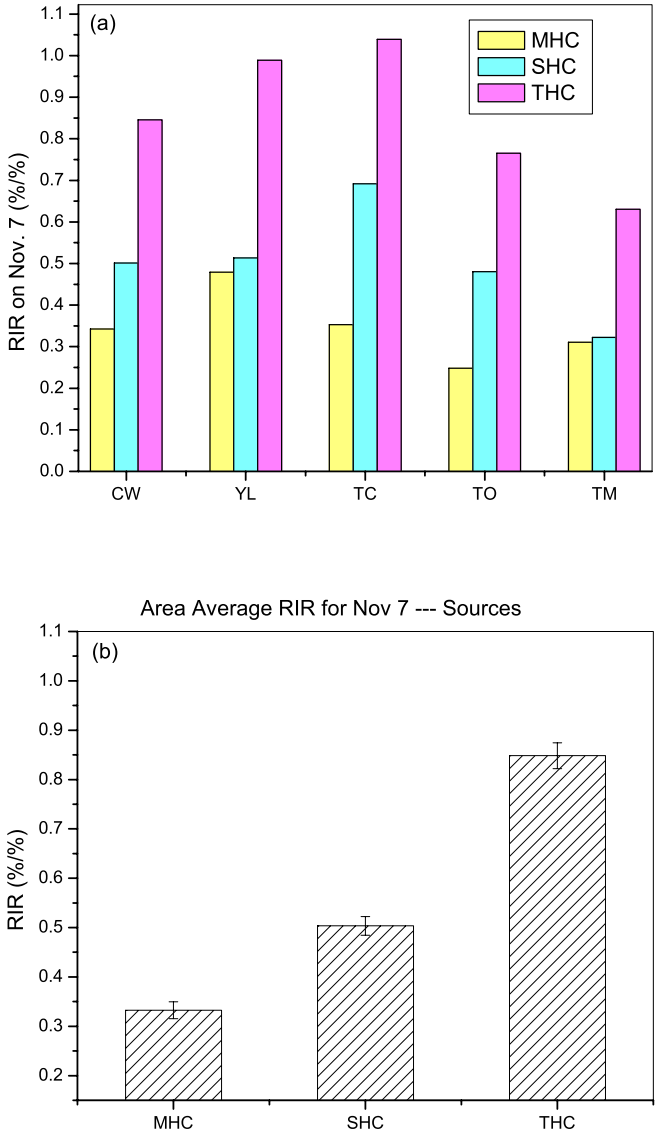

Figure 3.5.12 OBM-calculated RIRs associated with mobile (MHC), stationary (SHC), and total (THC) anthropogenic sources of VOC on Nov. 7: (a) RIR's at all five sites; (b) area-averaged RIR's with standard error of the means (σ) indicated by the vertical bars.

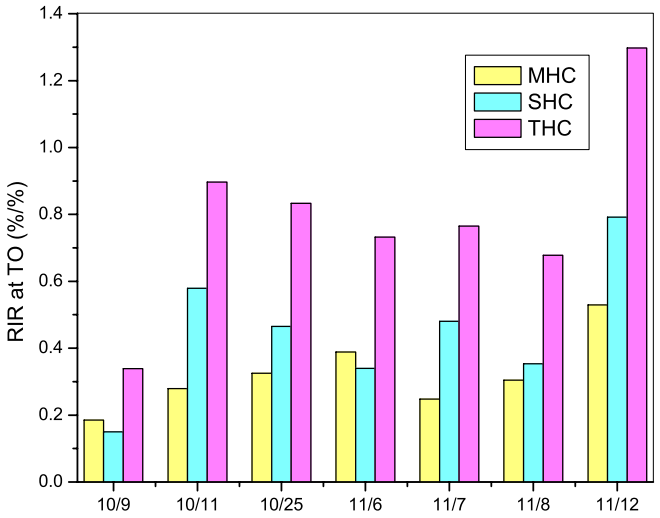

Figure 3.5.13 OBM-calculated RIRs at TO for episode days.

3.5.4.5. Summary: The OBM calculations indicate that the Hong Kong area was strongly VOC-limited during the period of the field campaign, with the RIR for AHC being considerably larger than those for NHC and CO and the RIR for NO_x being negative or close to zero. Of the groups of VOCs that make up AHC, R-AROM have the largest RIR. Thus, the results suggest that, on a ton-for-ton basis, emission controls of R-AROM would provide the most effective way to reduce O_3 in the area. The calculations also suggest that emission controls of both stationary sources and mobile sources of VOC would be effective with stationary-source controls being somewhat more efficacious.

3.6 Emission Inventories

In this section I present the results of a preliminary analyses using the speciated VOC measurements made during the field campaign to assess the accuracy of two existing VOC emission inventories for Hong Kong and the PRD area: (1) A speciated

VOC emissions inventory prepared by Dr. David Streets for the TRACE-P and ACE-ASIA field experiments and available at http://www.cgrer.uiowa.edu/EMISSION DATA/index_16.htm; and (2) the VOC emission inventory produced as part of the aforementioned earlier PRD study (see Section 3.3) and available on the Hong Kong EPD website (http://www.epd.gov.hk/epd/english/environmentinhk/air/studyrpts/study_pearl.html). (Note because the analyses presented here compare the emissions and observed ratios of selected VOC species, they require the existence of a speciated VOC inventory. However, the emissions inventory for VOC produced from the earlier PRD study was not speciated. In order to use this inventory here, the inventory was speciated as described in Appendix B.)

3.6.1 Butanes-to-Toluene

One useful approach to checking the speciation of VOC inventories is to compare ambient and emission ratios for VOC species that have similar lifetimes. As noted in Section 3.4.8, since VOC species with similar lifetimes react at the same rate, variations in their ratios should only reflect variations in their relative source strengths, and, on average, the ratio of their ambient concentrations should reflect the ratio of their emissions. Here, as in Section 3.4.8, I use the ratio butanes-to-toluene to assess the accuracy of the VOC inventories. Figure 3.6.1 shows the observed ambient butanes-to-toluene ratio at different sites in Hong Kong and the ratio from the two emission inventories for Hong Kong and for Guangdong Province. Inspection of the figure indicates that the ratios from the Streets inventory for both Hong Kong and Guangdong are considerably larger than that obtained from the ambient observations, indicating an inconsistency in the inventory. In the case of the inventory from the earlier PRD study,

on the other hand, I find that the ambient-measured ratios generally lie between the ratios derived from the emissions from Hong Kong and Guangdong. Given that emissions from Guangdong and Hong Kong both contribute to pollution in Hong Kong, this implies that the inventory from the earlier PRD study and its speciation are generally consistent with the butanes-to-toluene ratios observed at the sites during the field campaign.

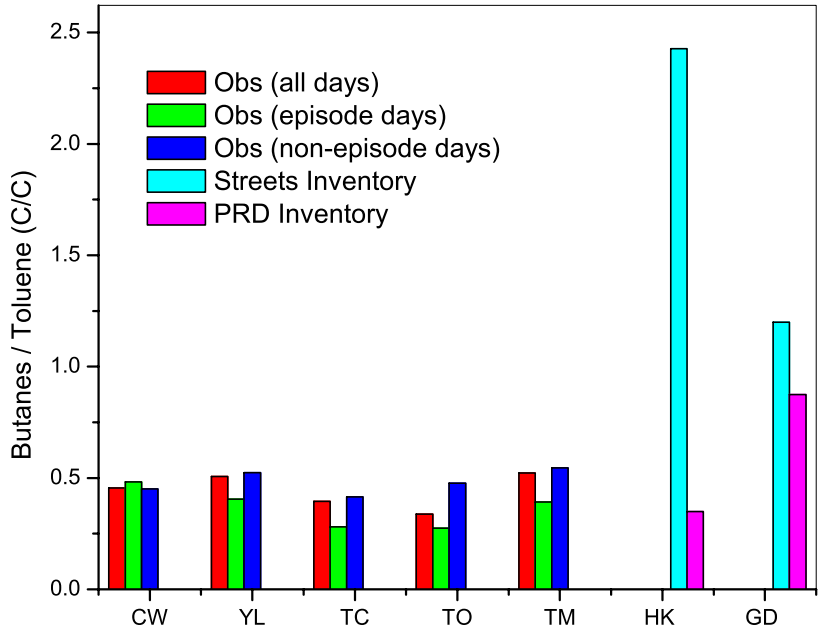

Figure 3.6.1 Average ratio of butanes-to-toluene observed in ambient air at different sites in Hong Kong and in the emissions inventories for Hong Kong (HK) and Guangdong Province (GD) from Streets [available at http://www.cgrer.uiowa.edu/EMISSION DATA/index_16.htm and the earlier PRD study [CH2M HILL (China) Limited, 2002].

3.6.2 Ratios of Alkanes

An alternate approach involves using two sets of ratios of VOC species with differing lifetimes and assessing how these ratios should vary in the atmosphere as they dilute and react. Extrapolation of the so-called "dilution lines" and reaction lines" back to time = 0 allows one to use the observed ratios of the VOCs to estimate the ratio of the

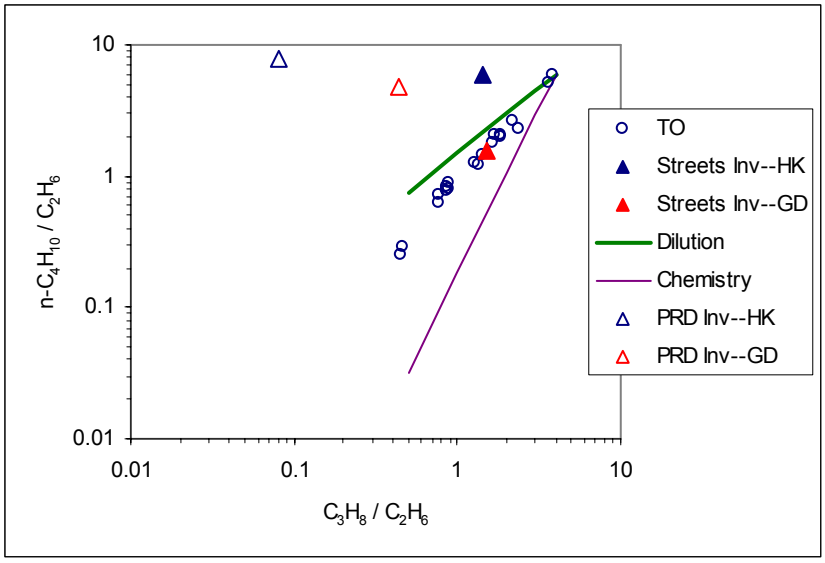

Figure 3.6.2 Ratios of n-butane-to-ethane vs. propane-to-ethane from observations of ambient air at TO and in the emission inventories for Hong Kong (HK) and Guangdong Province (GD) from Streets [available at http://www.cgrer.uiowa.edu/EMISSION DATA/index_16.htm and the earlier PRD study [CH2M HILL (China) Limited, 2002]. The two solid lines represent how these ratios would evolve in time as result of dilution only and photochemistry only.

emissions (see Mckeen and Liu, 1993 for complete discussions of this technique). Here I use the ratios of n-butane-to-ethane and propane-to-ethane. Figure 3.6.2 gives the relationship between the two ratios at TO on all episode days with VOC data and that from the speciation of the two VOC inventories. The two lines represent how these ratios would evolve in time as result of dilution only and photochemistry only; note all the data points lie inside these two lines reflecting their evolution from both dilution and photochemistry. The source of the VOCs should be on the right upper portion of the plot where the two lines intersect. However, the emissions ratios obtained from both inventories for both Hong Kong and Guangdong are located elsewhere. This suggests that the speciation of the VOC inventories in Hong Kong and Guangdong cannot be

rationalized with the ratios observed during the measurement period. (Note that n-butane is assumed to be ½ of butanes in the Streets emission inventory, since only the emission of total butanes is available at the website.)

3.6.3 Summary

Comparison of observed ambient ratios of selected VOCs and their ratios in speciated VOC emission inventories for Hong Kong and Guangdong Province provide mixed results. For butanes and toluene reasonable consistency between the ambient data and the speciated inventory derived from the earlier PRD study was obtained. This is encouraging since toluene (along with the xylenes) was generally found to be among the most important VOCs leading to the production of O_3 pollution in Hong Kong. However, the ratios of low-molecular weight alkanes in the emission inventories for both Hong Kong and Guangdong Province could not be rationalized with ratios observed for these species in ambient air. This lack of consistency could reflect inaccuracies in the gross inventories or in the methodology used to speciate the inventory or in the measurements themselves. And, in this regard it should be noted that the speciation for both the Streets inventory and the inventory from the earlier PRD study (see Appendix B) were based on emissions data obtained almost exclusively for sources operating in the United States and Europe and may very likely not be appropriate for sources operating in China. Clearly more measurements of the speciation of VOC sources in China will be needed in the future to resolve this issue.

3.7 Summaries

This study was designed to demonstrate the utility of observation-based approaches in air quality research and management by addressing four policy-relevant issues related to ozone pollution in the Hong Kong area. The specific issues and the insights gained from the project are outlined below.

1. **Identify those specific VOC and VOC-sources that contribute most to the formation of photochemical smog**

Results:

- The reactivity of the VOCs is dominated by anthropogenic VOC, with VOCs from natural or biogenic sources making a minor contribution;
- Of the anthropogenic VOCs, reactive aromatics (i.e., xylenes, toluene, trimethylbenzenes, ethylbenzene) dominate;
- Of the reactive aromatics, xylenes and toluene are the most important;
- The source of the reactive aromatics does not appear to be preferentially located in downtown Hong Kong, and does not appear to be dominated by mobile emissions. Specifically emissions from industrial, waterfront, and fuel storage activities appear to be implicated.

2. **Assess the relative contributions of local production and pollutant import from other locations to the presence of photochemical ozone in Hong Kong**

Results:

- Local emissions from Hong Kong as well as emissions from Guangdong Province appear to be able to act in concert or individually in fostering O_3 pollution episodes in Hong Kong;

- 5 out of the 10 Hong Kong O_3-pollution episodes studied show a "pollutant signature" that is indicative of impact from Guangdong Province;
  - one of these appears to be strongly influenced by emissions from Guangdong Province; the other 4 appear to have a more modest and transient impact from Guangdong;
- Approximately 50 – 100% of the O_3 increase observed in Hong Kong during O_3-pollution episodes can be explained by photochemical generation within the Hong Kong area and HONO (and to a lesser extent aldehydes) is predicted to play a critical role in local O_3 generation provided that HONO was present at the concentrations derived from the OBM calculations.

3. **Complete a preliminary investigation of the relative benefits of various emission-control strategies**

Results:

- The formation of O_3 throughout much of Hong Kong area is limited by VOC;
- High NO concentrations suppress O_3 production in much of Hong Kong;
- O_3 sensitivity to VOC is dominated by the contribution from reactive aromatics.

4. **Assess the accuracy of pollutant emission inventories for Hong Kong and the PRD region**

Results:

- The ratios of the concentrations of some VOC species (e.g., butanes-to-toluene) are consistent with a speciated version of the VOC emission inventory produced from an earlier PRD study. The ratios of selected alkanes are not. The reason for

this inconsistency could reflect inaccuracies in the inventory and/or the speciation method;

- VOC emissions in the region are dominated by reactive aromatics (i.e., xylenes, toluene, trimethylbenzenes, ethylbenzene);
  - A significant contribution to the reactive aromatics present in the Hong Kong area appears to be coming from non-mobile sources (e.g., related to industrial, waterfront, and/or fuel storage activities).

3.7.1 Caveat: The findings that the O_3 photochemistry in the Hong Kong area is strongly VOC-limited and dominated by anthropogenic VOCs are robustly supported by the data gathered during the field campaign. However, it should be borne in mind that these data were gathered in the fall season. The low light levels typical of this time of year tend to favor these results. Relative to the summer season: (1) natural emissions of VOCs are generally depressed and this tends to make anthropogenic VOC sources relatively more important; and (2) photolytic sources of OH are depressed and this tends to make the reactions that lead to O_3 productions limited by radicals and thus VOC-limited as opposed to NO_x-limited. It is therefore possible that different conclusions with regard to the relative roles of anthropogenic and natural VOCs and the VOC- versus NO_x-limitation of the photochemistry apply for portions of the Hong Kong area during the summer.

3.7.2 The Recommended Next Steps: On the basis of these findings a number of specific actions can be recommended. With regard to figure research and scientific investigations, it is recommended that studies be undertaken to:

- Identify source or sources of reactive aromatics;

- Confirm and quantify role of HONO in early morning chemistry;
- Expand measurements to include summer season;
- Expand measurements to PRD and new territories to characterize additional areas of significant O_3 photochemical production that likely impact the exposure of Hong Kong citizenry to O_3 pollution.

With regard to policy-relevant activities designed to mitigate O_3 pollution in the Hong Kong area during the fall:

- Initial emission controls should be aimed at lowering the emissions of reactive aromatics;
- These controls should be implemented within Hong Kong and Guangdong Province as both contribute to O_3 pollution in Hong Kong to a greater or lesser degree depending upon the specific meteorological conditions.

CHAPTER 4

CONCLUSION

This thesis focused on the use of observation-based methods and analyses to address two issues related to urban and regional air pollution. In one part, a mechanistic analysis was used to test the validity of the assumption of thermodynamic equilibrium between fine particulate ($PM_{2.5}$) nitrate (NO_3^-) and ammonium (NH_4^+) and gas-phase nitric acid ($HNO_3(g)$) and ammonia ($NH_3(g)$). In the other part, a variety of analytical approaches, including emissions tests, diagnostic analyses, source-receptor analyses, and an analysis of ozone control strategies, were undertaken to better understand the causes and possible remedies for ozone pollution in the Hong Kong area. The main conclusions of this thesis are summarized in Section 4.1 and suggestions and plans for future research are given in Section 4.2.

4.1 Major Results

4.1.1 An Evaluation of Thermodynamic Equilibrium Assumption for Fine Particulate Composition

A thermodynamic equilibrium model, ISORROPIA, was applied to 5-minute-averaged measurements of $PM_{2.5}$ inorganic composition and gas-phase concentrations of NH_3 and HNO_3 to determine the viability of the assumption of thermodynamic equilibrium. The model calculations suggest that the data collected during the Atlanta Supersite Experiment are consistent with the assumption of thermodynamic equilibrium on the time scale of 5 minutes; and ISORROPIA is, for the most part, capable of reproducing the partitioning of inorganic species between particulate and gas-phases

during the experiment. For this to be true, however, one or more of the following systematic errors must apply: The $PM_{2.5}$ PILS systematically overestimated the SO_4^{2-} concentration by 15%, or underestimated the concentration of the alkaline components by ~ 15%; and/or the ISORROPIA model systematically overestimated the acidity of the $PM_{2.5}$ encountered during the experiment.

4.1.2 Ground-Level Ozone Pollution in Hong Kong

A variety of observation-based approaches were used to assess ozone pollution in Hong Kong area using data gathered during the Hong Kong and the Pearl River Delta pilot air monitoring project. The specific VOC and VOC sources that contribute most to the formation of photochemical smog were identified. The reactivity of the VOCs is dominated by anthropogenic VOC, of which reactive aromatics dominate. Of the reactive aromatics, xylenes and toluene are the most important. The source of these reactive aromatics does not appear to be preferentially located in downtown Hong Kong, and does not appear to be dominated by mobile emissions. Emissions from industrial, waterfront, and fuel storage activities appear to be implicated as well.

The relative contributions of local production and pollutant import from other locations to the presence of photochemical ozone in Hong Kong were assessed. It was found that local emissions from Hong Kong as well as emissions from Guangdong Province appear to be able to act in concert or individually in fostering O_3 episodes in Hong Kong. About half of the O_3 episodes observed during the project show a "pollutant signature" that is indicative of impact from Guangdong Province. Approximately 50-100% of the O_3 increase observed in Hong Kong during the O_3 episodes can be explained by local photochemical production and HONO (and to a lesser extent aldehydes) is

predicted to play a critical role in local O_3 generation provided that HONO was present at the concentrations derived from the OBM calculations.

A preliminary investigation of the relative benefits of various emission-control strategies found that the O_3 formation throughout much of Hong Kong area is limited by VOC, and the O_3 sensitivity to these VOCs is dominated by the contribution from reactive aromatics. The high NO concentrations suppress O_3 in much of the area.

The accuracy of pollutant emission inventories for Hong Kong and the PRD region was also assessed. The ratio of butanes to toluene is consistent with a speciated version of the VOC emission inventory produced from an earlier PRD study. The ratios of selected alkanes are not. This may be caused by the inaccuracies in the inventory and/or the speciation method.

4.2 Suggestions and Plans for Future Research

In this thesis a variety of observation-based approaches were applied to analyze the air pollutants in Atlanta and Hong Kong area. These approaches utilized the ambient chemical data (e.g. aerosol and gas-phase composition) as the fundamental input for the analyses. One major limitation of the approaches encountered in both studies was related to the instrumentation and the reliability of the data. For example, in the mechanistic analysis of the first part, it was suggested that the $PM_{2.5}$ SO_4^{2-} concentration measured by the PILS were probably systematically overestimated by ~15%; or, the $PM_{2.5}$ PILS systematically underestimated the concentration of the alkaline components by ~ 15%. In the diagnostic analysis of the second part, it was noticed that the 24-hour averaged CO concentrations from high-time-resolution instrumentation operated by the HKEPD were

limited by the instrumentation sensitivity at low levels, and not consistent with those gathered with more sensitive but lower-resolution analyses using gas chromatography. The VOC data available at the four sites were 24 hour averages which needed to be deduced to hourly data for input of OBM calculations. Thus some of the data collected during the measurement campaign were not well-suited to the observation-based methods for which the data were, in part, collected.

Just as inaccuracies in emission inventories will always plague EBMs, the inaccuracies in observed ambient data can seriously limit observation-based methods that, in turn, were motivated in part by a desire to avoid some of the pitfalls of EBMs. As the development of the instrumentation, it can be expected that data with better accuracy and resolution will make observation-based methods easier to use and the results will have less uncertainties.

Aside from the limitation of observations, some observation-based methods that utilize chemical mechanisms are also subject to the restrictions of incompleteness of chemistry. For example, in the mechanistic analysis of the first part, only inorganic ions and gases were included; and in the OBM calculations of the second part, only gas-phase species were included. In both studies, the interactions of particulate composition and gas-phase pollutants in modeling analyses were not considered. Incorporation of this interaction in chemical mechanisms in the future will no doubt simulate the atmospheric processes better.

In spite of the flaws discussed above, observation-based methods, which complement EBMs as part of a weight-of-evidence approach to air quality control, are still a powerful tool for studying local or regional air pollution, especially in applications

of emission testing, source-receptor analyses, mechanistic analyses, diagnostic analyses, and analyses of ozone control strategies. To limit these drawbacks, both instrumentation and experimental design of data collection need to improve for accurate, well-suited data for the analyses; also the chemical mechanisms need to improve in the future, for example, by considering the interaction of particulate- and gas-phase pollutants in modeling analyses, to better simulate the atmospheric processes controlling the amounts of the pollutants in the atmosphere.

APPENDIX A

CALCULATION OF CHARACTERISTIC TIME TO ACHIEVE THERMODYNAMIC EQUILIBRIUM BETWEEN AEROSOL AND GAS PHASE SPECIES

According to Wexler and Seinfeld (1990), the characteristic time scale of a volatile species to equilibrate between aerosol and gas phases as a result of transport is

$$\tau_{\infty} = \frac{\beta + 1}{4\pi N R_p \overline{D}} \qquad \text{(A.1)}$$

where $\beta = \frac{0.065\mu m}{\alpha R_p}$ is a dimensionless surface accommodation factor (α is the accommodation coefficient), N is the number concentration of aerosol particles, R_p is the radius of the particle if the particle is assumed to have the shape of a sphere, and $\overline{D}$ is an average diffusivity of the gas-phase species.

The geometric mean diameter D_p of the $PM_{2.5}$ aerosol particle was 0.47 μm with a geometric standard deviation σ_g of 2.1 in 1990 Atlanta Supersite Experiment (Carrico et al, 2003). The count median diameter CMD of $PM_{2.5}$ particles is obtained from Equation A.2 following Hinds (1982)

$$CMD = \frac{MMD}{\exp(3\ln^2 \sigma_g)} \qquad \text{(A.2)}$$

where MMD is the mass median diameter which is the same as D_p shown above, and σ_g is the geometric standard deviation as mentioned above. CMD is calculated as 0.090 μm. Assuming the $PM_{2.5}$ aerosol particles are round, the volume of a particle with a diameter of the count median diameter CMD was 3.83×10^{-4} μm^3. The mass of such a particle is calculated as 5.75×10^{-10} μg by assuming the bulk aerosol density of 1.5 g cm^{-3} following McMurry et al. (2002). During the Atlanta Supersite Experiment, the arithmetic mean

$PM_{2.5}$ concentration measured was 31 μg m^{-3} (Carrico et al., 2003). Therefore the number concentration of $PM_{2.5}$ aerosol particles is calculated as 5.39×10^{10} m^{-3}.

Following Wexler et al. (1994), the diffusivity and accommodation coefficient are assumed to be 0.1 cm^2 s^{-1} and 0.01, respectively, for the gas-phase species. τ_∞ is calculated as 18 s from Equation A.1, which is comparable to 4 s estimated for inland conditions (hot, high aerosol mass concentrations, and small aerosol sizes) by Wexler and Seinfeld (1990).

Also according to Wexler and Seinfeld (1990), the characteristic time for the aqueous and gas phases to equilibrate as a result of changes in the gas-phase surface concentration, i.e. due to thermodynamics, is

$$\tau_p = \frac{m_w}{K_i} \tau_\infty \qquad \text{(A.3)}$$

where m_w is the liquid water mass of aerosol per unit volume of air, and K_i (kg m^{-3}) is the equilibrium constant between the aqueous and gas phases. Assuming the aqueous-phase particles are mostly water, m_w is nearly equal to 31 μg m^{-3}, the arithmetic mean $PM_{2.5}$ concentration measured during the Atlanta Supersite Experiment. This value represents an upper limit of m_w. The equilibrium constant K_i used is from Stelson and Seinfeld (1982a) for NH_4NO_3 (aq). The ratio of m_w/K_i is about 1.2 to 2 for temperature 25°C to 30°C, and τ_p ranges from about 22 s to 36 s.

From the calculation above, it can be found that for $PM_{2.5}$ measured during the Atlanta Supersite Experiment, τ_∞ and τ_p are about several tens seconds, which are much less than 5 min, the time scale of inorganic ion averages measured by PILS.

APPENDIX B

SPECIATION OF VOC EMISSIONS INVENTORY FROM EARLIER PRD STUDY

Using the emission inventories by sector for the year 2000 from the earlier PRD study [CH2M HILL (China) Limited, 2002; also found at the Hong Kong Environment Protection Department website http://www.epd.gov.hk/epd/english/environmentinhk/air/studyrpts/study pearl.html] (see Table B.1), a detailed analysis of the chemical speciation of VOC emissions from both Hong Kong (HKSAR) and Guangdong Province (PRDEZ) was performed. The VOC emissions were divided into the 47 species which were measured at TO and other sites operated by EPD, and into 4 categories that include species that were not measured based on functional groups. The speciation profiles for each source type were drawn from two major information sources: the USEPA SPECIATE database [USEPA, 2000, available at http://www.epa.gov/ttn/chief/software/speciate], and Andreae and Merlet [2001] for open biomass burning. For the first information source, it is assumed that the species profile for a given source type in Hong Kong and PRD is the same as for the same source type in the West. The speciated VOCs are listed in Table B.2.

Table B.1 Emission inventory of VOC by sector for the year 2000 from earlier PRD study.

	VOC emission	
Sector	HKSAR	PRDEZ
Energy	0.5 (1%)	7.0 (1%)
Industry	9.5 (17%)	51.6 (9%)
Transportation	13.6 (24%)	375.9 (66%)
VOC-containing products	31.4 (55%)	92.5 (16%)
Others	1.7 (3%)	47.2 (8%)

Note: The emissions are in unit of Gg (i.e. 10^9g). The data in parenthesis are in units of percent of total emissions. HKSAR = Hong Kong Special Administrative Region. PRDEZ = Pearl River Delta Economic Zone.

Table B.2 Hydrocarbons measured during the Hong Kong Supersite study and their apportionment among source categories.

Species	Percent Apportionment to Source Category					
	HKSAR			PRDEZ		
	Mobile	Stationary	Natural	Mobile	Stationary	Natural
Ethane	78	22	0	70	30	0
Propane	2	98	0	0	100	0
n-butane	70	30	0	95	5	0
i-butane	16	84	0	60	40	0
n-pentane	75	25	0	91	9	0
i-pentane	74	26	0	96	4	0
n-hexane	50	50	0	80	20	0
n-heptane	11	89	0	49	51	0
n-octane	100	0	0	100	0	0
n-nonane	97	3	0	100	0	0
n-decane	98	2	0	99	1	0
2,2-dimethylbutane	91	9	0	100	0	0
2,3-dimethylbutane	68	32	0	94	6	0
2-methylpentane	86	14	0	100	0	0
3-methylpentane	88	12	0	100	0	0
2-methylhexane	0	100	0	0	100	0
3-methylhexane	92	0	8	100	0	0
2,2,4-trimethylpentane	97	3	0	100	0	0
Methylcyclopentane	88	12	0	100	0	0
Cyclohexane	22	78	0	77	23	0
Ethene	100	0	0	96	4	0
Propene	99	1	0	90	10	0
i-butene	95	5	0	95	5	0
1-butene	64	36	0	78	22	0
1-pentene	77	23	0	100	0	0
1,3-butadiene	100	0	0	23	77	0
Isoprene	0	0	100	0	0	100
Cis-2-butene	67	33	0	97	3	0
Trans-2-butene	43	57	0	95	5	0
Acetylene	90	10	0	88	12	0
Benzene	78	22	0	91	9	0
Toluene	7	93	0	39	61	0
m-xylene	12	88	0	33	67	0
p-xylene	33	67	0	69	31	0
o-xylene	16	84	0	52	48	0
Ethylbenzene	32	68	0	72	28	0
i-propylbenzene	0	100	0	0	100	0
n-propylbenzene	78	22	0	96	4	0
m-ethyltoluene	79	21	0	96	4	0
p-ethyltoluene	0	100	0	0	100	0
o-ethyltoluene	42	58	0	83	17	0
1,3,5-trimethylbenzene	84	16	0	97	3	0
1,2,4-trimethylbenzene	93	7	0	99	1	0
1,2,3-trimethylbenzene	79	21	0	96	4	0
α-pinene	0	0	100	0	0	100
β-pinene	0	0	100	0	0	100

Note: HKSAR = Hong Kong Special Administrative Region
PRDEZ = Pearl River Delta Economic Zone

In general, the speciation of the VOC emissions from the earlier PRD study is quite different from that of the Streets inventory. For example, the emission of butanes in Hong Kong from the earlier PRD study is about 1/6 of that from the Streets inventory, while the emission of toluene in Hong Kong is 12% higher.

REFERENCES

Alicke, B., U. Platt, and J. Stutz (2002), Impact of nitrous acid photolysis on the total hydroxyl radical budget during the Limitation of Oxidant Production/Pianura Padana Produzione di Ozono study in Milan, *Journal of Geophysical Research, 107*(D22), 8196, doi: 10.1029/2000JD000075.

Alicke, B., A. Geyer, A. Hofzumahaus, F. Holland, S. Konrad, H. W. Patz, J. Schafer, J. Stutz, A. Volz-Thomas, and U. Platt (2003), OH formation by HONO photolysis during the BERLIOZ experiment, *Journal of Geophysical Research, 108*(D4), 8247, doi: 10.1029/2001JD000579.

Andreae, M. O., and P. Merlet (2001), Emissions of trace gases and aerosols from biomass burning, *Global Biogeochemical Cycles, 15*, 955-966.

Ansari, A. S., and S. N. Pandis (2000), The effect of metastable equilibrium states on the partitioning of nitrate between the gas and aerosol phases, *Atmospheric Environment, 34*, 157-168.

Baumann, K., F. Ift, J. Z. Zhao, and W. L. Chameides (2003), Discrete measurements of reactive gases and fine particle mass and composition during the 1999 Atlanta Supersite Experiment, *Journal of Geophysical Research, 108*(D7), 8416, doi:10.1029/2001JD001210.

Bell, M. L. and D. L. Davis (2001), Reassessment of the Lethal London Fog of 1952: Novel Indicators of Acute and Chronic Consequences of Acute Exposure to Air Pollution, *Environmental Health Perspectives, 109(3)/Supplements*, 389-394.

Berge, E, and H. A. Jakobsen (1998), A regional scale multi-layer model for the calculation of long-term transport and deposition of air pollution in Europe, *Tellus 50B,* 205-223.

Bergin, M. H., R. Greenwald, J. Xu, Y. Berta, and W. L. Chameides (2001), Influence of aerosol dry deposition on photosynthetically active radiation available to plants: A case study in the Yangtze delta region of China, *Geophysical Research Letters, 28*, 3605-3608.

Blanchard, C. L., F. W. Lurmann, P. M. Roth, H. E. Jeffries, M. Korc (1999), The use of ambient data to corroborate analyses of ozone control strategies, *Atmospheric Environment, 33*, 369-381.

Blanchard, C. L. (2000), Ozone process insights from field experiments – Part III: extent of reaction and ozone formation, *Atmospheric Environment, 34*, 2035-2043.

Brimblecombe, P. (1982), Long term trends in London fog, *Scientific Total Environment, 22*, 19-29.

Brown, M. (1995), The singular value decomposition method applied to the deduction of the emissions and the isotopic composition of atmospheric methane, *Journal of Geophysical Research, 100*(D6), doi: 10.1029/95JD00367, 11425-11446.

Brune, W. H., D. Tan, I. F. Faloona, L. J. Jacob, B. G. Heikes, J. Snow, Y. Kondo, R. Shetter, G. W. Sachse, B. Anderson, G. L. Gregory, S. Vay, H. B. Singh, D. D. Davis, J. H. Crawford, and D. R. Blake (1999), OH and HO_2 chemistry in the North Atlantic free troposphere, *Geophysical Research Letters, 26*, 3077-3080.

Cadle, R. D., and H. S. Johnston (1952), Chemical reaction in Los Angeles smog, *Proceedings of the National Air Pollution Symposium, 2nd*.

Calvert, J. G. (1976), Test of the theory of ozone generation in Los Angeles atmosphere, *Environmental Science & Technology, 10*, 248-262.

Cantrell, C. A., R. E. Shetter, T. M. Gilpin, J. G. Calvert, F. L. Eisele, and D. J. Tanner (1996), Peroxy radical concentrations measured and calculated from trace gas measurements in the Mauna Loa Observatory Photochemistry Experiment 2, *Journal of Geophysical Research, 101*, 14653-14664.

Cantrell, C. A., L. Mauldin, M. Zondlo, F. Eisele, E. Kosciuch, R. Shetter, B. Lefer, S. Hall, T. Campos, B. Ridley, J. Walega, A. Fried, B. Wert, F. Flocke, A. Weinhermer, J. Hannigan, M. Coffey, E. Atlas, S. Stephens, B. Heikes, J. Snow, D. Blake, N. Blake, A. Katzenstein, J. Lopez, E. V. Browell, J. Dibb, E. Scheuer, G. Seid, and R. Talbot (2003), Steady state free radical budgets and ozone photochemistry during TOPSE, *Journal of Geophysical Research, 108* (D4), 8361, doi:10.1029/2002JD 002198.

Capaldo, K. P., C. Pilinis, and S. N. Pandis (2000), A computationally efficient hybrid approach for dynamic gas/aerosol transfer in air quality models, *Atmospheric Environment, 34*, 3617-3627.

Cardelino, C. (1998), Daily variability of motor vehicle emissions derived from traffic counter data, *Journal of the Air & Waster Management Association, 48*, 637-645.

Cardelino, C. and W. L. Chameides (1995), An observation-based model for analyzing ozone precursor relationships in the urban atmosphere, *Journal of Air & Waster Management Association, 45*, 161-180.

Cardelino, C. and W. L. Chameides (2000), The application of data from photochemical assessment monitoring stations to the observation-based model, *Atmospheric Environment, 34*, 2325-2332.

Carrico, C. M., M. H. Bergin, J. Xu, K. Baumann, and H. Maring (2003), Urban aerosol radiative properties: Measurements during the 1999 Atlanta Supersite Experiment, *Journal of Geophysical Research, 108*(D7), doi:10.1029/2001JD001222, 8422-8438.

Carslaw, N., D. J. Creasey, D. Harrison, D. E. Heard, M. C. Hunter, P. J. Jacobs, M. E. Jenkin, J. D. Lee, A. C. Lewis, M. J. Pilling, S. M. Saunders, and P. W. Seakins (2001), OH and HO_2 radical chemistry in a forested region of north-western Greece, *Atmospheric Environment, 35*, 4725-4737.

Carslaw, N., D. J. Creasey, D. E. Heard, P. J. Jacobs, J. D. Lee, A. C. Lewis, J. B. McQuaid, M. J. Pilling, S. Bauguitte, S. A. Penkett, P. S. Monks, and G. Salisbury (2002), Eastern Atlantic Spring Experiment 1997 (EASE97) 2. Comparisons of model concentrations of OH, HO_2, and RO_2 with measurements, *Journal of Geophysical Research, 107*(D14), doi: 10.1029/2001JD001568.

Carter, W. P. L., R. Atkinson (1987), An experimental study of incremental hydrocarbon reactivity, *Environmental Science & Technology, 21*, 670-679.

Carter, W. P. L., and R. Atkinson (1989), Computing modeling study of incremental hydrocarbon reactivity, *Environmental Science & Technology, 23*, 864-880.

Cass, G. R., and G. J. McRae (1983), Source-receptor reconciliation of routine air monitoring data for trace metals: An emission inventory assisted approach, *Environmental Science & Technology, 17*, 129-139.

Castro, T., S. Madronich, S. Rivale, A. Muhlia, and B. Mar (2001), The influence of aerosols on photochemical smog in Mexico City, *Atmospheric Environment, 35*, 1765-1772.

CH2M HILL (China) Limited (2002), Final report: agreement No. CE 106/98: Study of Air Quality in the Pearl River Delta Region, April 2002.

Chameides, W. L., and A. Tan (1981), The two-dimensional diagnostic model for tropospheric OH: An uncertainty analysis, *Journal of Geophysical Research, 86*, 5209-5223.

Chameides, W. L., and J. C. G. Walker (1973), A photochemical theory of tropospheric ozone, *Journal of Geophysical Research, 78*, 8751-8760.

Chameides, W. L., and J. C. G. Walker (1974), Reply, *Journal of Geophysical Research, 79*, 4126.

Chameides, W. L., D. D. Davis, J. Bradshaw, S. Sandholm, M. Rodgers, B. Baum, B. Ridley, S. Madronich, M. A. Carroll, G. Gregory, H. I. Schiff, D. R. Hastie, A. Torres, and E. Condon (1990), Observed and model-calculated NO_2:NO ratios in

tropospheric air sampled during the NASA GTE/CITE 2 field study, *Journal of Geophysical Research, 95*, 10235-10247.

Chameides, W. L., D. Davis, M. O. Rodgers, J. Bradshaw, S. Sandholm, G. Sachse, G. Hill, G. Gregory, and R. Rasmussen (1987), Net ozone photochemical production over the eastern and central North Pacific as inferred from GTE/CITE 1 observations during fall 1983, *Journal of Geophysical Research, 92*, 2131-2152.

Chameides, W. L., F. Fehsenfeld, M. O. Rodgers, C. Cardelino, J. Martinez, J., D. Parrish, W. Lonneman, D. R. Lawson, R. A. Rasmussen, P. Zimmerman, J. Greenberg, P. Middleton, and T. Wang (1992), Ozone precursor relationships in the ambient atmosphere, *Journal of Geophysical Research, 97*, 6037-6055.

Chang, J. S., R. A. Brost, I. S. A. Isaksen, P. Madronich, W. R. Stockwell, and C. J. Walcek (1987), A three-dimensional Eulerian acid deposition model: Physical concepts and formulation, *Journal of Geophysical Research, 92*, 14681-14700.

Chang, M. E., D. E. Hartley, C. Cardelino, and W.-L. Chang (1996), Inverse modeling of biogenic isoprene emissions, *Geophysical Research letters, 23*, 3007-3010.

Chang, M. E., D. E. Hartley, C. Cardelino, D. Haas-Lauresen, and W.-L. Chang (1997), On using inverse methods for resolving emissions with large spatial inhomogeneities, *Journal of Geophysical Research, 102*, 16023-16036.

Chang, T. Y., D. P. Chock, B. I. Nance, S. L. Winkler (1997), A photochemical extent parameter to aid ozone air quality management, *Atmospheric Environment, 31*, 2787-2794.

Chatfield, R. B., and H. Harrison (1976), Ozone in the remote troposphere: Mixing versus photochemistry, *Journal of Geophysical Research, 81*, 421-423.

Chin, M., D. J. Jacob, J. W. Munger, D. D. Parrish, and B. G. Doddridge (1994), Relationship of ozone and carbon monoxide over North America, *Journal of Geophysical Research, 99*, 14565-14573.

Chock, D. P., T. Y. Chang, S. L. Winkler, B. I. Nance (1999), The impact of an 8 h ozone air quality standard on ROG and NO_x controls in Southern California, *Atmospheric Environment, 33*, 2471-2485.

Chow, J. (1995), Critical review of measurement methods to determine compliance with ambient air quality standards for suspended particulates, *Journal of Air & Waste Management Association, 45*, 320-382.

Cope, M. E. and J. Ischtwan (1995), Perth Photochemical Smog Study: Airshed Modelling Component, *Final Report*, pp. 320, Environmental Protection Authority of Victoria, Melbourne, Australia.

Crawford, J., D. Davis, G. Chen, J. Bradshaw, S. Sandholm, G. Gregory, G. Sachse, B. Anderson, J. Collins, D. Blake, H. Singh, B. Heikes, R. Talbot, and J. Rodriguez (1996), Photostationary state analysis of the NO_2-NO system based on airborne observations from the western and central North Pacific, *Journal of Geophysical Research, 101*, 2053-2072.

Cruz, C. N., K. G. Dassios, and S. N. Pandis (2000), The effect of dioctyl phthalate films on the ammonium nitrate aerosol evaporation rate, *Atmospheric Environment, 34*, 3897-3905.

Cruzen, P. (1973), A discussion of the chemistry of some minor constituents in the stratosphere and troposohere, *Pure and Applied Geophysics, 106-108*, 1385-1399.

Cunnold, D. M., R. G. Prinn, R. A. Rasmussen, P. G. Simmonds, F. N. Alyea, C. A. Cardelino, A. J. Crawford, P. J. Fraser, and R. D. Rosen (1983), The atmospheric lifetime experiment, 3, Lifetime methodology and application to three years of $CFCl_3$ data, *Journal of Geophysical Research, 88*, 8379-8400.

Cunnold, D. M., R. G. Prinn, R. A. Rasmussen, P. G. Simmonds, F. N. Alyea, C. A. Cardelino, A. J. Crawford, P. J. Fraser, and R. D. Rosen (1986), Atmospheric lifetime and annual release estimates for $CFCl_3$ and CF_2Cl_2 from 5 years of ALE data, *Journal of Geophysical Research, 91*, 10797-10817.

Dassios, K. G., and S. N. Pandis (1999), The mass accommodation coefficient of ammonium nitrate aerosol, *Atmospheric Environment, 33*, 2993-3003.

Davis, D. D. (1993), A photostationary state analysis of the NO_2-NO system based on airborne observations from the subtropical/tropical North and South Atlantic, *Journal of Geophysical Research, 98*, 23501-23523.

Davis, D. D., J. Crawford, G. Chen, W. Chameides, S. Liu, J. Bradshaw, S. Sandholm, G. Sachse, G. Gregory, B. Anderson, J. Barrick, A. Bachmeier, J. Collins, E. Browell, D. Blake, S. Rowland, Y. Kondo, H. Singh, R. Talbot, B. Heikes, J. Merrill, J. Rodriguez, and R. E. Newell (1996), Assessment of ozone photochemistry in the western North Pacific as inferred from PEM-West A observations during the fall 1991, *Journal of Geophysical Research, 101*, 2111-2134.

Dennis, R. L., J. N. McHenry, W. R. Barchet, F. S. Binkowski, and D. W. Byun (1993), Correcting RADM's sulfate underprediction: Discovery and correction of model errors and testing the corrections through comparisons against field data, *Atmospheric Environment, 27A*, 975-997.

Diamond, D. (2002), New York Supersite Instrument Intercomparison and Analysis, MS thesis, pp12, Georgia Institute of Technology, Atlanta, GA.

Doyle, G. J., E. C. Tuazon, R. A. Graham, T. M. Mischke, A. M. Winer, and J. N. Pitts (1979), Simultaneous concentrations of ammonia and nitric acid in a polluted atmosphere and their equilibrium relationship to particulate ammonium nitrate, *Environmental Science & Technology, 13*, 1416-1419.

Edgerton, E., B. Hartsell, A. Hansen, and J. Jansen (2000a), Continuous measurements of fine particulate ammonium, nitrate, organic carbon and elemental carbon, paper presented at AGU 2000 Fall Meeting, San Francisco, USA.

Edgerton, E., B. Hartsell, J. Jansen, and J. S. John (2000b), Chemical and meteorological characteristics of the Jefferson Street monitoring site, paper presented at AGU 2000 Fall Meeting, San Francisco, USA.

Eisele, F. L., D. J. Tanner, C. A. Cantrell, and J. G. Calvert (1996), Measurements and steady state calculations of OH concentrations at Mauna Loa Observatory, *Journal of Geophysical Research, 101*, 14665-14679.

Enting, I., and J. Mansbridge (1989), Seasonal sources and sinks of atmospheric CO2 direct inversion of filtered data, *Tellus, 41B,* 111-129.

Fabian, P. (1974), Comments on 'A photochemical theory of tropospheric ozone' by W. Chameides and J. C. G. Walker, *Journal of Geophysical Research, 79*, 4124-4125.

Fabian, P., and P. G. Pruchniewicz (1977), Meridional distribution of ozone in the troposphere and its seasonal variation, *Journal of Geophysical Research, 82*, 2063-2073.

Fehsenfeld, F. C., M. J. Bollinger, S. C. Liu, D. D. Parrish, M. McFarland, M. Trainer, D. Kley, P. C. Murphy, D. L. Albritton, and D. H. Lenschow (1983), A study of ozone in the Colorado mountains, *Journal of Atmospheric Chemistry, 1*, 87-105.

Finlayson-Pitts, B. J., L. M. Wingen, A. L. Sumner, D. Syomin, and K. A. Ramazan (2003), The heterogeneous hydrolysis of NO_2 in laboratory systems and in outdoor and indoor atmospheres: An integrated mechanism, *Physical Chemistry Chemical Physics, 5*, 223-242.

Fishman, J., and P. Crutzen (1977), A numerical study of tropospheric photochemistry using a one-dimensional model, *Journal of Geophysical Research, 82*, 5897-5906.

Fishman, J., and R. Kalish (1990) *Global Alert: The Ozone Pollution Crisis*, pp. 257-262, Plenum Press, New York.

Fridlind, A. M., and M. Z. Jacobson (2000), A study of gas-aerosol equilibrium and aerosol pH in the remote marine boundary layer during the first aerosol characterization experiment (ACE1), *Journal of Geophysical Research, 105*, 17325-17340.

Fridlind, A. M., M. Z. Jacobson, V. M. Kermnen, R. E. Hillamo, V. Ricard, and J. L. Jaffrezo (2000), Analysis of gas-aerosol partitioning in the Arctic: comparison of size-resolved equilibrium model results with field data, *Journal of Geophysical Research, 105*, 19891-19903.

Friedlander, S. K. (1973), Chemical element balances and identification of air pollution sources, *Environmental Science & Technology, 7*, 235-240.

Geron, C. D., A. B. Guenther, T. E. Pierce (1994), An improved model for estimating emissions of volatile organic compounds from forests in the eastern United States, *Journal of Geophysical Research, 99*, 12773-12791.

Gertler, A. W., D. N. Wittorff, R. Mclaren, W. Belzer, and T. Dann (1997), Characterization of vehicle emissions in Vancouver BC during the1993 Lower Fraser Valley Oxidants Study, *Atmospheric Environment, 31*, 2107-2112.

Groblicki, P. J., G. T. Wolff, and R. J. Countess (1981), Visibility-reducing species in the Denver Brown Cloud – 1, Relationship between extinctin and chemical composition, *Atmospheric Environment, 15*, 2473-2484.

Guenther, A., C. Geron, T. Pierce, B. Lamb, P. Harley, R. Fall (2000), Natural emissions of non-methane volatile organic compounds, carbon monoxide , and oxides of nitrogen from North America, *Atmospheric Environment, 34*, 2205-2230.

Gusten, H., G. Heinrich, T. Cvitas, L. Klasinc, B. Ruscic, D. Lalas, and M. Petrakis (1988), Photochemical formation and transport of ozone in Athens, Greece, *Atmospheric Environment, 22,* 1855-1861.

Haagen-Smit, A. J. (1950), The air pollution problem in Los Angeles, *Engineering and Science XIV*, 7-13.

Haagen-Smit, A. J. (1952), Chemistry and physiology of Los Angeles smog, *Industrial & Engineering Chemistry, 44*, 1342-1346.

Haagen-Smit, A. J., E. F. Darley, et al. (1951), Investigation on injury to plants from air pollution in the Los Angeles area, *Plant Physiology, 27*, 18.

Haagen-Smit, A. J. and M. M. Fox (1954), Photochemical ozone formation with hydrocarbons and automobile exhaust, *Journal of Air Pollution Control Association, 4*, 105-109.

Hanna, S. R., G. E. Moore, M. E. Fernau (1996), Evaluation of photochemical grid models (UAM-IV, UAM-V, and the ROM/UAM-IV couple) using datafrom the Lake Michigan Ozone Study (LMOS), *Atmospheric Environment, 30*, 3265-3279.

Harrison, R. M., J. D. Peak, and G. M. Collins (1996), Tropospheric cycle of nitrous acid, *Journal of Geophysical Research, 101*, 14429-14439.

Hartley, D. and R. Prinn (1993), Feasibility of determining surface emissions of trace gases using an inverse method in a three-dimensional chemical transport model, *Journal of Geophysical Research, 98*, 5183-5197.

Hass, H., H. J. Jakobs, M. Memmesheimer, A. Ebel and J. S. Chang (1991), Simulation of a wet deposition case in Europe using the European Acid Deposition Model (EURAD), in *Air Pollution Modeling and Its Application VIII*, edited by H. van Dop and D. G. Steyn, Plenum Press, 205-214.

Hass, H, A. Ebel, H. Feldmann, H. J. Jakobs, and M. Memmesheimer (1993), Evaluation studies with a regional chemical transport model (EURAD) using air quality data from the EMEP monitoring network, *Atmospheric Environment, 27A*, 867-887.

Heintzenberg J. (1989), Fine particles in the global troposphere, A review, *Tellus 41B*, 149-160.

Hidy, G. (2000), Ozone process insights from field experiments---Part I. NARSTO Critical Review Papers Special Issue, *Atmospheric Environment, 34*, 2001-2022.

Hinds, W. C. (1982), *Aerosol technology*, John Wiley & Sons, USA.

Holzworth, G. C. (1967), Mixing depths, wind speeds and air pollution potential for selected locations in the United States, *Journal of Applied Meteorology, 6*, 1039-1044.

Hogo, H, and M. W. Gery (1988), User's Guide for Executing OZIPM-4 with CBM-IV or Optional Mechanisms, U.S. Environmental Protection Agency: Research Triangle Park, NC, EPA/600/8-88/082.

Intergovernmental Panel on Climate Change (IPCC) 1995 (1996), I, pp. 20, Cambridge University Press, UK.

Iversen, T (1993), Modeled and measured transboundary acidifying pollution in Europe – Verification and trends, *Atmospheric Environment, 27A*, 889-920.

Jacobson, M. Z. (1999), *Fundamentals of Atmospheric Modeling*, Cambridge University Press, 385-393.

Jenkin, M. I., R. A. Cox, and D. J. Williams (1988), Laboratory studies of the kinetics of formation of nitrous acid from the thermal reaction of nitrogen dioxide and water vapor, *Atmospheric Environment, 22*, 487-498.

Joe, H., D. G. Steyn, and E. Susko (1996), Analysis of trends in tropospheric ozone in the Lower Fraser Valley, British Columbia, *Atmospheric Environment, 30*, 3413-3421.

Kalman, R. E. (1960), A new approach to linear filtering and prediction problems, *Trans. ASME, Journal of Basic Engineering, 82D*, 35-45.

Kasibhatla, P., W. L. Chameides, R. D. Saylor, and D. Olerud (1998), Relationships between regional ozone pollution and emissions of nitrogen oxides in the eastern United States, *Journal of Geophysical Research, 103*, 22663-22669.

Kok, G. L., J. A. Lind, and M. Fang (1997), An airborne study of air quality around the Hong Kong Territory, *Journal of Geophysical Research, 102*, 19043-19057.

Kuklin, A. and J. H. Seinfeld (1995), Emissions reductions needed to meet the standard for ozone in Southern California: effect of boundary conditions, *Journal of the Air & Waste Management Association, 45*, 899-901.

Kumar, N., and A. G. Russell (1996), Comparing prognostic and diagnostic meteorological fields and their impacts on photochemical air quality modeling, *Atmospheric Environment, 30*, 1989-2010.

Lalas, D. P., D. N., Asimakopoulos, D. G., Deligiorgi, and C. G. Helmis (1983), Sea-breeze circulation and photochemical pollution in Athens, Greece, *Atmospheric Environment, 17*, 1621-1632.

Leighton, P. A. (1961), *Photochemistry of Air Pollution*, Academic, San Diego, California.

Liu, S. C., D. Kley, M. McFarland, J. D. Mahlman, and H. Levy (1980), On the origin of tropospheric ozone, *Journal of Geophysical Research, 85*, 7546-7552.

Lu, C., and J. S. Chang (1998), On the indicator-based approach to assess ozone sensitivities and emissions features, *Journal of Geophysical Research, 103*, 3453-3462.

Malm, W. C., K. A. Gebhart, J. Molenar, T. Cahill, R. Eldred, and D. Huffman (1994a), Examining the relationship between atmospheric aerosols and light extinction at Mount Rainer and North Cascade National Parks, *Atmospheric Environment, 28*, 347-360.

Malm, W. C., J. F. Sisler, D. Huffman, R. A. Eldred, and T. A. Cahill (1994b), Spatial and seasonal trends in particle concentration and optical extinction in the United States, *Journal of Geophysical Research, 99*, 1347-1370.

Mantis, H. T., C. C. Repapis, C. S. Zerefos, and J. C. Ziomas (1992), Assessment of the potential for photochemical air pollution in Athens: A comparison of emissions and

air-pollutant levels in Athens with those in LA, *Journal of Applied Meteorology, 31*, 1467-1476.

Massambani, O. and F. Andrade (1994). Seasonal behavior of tropospheric ozone in the Sao Paulo (Brazil) metropolitan area, *Atmospheric Environment, 28*, 3165-3169.

McHenry, J., and R. L. Dennis (1994), The relative importance of oxidation pathways and clouds to atmospheric ambient sulfate production as predicted by the regional acid deposition model, *Journal of Applied Meteorology, 33*, 890-905.

Mckeen, S. A., and S. C. Liu (1993), Hydrocarbon ratios and photochemical history of air masses, *Geophysical Research Letters, 20*, 2363-2366.

McKeen, S. A., G. Mount, F. Eisele, E. Williams, J. Harder, P. Coldan, W. Kuster, S. C. Liu, K. Baumann, D. Tanner, A. Fried, S. Sewell, C. Cantrell, and R. Shetter (1997), Photochemical modeling of hydroxyl and its relationship to other species during the Tropospheric OH Photochemistry Experiment, *Journal of Geophysical Research, 96*, 6467-6493.

Meng, Z., and J. H. Seinfeld (1996), Time scales to achieve atmospheric gas-aerosol equilibrium for volatile species, *Atmospheric Environment, 30*, 2889-2900.

Miller, M. S., S. K. Friedlander, and G. M. Hidy (1972), A chemical element balance for the Pasadena aerosol, *Journal of Colloid and Interface Science, 39*, 165-176.

Mitchell, J. F. B., T. C. Johns, J. M. Gregory, and S. F. B. Tett (1995), Climate response to increasing levels of greenhouse gases and sulphate aerosols, *Nature, 376*, 501-504.

Moussiopoulos N., P. Sahm, and C. Kessler (1995), Numerical simulation of photochemical smog formation in Athens, Greece-a case study, *Atmospheric Environment, 29*, 3619-3632.

Moya, M., A. S. Ansari, and S. N. Pandis (2001), Partitioning of nitrate and ammonium between the gas and particulate phases during the 1997 IMADA-AVER study in Mexico City, *Atmospheric Environment, 35*, 1792-1804.

Mulholland, M. and J. H. Seinfeld (1995), Inverse air pollution modeling of urban-scale CO emissions, *Atmospheric Environment, 28*, 497-516.

North American Research Strategy for Tropospheric Ozone (NARSTO) (2000), An assessment of tropospheric ozone pollution: A North American Perspective.

National Acid Precipitation Assessment Program (NAPAP) (1989), Models planned for use in the NAPAP integrated assessment, The NAPAP Office of the Director, Washington, D.C.

National Acid Precipitation Assessment Program (NAPAP) (1991), The U.S. National Acid Precipitation Assessment Program, 1990 integrated assessment report, The NAPAP Office of the Director, Washington, D.C.

Nelson, P. F. and S. M. Quigley (1983), The m,p-xylenes:ethylbenzene ratio. A technique for estimating hydrocarbon age in ambient atmospheres, *Atmospheric Environment, 17*, 659-662.

Nenes, A., S. N. Pandis, and C. Pilinis (1998), ISORROPIA: a new thermodynamic equilibrium model for multiphase multicomponent inorganic aerosols, *Aquatic Geochemistry, 4*, 123-152.

Olszyna, K. J., E. M. Bailey, R. Simonaitis, and J. F. Meagher (1994), O_3 and NO_y relationships at a rural site, *Journal of Geophysical Research, 99*, 14557-14563.

Parrish, D. D., M. Trainer, M. P. Buhr, B. A.Watkins, and F. C. Fehsenfeld (1991), Carbon monoxide concentrations and their relation to concentrations of total reactive oxidized nitrogen at two rural U.S. sites, *Journal of Geophysical Research, 96*, 9309-9320.

Parrish, D. D., M. Trainer, E. J. Williams, D. W. Fahey, G. Hubler, C. S. Eubank, S. C. Liu, P. C. Murphy, D. L. Albritton, and F. C. Fehsenfeld (1986), Measurements of the NO-O3 photostationary state at Niwot Ridge, Colorado, *Journal of Geophysical Research, 91*, 5361-5370.

Perdue, E. M., K. C. Beck (1988), Chemical consequences of mixing atmospheric droplets of varied pH, *Journal of Geophysical Research, 93*, 691-698.

Pierson, W. R., A. W. Gertler, R. L. Bradow (1990), Comparison of the SCAQS tunnel study with other on-road vehicle emission data, *Journal of Air & Waste Management Association, 40*, 1495-1504.

Poppe, D, J. Zimmermann, R. Bauer, T. Brauers, D. Bruning, J. Callies, H.-P. Dorn, A. Hofzumahaus, F.-J. Johnen, A. Khedim, H. Koch, R. Koppmann, H. London, K.-P. Muller, R. Neuroth, C. Plass-Dulmer, U. Platt, F. Rohrer, E.-P. Roth, J. Rudopph, U. Schmidt, M. Wallasch, and D. H. Ehhalt (1994), Comparison of measured OH concentrations with model calculations, *Journal of Geophysical Research, 99*, 16633-16642.

Potukuchi S, and A. S. Wexler (1995), Identifying solid-aqueous phase transitions in atmospheric aerosols—I. Neutral-acidity solutions, *Atmospheric Environment, 29*, 1663-1676.

Prinn, R. G., D. Cunnold, R. Rasmussen, P. Simmonds, F. Alyea, A. Crawford, P. Fraser, and R. Rosen (1990), Atmospheric emissions and trends of nitrous oxide deduced

from 10 years of ALE-GAGE data, *Journal of Geophysical Research, 95*, 18369-18385.

Pryor, S. C. (1988), A case study of emission changes and ozone responses, *Atmospheric Environment, 32*, 123-131.

Raga, G. B., and A. C. Raga (2000), On the formation of an elevated ozone peak in Mexico City, *Atmospheric Environment, 34*, 4097-4102.

Raga, G. B., T. Castro, and D. Baumgardner (2001), The impact of megacity pollution on local climate and implications for the regional environment: Mexico City, *Atmospheric Environment, 35*, 1805-1811.

Ridley, B. A. S. Madronich, R. B. Chatfield, J. G. Walega, R. E. Shetter, M. A. Carroll, and D. D. Montzka (1992), Measurements and model simulations of the photostationary state during the Mauna Loa Observatory Photochemistry Experiment: Implications for radical concentrations and ozone production and loss rates, *Journal of Geophysical Research, 97*, 10375-10388.

Russell, A. G., and R. L. Dennis (2000), Critical review of photochemical models and modeling. NARSTO Critical Review Papers Special Issue, *Atmospheric Environment, 34*, 2283-2324.

Rye, P. J., K. Rayner, and P, Weir (1996), The Perth photochemical smog study, Western Power Report CS20/96, Department of Environmental Protection Report 16, Perth, Austrilia.

Ryerson, T. B., M. Trainer, M. P. Buhr, G. Frost, P. D. Goldan, J. S. Holloway, G. Hubler, B. T. Jobson, W. C. Kuster, S. A. McKeen, D. D. Parrish, J. M. Roberts, D. M. Sueper, J. Williams, F. C. Fehsenfeld (1998), Emissions, lifetimes and ozone formation in power plant plumes, *Journal of Geophysical Research, 103*, 22569-22583.

St. John, J. C., W. L. Chameides (1997), Climatology of ozone exceedance in the Atlanta metropolitan area: 1-hour vs. 8-hour standard and the role of plume recirculation air pollution episodes, *Environmental Science & Technology, 31*, 2797-2804.

St. John, J. C., W. L. Chameides, and R. Saylor (1998), Role of anthropogenic NOx and VOC as ozone precursors: a case study from the SOS Nashville/Middle Tennessee ozone study, *Journal of Geophysical Research, 103*, 22415-22434.

Schauer, J. J., and G. R. Cass (2000), Source apportionment of wintertime gas-phase and particle-phase air pollutants using organic compounds as tracers, *Environmental Science & Technology, 34*, 1821-1832.

Schauer, J. J., W. F. Rogge, L. M. Hildemann, M. A. Mazurek, G. R. Cass, and B. R. T. Simoneit (1996), Source apportionment of airborne particulate matter using organic compounds as tracers, *Atmospheric Environment, 30*, 3837-3855.

Seinfeld, J. H., and S. N. Pandis (1997), *Atmospheric Chemistry and Physics: From Air Pollution to Climate Change*, John Wiley & Sons, Inc., New York.

Sillman, S. (1995), The use of NO_y, H_2O_2 and HNO_3 as indicators for O_3-NO_x-ROG sensitivity in urban locations, *Journal of Geophysical Research, 100*, 14175-14188.

Sillman, S. (1999), The method of photochemical indicators as a basis for analyzing O_3-NO_x-ROG sensitivity, NARSTO Critical Review (http://www.cgenv.com/Narsto)

Sillman, S., D. He, C. Cardelino, and R. E. Imhoff (1997), The use of photochemical indicators to evaluate ozone-NO_x-hydrocarbon sensitivity: Case studies from Atlanta, New York and Los Angeles, *Journal of the Air & Waste Management Association, 47*, 642-652.

Sillman, S., and D. He (2002), Some theoretical results concerning O_3-NO_x-VOC chemistry and NOx-VOC indicators, *Journal of Geophysical Research, 107*(D22), 4659, doi:10.1029/2001JD001123.

Simon, P. K. and P. K. Dasgupta (1995), Continuous automated measurement of the soluble fraction of atmospheric particulate matter, *Analytical Chemistry, 67*, 71-78.

Simpson, D. (1995), Biogenic emissions in Europe, 2, implications for ozone control strategies, *Journal of Geophysical Research, 100*, 22891-22906.

Slanina, J., P. J. de Wild, and G. P. Wyers (1992), The application of denuder systems to the analysis of atmospheric components, in *Gaseous Pollutants, Characterization and Cycling*, edited by J. O. Nriagu, pp. 129-154, Wiley, New York.

Slanina, J., H. M. Brink, R. P. Otjes, A. Even, P. Jongejan, A. Khlystov., A. Waijers-Ijpelaan, M. Hu, and Y. Lu (2001), The continuous analysis of nitrate and ammonium in aerosols by the steam jet aerosol collector (SJAC): extension and validation of the methodology, *Atmospheric Environment, 35*, 2319-2330.

Solomon, P. A. (1995), Regional photochemical measurement and modeling studies: a summary of the A&WMA International Specialty Conference, Feature Article, *Journal of the Air & Waste Management Association, 45*, 253-286.

Solomon, P. A., W. L. Chameides, C. S. Kiang, T. Russell, A. Butler, D. Mikel, R. Scheffe, E. Cowling, E. Edgerton, J. Jansen, P. McMurry, S. Hering, T. Bahadori (2003), Overview of the 1999 Atlanta Supersites Project, *Journal of Geophysical Research, 108*(D7), 8413, doi:10.1029/2001JD001458.

Stelson, A. W., S. K. Friedlander, and J. H. Seinfeld (1979), A note on the equilibrium relationship between ammonia and nitric acid and particulate ammonium nitrate, *Atmospheric Environment, 13*, 369-371.

Stelson, A. W., and J. H. Seinfeld (1982a), Relative humidity and temperature dependence of the ammonium nitrate dissociation constant, *Atmospheric Environment, 16*, 983-992.

Stelson, A. W., and J. H. Seinfeld (1982b), Relative humidity and pH dependence of the vapor pressure of ammonium nitrate – nitric acid solutions at 25^{o}C, *Atmospheric Environment, 16*, 993-1000.

Stelson, A. W., and J. H. Seinfeld (1982c), Thermodynamic prediction of the water activity, NH_4NO_3 dissociation constant, density and refractive index for the NH_4NO_3-$(NH_4)_2SO_4$-H_2O system at 25^{o}C, *Atmospheric Environment, 16,* 2507-2514.

Stevens, P. S., J. H. Mather, W. H. Brune, F. Eisele, D. Tanner, A. Jefferson, C. Cantrell, R. Shetter, S. Sewall, A. Fried, B. Henry, E. Williams, K. Baumann, P. Goldan, and W. Kuster (1997), HO_2/OH and RO_2/HO_2 ratios during the Tropospheric OH Photochemistry Experiment: Measurement and theory, *Journal of Geophysical Research, 102*, 6379-6391.

Stolzenburg, M. ., and S. V. Hering (2000), A method for the automated measurement of fine particle nitrate in the atmosphere, *Environmental Science & Technology, 34*, 907-914.

Streets, D. G., T. C. Bond, G. R. Carmichael, S. D. Fernandes, Q. Fu, D. He, Z. Klimont, S. M. Nelson, N. Y. Tsai, M. Q. Wang, J.-H. Woo, and K. F. Yarber (2003), An inventory of gaseous and primary aerosol emissions in Asia in the year 2000, *Journal of Geophysical Research, 108*(D21), 8809, doi:10.1029/2002JD003093.

Tiao, G. C., G. E. D. Box, and W. J. Hamming (1975), Analysis of Los Angeles photochemical smog data: a statistical overview, *Journal of Air Pollution Control Association, 25*, 260-268.

Trainer, M, D. D. Parrish, M. P. Buhr, R. B. Norton, F. C. Fehsenfeld, K. G. Anlauf, J. W. Bottenheim, Y. Z. Tang, H. A. Wiebe, J. M. Roberts, R. L. Tanner, L. Newman, V. C. Bowersox, J. F. Meagher, K. J. Olszyna, M. O. Rodgers, T. Wang, H. Berresheim, K. L. Demerjian, and U. K. Roychowdhury (1993), Correlation of ozone with NO_y in photochemically aged air, *Journal of Geophysical Research, 98*, 2917-2925.

Trainer, M., B. A. Ridley, M. P. Buhr, G. Kok, J. Walega, G. Hubler, D. D. Parish, and F. C. Fehsenfeld (1995), Regional ozone and urban plumes in the southeastern United States: Birmingham, a case study, *Journal of Geophysical Research, 100*, 18823-18834.

Vedal, S. (1997), Ambient particles and health: lines that divide, *Journal of Air & Waste Management Association, 47*, 551-581.

Vingarzan, R., and B. Taylor (2003), Trend analysis of ground level ozone in the greater Vancouver/Fraser Valley area of British Columbia, *Atmospheric Environment, 37*, 2159-2171.

Wakamatsu S., I. Uno, and M. Suzuki (1990), A field study of photochemical smog formation under stagnant meteorological conditions, *Atmospheric Environment, 24A*, 1037-1050,

Wakamatsu, S., T. Ohara, and I, Uno (1996), Recent trends in precursor concentrations and oxidant distributions in the Tokyo and Osaka areas. *Atmospheric Environment, 30*, 715-721.

Wakamatsu, S., I. Uno, T. Ohara, and K. L., Schere (1999), A study of the relationship between photochemical ozone and its precursor emissions of nitrogen oxides and hydrocarbons in Tokyo and surrounding areas, *Atmospheric Environment, 33*, 3097-3108.

Wang, T., Y. Y. Wu, T. F. Cheung, K. S. Lam (2001a), A study of surface ozone and the relation to complex wind flow in Hong Kong, *Atmospheric Environment, 35*, 3203-3215.

Wang, T., V. T. F. Cheung, K. S. Lam, G. L. Kok, J. M. Harris (2001b), The characteristics of ozone and related compounds in the boundary layer of the South China coast: temporal and vertical variations during autumn season, *Atmospheric Environment, 35*, 2735-2746.

Weber R., D. Orsini, Y. Duan, Y.-N. Lee, P. Klotz, and F. Brechtel (2001), A particle-into-liquid collector for rapid measurements of aerosol chemical composition, *Aerosol Science and Technology, 35*, 718-727.

Weber R., D. Orsini, Y. Duan, K. Baumann, C. S. Kiang, W. Chameides, Y.-N. Lee, F. Brechtel, P. Klotz, P. Jongejan, H. t. Brink, J. Slanina, P. Dasgupta, S. Hering, M. Stolzenburg, E. Edgerton, B. Harstell, P. Solomon, and R. Tanner (2003), Intercomparison of near real-time monitors of $PM_{2.5}$ of nitrate and sulfate at the EPA Atlanta Supersite, *Journal of Geophysical Research, 108*(D7), 8421, doi:10.1029/2001JD001220.

Weber, R. J., P. H. McMurry, F. L. Eisele, and D. J. Tanner (1995), Measurement of expected nucleation precursor species and 3 to 500 nm diameter particles at Mauna Loa Observatory, Hawaii, *Journal of Atmospheric Sciences, 52*, 2242-2257.

Weber, R. J., J. J. Marti, P. H. McMurry, F. L. Eisele, D. J. Tanner, and A. Jefferson (1996), Measured atmospheric new particle formation rates: Implications fro nucleation mechanisms, *Chemical Engineering Communications, 151*, 53-64.

Weber, R. J., J. J. Marti, P. H. McMurry, F. L. Eisele, D. J. Tanner, and A. Jefferson (1997), Measurements of new particle formation and ultrafine particle growth rates at a clean continental site, *Journal of Geophysical Research, 102*, 4375-4385.

Weber, R. J., P. H. McMurry, L. Mauldin, D. Tanner, F. Eisele, F. Brechtel, S. Kreidenweis, G. Kok, R. Schillawski, and D. Baumgardner (1998), A study of new particle formation and growth involving biogenic trace gas species measured during ACE 1, *Journal of Geophysical Research, 103*, 16385-16396.

Weber, R. J., P. H. McMurry, L. Mauldin, D. Tanner, F. Eisele, A. Clarke, and V. N. Kapustin (1999), New particle production in the remote troposphere: A comparison of observations at various sites, *Geophysical Research Letters, 26*, 307-310.

Wexler, A. S., and J. H. Seinfeld (1990), The distribution of ammonium salts among a size and composition dispersed aerosol, *Atmospheric Environment, 24A*, 1231-1246.

Wexler, A. S., and J. H. Seinfeld (1991), Second-generation inorganic aerosol model, *Atmospheric Environment, 25A*, 2731-2748.

Wexler, A. S., and J. H. Seinfeld (1992), Analysis of aerosol ammonium nitrate: departures from equilibrium during SCAQS, *Atmospheric Environment, 26A*, 579-591.

Wexler, A. S., F. W. Lurmann, and J. H. Seinfeld (1994), Modelling urban and regional aerosol – I. Model development, *Atmospheric Environment, 28A*, 531-546.

Wigley, T. M. L. (1989), Possible climate change due to SO_2 derived cloud condensation nuclei, *Nature, 339*, 365-367.

Wilkins, E. T. (1954), Air pollution and the London fog of December 1952. *Journal of the Royal Sanitary Institute, 74(1)*, 1-21.

Xu, J., M. H. Bergin, X. Yu, G. Liu, J. Zhao, C. M. Carrico, and K. Baumann (2002), Measurement of aerosol chemical, physical and radiative properties in the Yangtze delta region of China, *Atmospheric Environment, 36*, 161-173.

Xu, J., M. H. Bergin, R. Greenwald, and P. B. Russell (2003), Direct aerosol radiative forcing in the Yangtze delta region of China: Observation and model estimation, *Journal of Geophysical Research, 108*(D2), 4060, doi:10.1029/2002JD002550.

Zheng, M., G. R. Cass, J. J. Schauer, and E. S. Edgerton (2002), Source apportionment of PM2.5 in the Southeastern United States using solvent-extractable organic compounds as tracers, *Environmental Science & Technology, 36*, 2361-2371.

VITA

Jing Zhang was born in Kaiyuan, Liaoning Province, China. She spent four years at Beijing (Peking) University studying Applied Chemistry in Department of Technical Physics before she gained a B.S. in 1990. Then she studied toward a M.S. at Research Center for Eco-Environmental Sciences, Chinese Academy of Sciences from 1990 to 1993, with Atmospheric Chemistry as her research field. After that she worked at Atmospheric Environment Institute, Chinese Research Academy of Environmental Sciences till 1999. She enrolled in School of Earth and Atmospheric Sciences, Georgia Institute of Technology in 1999 and studied for her Ph.D. degree until now.